ANTI-S2 PEPTIDES AND ANTIBODIES BINDING EFFECT ON MYOSIN S2 AND ANTI-S2 PEPTIDE'S ABILITY TO REACH THE CARDIOMYOCYTES IN VIVO AND INTERFERE IN MUSCLE CONTRACTION

Duaa Mohamad Alhaj Mahmoud Quedan, D.D.S.

Dissertation Prepared for the Degree of

DOCTOR OF PHILOSOPHY

UNIVERSITY OF NORTH TEXAS

July 2023

APPROVED:

Douglas D. Root, Major Professor
Pamela A. Padilla, Committee Member
Rajeev Azad, Committee Member
Robert C. Benjamin, Committee Member
Jyoti Shah, Chair of the Department of Biological Sciences
John Quintanilla, Dean of the College of Science
Victor Prybutok, Dean of the Toulouse Graduate School

Quedan, Duaa Mohamad Alhaj Mahmoud. *Anti-S2 Peptides and Antibodies Binding Effect on Myosin S2 and Anti-S2 Peptide's Ability to Reach the Cardiomyocytes in vivo and Interfere in Muscle Contraction*. Doctor of Philosophy (Biochemistry and Molecular Biology), July 2023, 97 pp., 11 tables, 37 figures, 116 numbered references.

The anti-S2 peptides, the stabilizer and destabilizer, were designed to target myosin sub-fragment 2 (S2) in muscle. When the peptides are coupled to a heart-targeting molecule, they can reach the cardiomyocytes and interfere with cardiac muscle contraction. Monoclonal antibodies, MF20 and MF30, are also known to interact with light meromyosin and S2 respectively. The MF30 antibody compared to anti-S2 peptides and the MF20 antibody is used as a control to test the central hypothesis that: Both the anti-S2 peptides and antibodies bind to myosin S2 with high affinity, compete with MyBPC, and possibly interact with titin, in which case the anti-S2 peptides have further impact on myosin helicity and reach the heart with the aid of tannic acid to modulate cardiomyocytes' contraction in live mice. In this research, the effects of anti-S2 peptides and antibodies on myosin S2 were studied at the molecular and tissue levels. The anti-myosin binding mechanism to whole myosin was determined based on total internal reflectance fluorescence spectroscopy (TIRFS), and a modified cuvette was utilized to accommodate this experiment. The binding graphs indicated the cooperative binding of the peptides and antibodies with high affinity to myosin. Anti-myosin peptides and antibodies competition with Myosin Binding Protein C (MyBPC) was revealed through the super-resolution expansion microscopy using wildtype skeletal and cardiac myofibrils, and MyBPC knock-out cardiac myofibril. This new emerging technique depends on using the regular confocal microscope in imaging expanded myofibril after embedding in a swellable hydrogel polymer and digestion. A decrease in the fluorescent intensity at the C-zone was observed in myofibrils labeled with fluorescently labeled anti-S2 peptides or

antibodies supporting the competition with MyBPC, which further was confirmed by the absence of this reduction at the C-zone in the knockout MyBPC cardiac tissue. The anti-S2 peptide's ability to reach inside the cardiomyocytes was tested by injecting fluorescently labeled anti-S2 peptides bound to tannic acid in live mice, the destabilizer peptide reached the heart 6X more than the stabilizer peptide. Some of the peptides labeled cardiac arterioles and T-tubules as detected by super-resolution microscopic images, meanwhile some peptides reached inside the cardiomyocytes and labeled some sarcomeres. This dissertation demonstrates the ability of anti-S2 peptides and antibodies in modifying myosin as they bind cooperatively with high affinity to myosin and compete with the regulatory protein MyBPC, in addition to the possible interaction between the stabilizer peptide and titin. Lastly, the peptides succeeded in labeling some cardiac sarcomeres in live mice.

ACKNOWLEDGMENTS

By the name of God, the most merciful, I have accomplished my PhD without God will who gave me the strength to reach where I am today. Unconditional thanks to Dr Douglas Root who helped me throughout this journey, he is my model for science knowledge. Special thanks to my committee members for their continuous support Dr. Pamela A. Padilla, Dr. Xiaoqiang Wang, Dr. Rajeev Azad, and Dr. Robert C. Benjamin. I cannot deny Dr. Andrea L Bernardino support and guidance in my expansion experiments. Special thanks to Dr. Arland Alberts who is the best supervisor, she gave me the strength and confidence during teaching the labs. Also special thanks to my previous lab members Dr. Rohit Singh, Dr. Motamed Qadan, Dr. Negar Aboonasrshiraz, Sabrina Shalabli, and Julia Migliore they all are great companions with their support.

I gift this degree to my parents who always push me to be the best, their prayers showered me with strength and patience. Special thanks to my second half, Motamed, I won't reach here without your continuous help and support. My little team, Talyah, Maryam, and Ibrahim we survived this together. My brothers, sisters, and in laws thank you all for your endless support and prayers.

Special thanks to our collaborators: Kenneth S. Campbell (University of Kentucky), Richard L. Moss (University of Wisconsin), and Daniel P. Fitzsimons (University of Idaho), and to the National Institutes of Health (R01HL149164) for the grant to support this work.

TABLE OF CONTENTS

Page

LIST OF TABLES

Page

LIST OF FIGURES

Page

ABBREVIATIONS

α	Alpha symbol
A-band	Anisotropic band
ADP	Adenosine diphosphate
APS	Ammonium persulfate
ATP	Adenosine triphosphate
C-zone	Central region where Myosin Binding Protein C localized
°C	Celsius degree
Ca^{2+}	Calcium ions
D-zone	Distal zone in the A-band
Da	Dalton
DAB	Diaminobenzodine
DCM	Dilated cardiomyopathy
DIC	Differential interference contrast
DMF	Dimethyl formamide
DVB	Divinylbenzene
EDTA	Ethylenediaminetetraacetic acid
ELISA	Enzyme linked immunosorbent assay
FRET	Fluorescence resonance energy transfer
GFS	Gravitational force spectroscopy
HCM	Hypertrophic cardiomyopathy
HEPES	2-[4-(2-Hydroxyethyl)piperazin-1-yl]ethane-1- sulfonic acid
I-band	Isotropic band

IgG	Immunoglobulin
K_2HPO_4	Dipotassium hydrogen phosphate
kDa	Kilodaltons
L	Liter
Min	Minute
M-line	Mittel line or middle line in the sarcomere
MyBPC	Myosin binding protein C
NaH_2PO_4	Sodium dihydrogen phosphate
nM	Nanomolar
NMR	Nuclear magnetic resonance
P-zone	Proximal zone in the A-band
PAGE	Polyacrylamide gel electrophoresis
P_i	Phosphate ion
RCF	Relative centrifugal force
RPC	Reverse phase chromatography
S1	Myosin sub-fragment 1
S2	Myosin sub-fragment 2
SDS	Sodium dodecyl sulfate
TA	Tannic acid
TFA	Trifluoroacetic acid
TIRFS	Total internal reflectance fluorescence spectroscopy
Tm	Tropomyosin
TnC	Calcium binding troponin

TnI	Inhibitory troponin I
TnT	Tropomyosin binding troponin
TRIS	Tris(hydroxymethyl)aminomethane
UV	Ultraviolet
Vis	Visible
Wt	Wild type
Xg	Centrifuge unit means times gravity
Z-disc	Zwischenscheibe (German) spacer

CHAPTER 1

INTRODUCTION

1.1 Sarcomere: The Unit of Contraction

Striated muscles, which include the skeletal and the cardiac muscles, are organized in a fascinating repeated unit called the sarcomere. This repeated unit displays a banding pattern under the light microscope and gives the striated muscle this name. The sarcomeres work side by side to achieve muscle contraction by myosin and actin filaments interdigitation (1). This contraction is regulated by accessory proteins like troponin, tropomyosin, titin, myosin binding protein C (MyBPC), nebulin, and others (2).

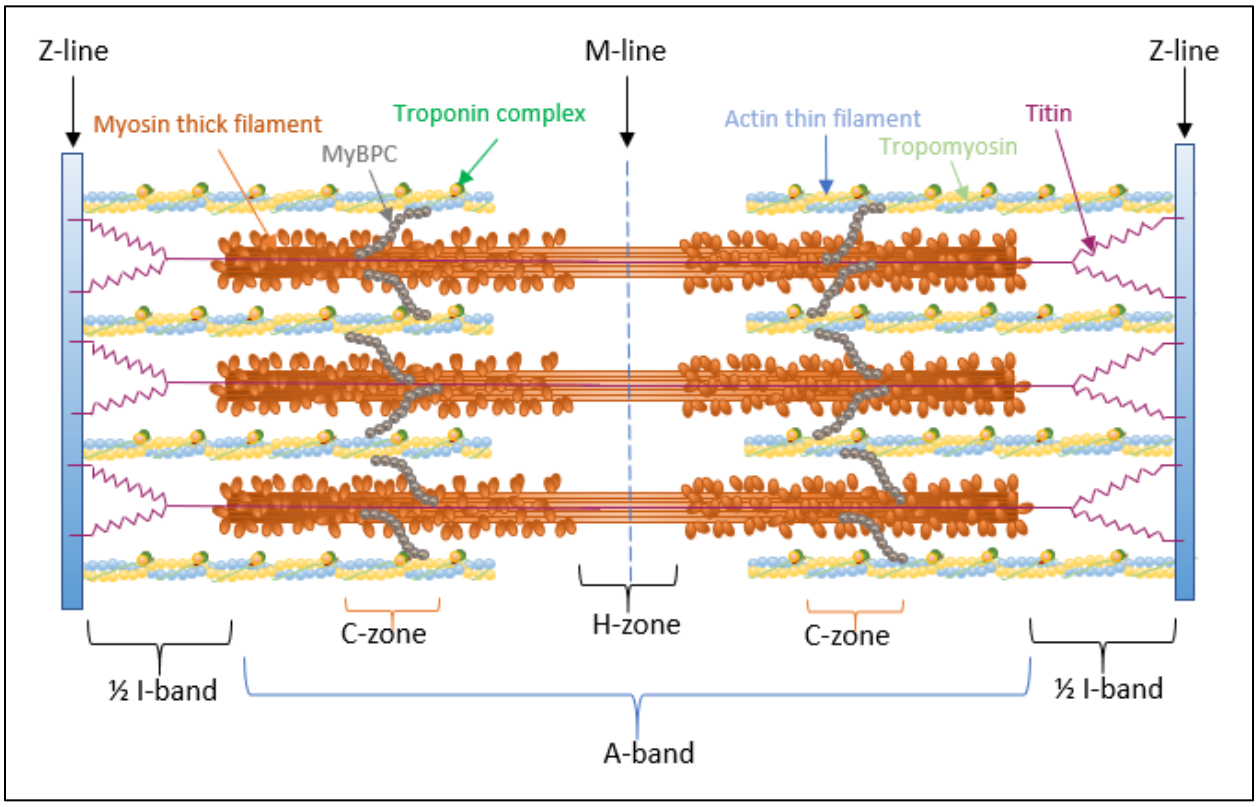

Figure 1: Muscle sarcomere diagram. Actin and myosin filaments interdigitation in muscle sarcomere and the regulatory proteins.

The sarcomere is defined by two Z-discs at the edges with a 2.2 -3.2 µm separation distance between them (3). The actin thin filaments run from both sides of the Z-disc toward the middle of

the sarcomere, where they interdigitate with the bipolar myosin thick filaments in the center of the sarcomere (Figure 1). The entire length of the myosin thick filament is dominated by A-band, which is approximately 1.6 μm that does not change during muscle contraction (4). The A-Band is bisected by the M-line in the middle of the sarcomere. The distance between the two ends of myosin thick filament from adjacent sarcomeres passing by the Z-disc is called the I-band. The I-band shortens during muscle contraction. The sarcomere length reaches 1.6 μm (the entire length of the A-band) in a fully contracted sarcomere (5), or beyond that in super-contracted state when myosin thick filaments of neighboring sarcomeres overlap through the perforations in the Z-disc (6).

1.1.1 Myosin Filament

In muscles, myosin type 2 is the abundant myosin that is involved in muscle contraction; it is organized as a bipolar thick filament. Myosin filament is composed of one pair of identical heavy chains (223 kDa each), and two pairs of light chains (22 kDa each) called the essential and the regulatory light chains (7). Myosin heavy chain is subdivided into three parts: head, neck, and tail (Figure 2). Myosin head or sub-fragment 1 (S1) is a globular protein that is protruding out of myosin thick filament. It is the motor part of myosin protein that is responsible for ATP hydrolysis to slide over the actin filament (8). Hundreds of myosin heads cooperatively interact with actin and initiate contraction (9). Myosin neck or sub-fragment 2 (S2) is a coiled-coil structure that links the head to the tail and undergoes a conformational change to facilitate muscle contraction. Myosin tail or light meromyosin (LMM) is a coiled-coil structure that is organized rods and meets at the M line from its ends constructing the bulk of myosin thick filament (9). Each thick filament is composed of approximately 300 myosin thick filaments and their regulatory proteins. The heads are organized in the opposite direction on both sides of the filament leaving a bare zone in the

middle without myosin heads (H-zone in Figure 1) (4).

The residues on the myosin S2 and LMM strands form heptad repeat (a-b-c-d-e-f-g) where residue a from one strand form a hydrophobic interaction with residue d on the other strand. The a-d hydrophobic interaction between the two strands stabilizes the coiled-coil structure and gives the myosin S2 the required flexibility (10, 11).

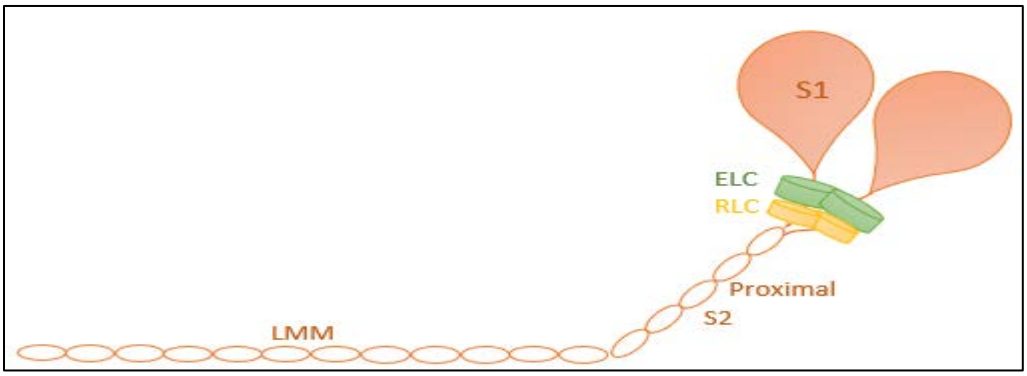

Figure 2: Myosin thick filament scheme. Composed of a pair of heavy chains and two pairs of light chains.

1.1.2 Actin Filament

Actin filaments in sarcomere are precisely organized to be equal in length. This filament is composed of the globular actin monomer (G-actin) that polymerizes to form the fibrous actin polymer (F-actin) (12). In muscles, two strands of F-actin are twisted together to form the thin filament helix that repeats every 36 nm, and it is embellished with tropomyosin and troponin complex that regulate muscle contraction (Figure 1) (13, 14). They are more abundant than myosin thick filament in sarcomere with a ratio of 2:1 (15). The C-terminus of the actin filament is attached to the Z-disc and the N-terminus is facing toward the M-line (16). The actin thin filaments interdigitate with the myosin thick filaments giving the muscle a striated appearance.

1.1.3 Tropomyosin and Troponin Complex

Actomyosin binding is modulated by tropomyosin and troponin complex. Tropomyosin is

an α-helical coiled coil dimer with negative side chains that run along the main groove of the actin filament which is positively charged. The C-terminus of the tropomyosin overlaps and noncovalently binds with the N-terminus of the next tropomyosin to form a continuous string along the actin filament groove (17, 18). The tropomyosin stabilizes the actin filament and regulates muscle contraction by shifting away from the myosin heads binding sites on actin filament upon receiving signal to initiate muscle contraction (19).

Meanwhile, Troponin complex is composed of 3 subunits: The Ca^{2+} binding troponin C (TnC), the inhibitory troponin I (TnI), and the Tm-binding troponin T (TnT); they regulate muscle contraction upon an increase in Ca^{2+} concentration (20). When a muscle cell is stimulated, TnC senses Ca^{2+} that evokes a conformational change in the troponin complex and translocates tropomyosin away from the myosin binding site on the actin filaments, which becomes accessible for myosin heads to initiate contraction (21).

1.1.4 Myosin Binding Protein C

The regulatory myosin binding protein C (MyBPC) is a 150 kDa protein localized within the C-zone of muscle sarcomere. It is composed of 10 domains C1-C10 in skeletal muscles and 11 domains C0-C10 in cardiac muscles (22). The N-terminus of this protein interacts with the actin filament and extends to interact with titin and myosin S2, and the C-terminus is anchored in the LMM (23). It is suggested that MyBPC regulates muscle contraction by stabilizing the folded S1 domain of myosin to the back over S2 during the OFF state, and releasing S1 to interact with actin filament during the ON state (24).

Mutations within this protein have an impact on its structure and function (25). Some mutations disrupt the role of MyBPC in facilitating myosin heads bending toward the myosin rods (26, 27). In this case, myosin heads remain in the ON state available for binding to the actin

filament and initiating muscle contraction (28).

1.1.5 Titin

The giant protein titin ,or connectin, is the longest single polypeptide known, and the third abundant protein in the striated muscles after myosin and actin. It is composed of 38,138 residues in human and weigh ~4.2 mDa (29). Titin runs from the Z-disc (N-terminus) and is inserted in the thick filament close to the M-line (C-terminus). Each titin overlaps with the neighboring titin from the same sarcomere or the adjacent sarcomeres to form one unit of titin along the myofilament (30).

The part of titin located in the I-band is extensible; it resembles an elastic spring that maintains the passive force in the sarcomere during diastolic stretch that elongates the sarcomere. The embedded part of titin close to the M-line keeps the thick filaments aligned during muscle contraction to control sarcomere stiffness. Titin also works as a restoring force to bring the sarcomere back to its normal length after muscle contraction (31, 32).

1.2 Muscle Contraction

Sliding filament theory is more complicated than actin thin filaments sliding over myosin thick filaments. It is rather controlled and regulated by many proteins and ions. When an electric activation reaches the neuromuscular junction, acetylcholine is released from the neuronal terminal ending and passes the synapse to bind at specific receptors on the sarcolemma (muscle cell membrane). Subsequently, an action potential is initiated along the sarcolemma causing transmembrane Ca^{2+} ions influx into the myocyte. Ca^{2+} ions bind to the sarcoplasmic reticulum and prompt Ca^{2+} ions release (33). The released Ca^{2+} ions must bind to troponin C to interact with troponin I and T. The interactions between the troponin complex cause sliding of the tropomyosin away from the binding site of myosin on the actin filament (34).

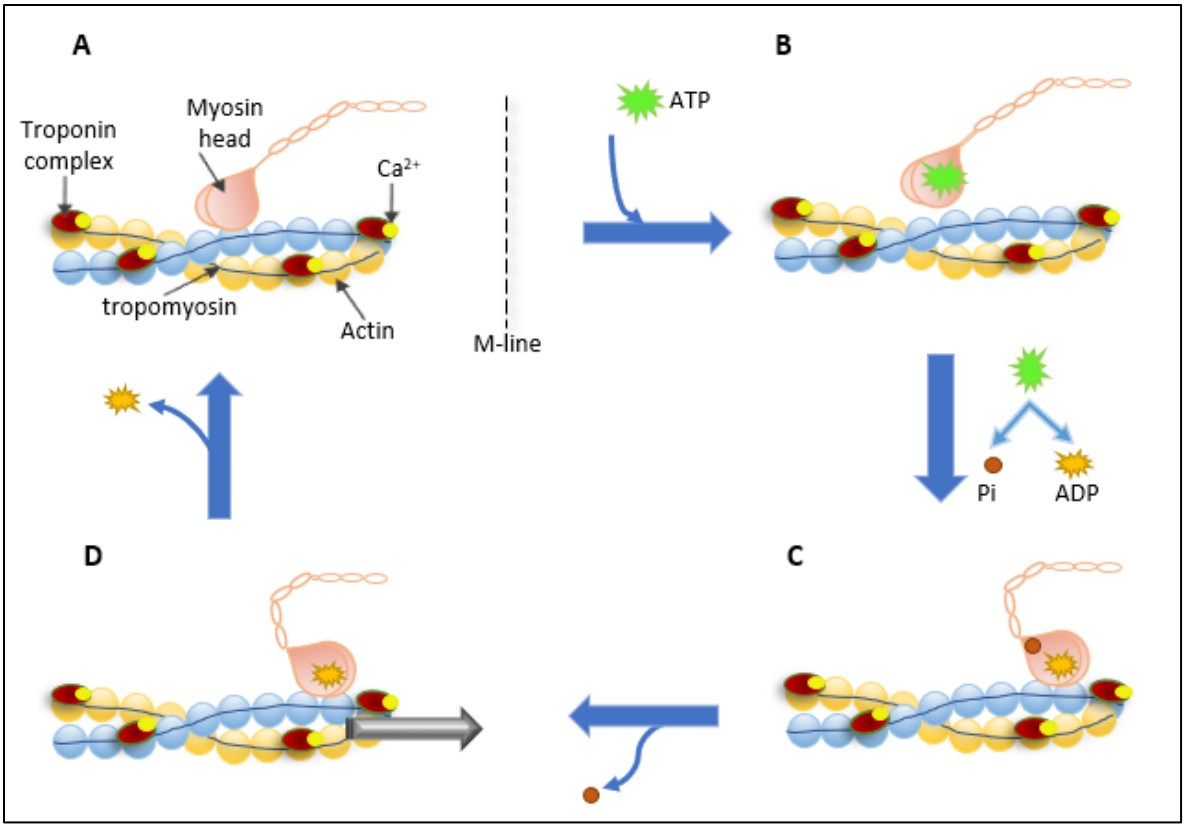

Figure 3: **Actin myosin cross-bridging during muscle contraction.**

A: In the presence of Ca^{2+} ions, troponin complex slides tropomyosin away from the myosin binding site on the actin filament. But in the absence of ATP myosin heads are cross bridged with actin filaments (rigor state). B: In the presence of ATP, myosin heads are detached from the actin filament. C: ATP hydrolysis causes a conformational change in myosin and strong binding to actin. D: The release of P_i initiates the power stroke that pulls the actin filament toward the M-line (grey arrow). ADP is released leaving the myosin head attached to the actin till another ATP binds and initiates a new power stroke cycle in the presence of Ca^{2+}.

In the presence of adenosine triphosphate (ATP), which binds to the ATPase binding site on the myosin head, the myosin-actin complex is separated. Afterward, ATP is hydrolyzed and induces a conformational change in the myosin, which promotes myosin head to bind to the actin filament at a location closer to the M-line. The release of P_i provokes the power stroke by pulling the actin filament toward the M-line which causes shortening of the sarcomere. Finally, the adenosine diphosphate (ADP) is released leaving the myosin head firmly attached to the actin filament (rigor state). As long as Ca^{2+} ions and ATP are available the cycle will repeat and the actin filament will slide over the myosin filament till muscle contracts (35, 36) (Figure 3). When the

nerve stimulus is ceased from the muscle, the Ca^{2+} ions are pumped back into the sarcoplasmic reticulum and the myosin binding site on the actin filament is blocked again by tropomyosin. As a result, myosin heads detach from the actin filament and the muscle relaxes (33).

1.3 Myosin Sub-Fragment 2 (S2)

This flexible segment is composed of 429 residues (from residue 841 to 1280) that tends to form a helix (37, 38). The N-terminus of S2 is located at the hinge region that connects the myosin head with S2, and the C terminus is located within the hinge region that connects S2 with LMM (Figure 2). The flexibility of myosin S2 is derived from the two hinges at both ends and the extensible coiled-coil structure (39). Some studies suggest that the part of S2, specifically at the hinges, are random coils which add extra flexibility to this segment. The flexibility of myosin S2 allows myosin heads to swivel around myosin by more than 360° (40).

Myosin S2 has a significant role in stabilizing myosin head when it folds to the back during the OFF state (41, 42). During this state, the actin binding site on myosin head becomes close to the S2, and the intermolecular interaction keeps the head blocked and inaccessible from the actin filament during muscle relaxation (43, 44).

Some mutations associated with myosin S2 have detrimental effects on the intermolecular interaction. For example, R870H and E924K are two substitute mutations that disrupt the interaction between myosin S2 and MyBPC. Therefore, the bending of myosin head during the OFF state will be unstable causing a decompensation in the cardiac muscle on the long term (45). Another important mutation located within the S2 region is the E930del. Glutamic acid deletion causes disruption in the heptad repeat of the coiled-coil, which leads to an increase in the myosin dimer flexibility, subsequently cardiac myocyte contraction increases leading to hypertrophic cardiomyopathy (46, 47).

1.4 Cardiomyopathy

The heart is a hard-working muscle in our bodies that keeps pumping the blood throughout our life without stopping or having a rest. Cardiomyopathy is a term used for a diseased heart, it could be a primary cardiomyopathy that mostly results from genetic mutations in cardiac myocytes like dilated cardiomyopathy (DCM) and hypertrophic cardiomyopathy (HCM), or a secondary cardiomyopathy that is caused as a result of a medical condition (48).

DCM is a common disease that affects 1 out of 2500 individuals in the USA (49). Most of the patients have mutations in the cytoskeletal proteins. These mutations affect myocyte organization and function leading to cardiac myocyte death and replacement with fibrous tissues. DCM causes dilation in the ventricular cavity with thin ventricular walls, and this will affect the efficiency of the heart causing systolic dysfunction and heart failure in some cases (50).

HCM is more common than DCM, it is a heterogenous autosomal dominant disease that affects 1 individual out of 500. More than 70% of the mutations are located in 2 genes: β- myosin heavy chain and MyBPC (51). The location of the mutation on the gene determines the severity of the disease (50). Some patients are symptomless, while others suffer from arrhythmia, atrial fibrillation, and heart failure up to sudden death specially at young ages. 10-20% of the patients develop DCM as a result of persistent HCM (52). At the cellular level, the cardiac myocyte increases in size and has distorted alignment. Apoptosis occurs more frequently at the beginning then it slows down, the dead cell will be replaced by fibrous tissue and collagen (50). For the heart to compensate for the high demand and the stress, it adapts by increasing the heart mass, leading to an asymmetrical thickening of the interventricular septum and decreasing the chamber size of the ventricle (51, 53).

The treatment options depend on the severity of the case. Some mild conditions are

controlled by drug administration, β-blockers or calcium channel blockers which are the most commonly used drugs (54, 55). Defibrillator implanting is also undertaken in some cases to control heart beat rhythm (56); however, in some severe cases surgical myectomy is required to decrease the heart mass and relief the stress from the heart walls (53).

1.5 Hypothesis and Testing

The critical role of myosin S2 in regulating muscle contraction is demonstrated by the several mutations that occur in this segment (11). Since some of these mutations disrupt the stability of this region by causing disruption of the OFF state leading to cardiomyopathies (57, 58). Then altering S2 stability in a manner similar to mutations may modify muscle function. For example, if S2 is altered to be unstable, the myosin heads are more in the ON state compared to the regular muscle filament, this could increase the chance of myosin heads binding to the actin filaments leading to an increase in muscle contraction. If this modification can be applied to patients with heart failure, cardiac muscle contraction can be improved.

In view of the importance of S2, stabilizer and destabilizer peptides were designed in our lab based on computational simulation to target myosin S2 specifically and interfere with muscle contraction. The peptides were tested in the lab for their ability to bind to purified myosin S2 in myofilaments and modulate their contraction. Then, upon gathering sufficient data at the molecular and tissue levels, the peptides were advanced to animal models to target the heart. And with that came the demand for a heart homing molecule that would guide the peptides to the heart. One good fit was the tannic acid (TA). This molecule is naturally available and was found to be able to bind anti-S2 peptides and guide them to the heart, thus it was chosen to perform this task (59).

My work focused on testing the effect of anti-S2 peptides on myosin at the molecular level, at the cellular level by imaging skeletal and cardiac myocytes, and at the animal model level by

analyzing the data (from our collaborators). In addition to that, I compared the synthetic peptides with antibodies against myosin, which were used as a control in later experiments.

Based on the preceding findings, the following central hypothesis was formulated: Both the anti-S2 peptides and antibodies bind to myosin S2 with high affinity, compete with MyBPC, and possibly interact with titin, in which case the anti-S2 peptides have further impact on myosin helicity, and reach the heart with the aid of tannic acid to modulate cardiomyocyte's contraction in live mice. To test this hypothesis, it was organized into 3 aims to answer it.

The first aim is organized into three parts. First, testing if the anti-S2 peptides bind to myosin dimer through anisotropy. The change in anisotropy reading can predict if anti-S2 peptides bind to myosin or not through molecule rotation alternation upon binding.

Second, testing the structural modification in myosin S2 upon binding to anti-S2 peptide through alpha helical content changes in synthetic myosin S2. The destabilizer was designed to break the coiled coil structure of myosin S2, therefore, estimating the helicity changes in myosin S2 indicates if the destabilizer peptide disrupts the dimer formation of myosin S2. On the other hand, the stabilizer peptide was designed to wrap around myosin S2 and increase helicity. Improvement in S2 helicity would indicate the development of more stable myosin. The changes in myosin helicity were measured using UV absorbance spectrophotometer.

Lastly in this aim, the affinity of the anti-S2 peptide/antibody to myosin has a significant role in estimating the optimal concentration that will be injected into the mice in live animal model. The measured affinity of the fluorescently labeled anti-S2 peptide/antibody was measured using fluorescence anisotropy, total internal reflectance spectroscopy (TIRFS), or competitive TIRFS.

In the second aim, microscopy was used to locate the labeled anti-S2 peptide/antibody within the muscle sarcomere. Along with actin and myosin filaments, there are regulatory proteins

in the sarcomere that share the same binding site with the anti-S2 peptide/antibody. These anti-S2 peptides/antibodies can compete with MyBPC and could block their binding site. This competition was detected by analyzing super-resolution images for myofibrils imaged using the new arising expansion microscopy technique. In this technique, the labeled myofibrils were embedded in a swellable polymer gel and were digested afterward. Tracing the crosslinked fluorophores to the gel revealed the binding sites of the labeled anti-S2 peptides/antibodies within the muscle sarcomere and their competition with MyBPC.

Further in this aim, anti-S2 peptides and antibodies were tested to see if they interact with titin. Anti-titin competition with the peptides or antibodies to bind at titin might shed any possible interaction with titin.

Lastly in the third aim, the labeled/unlabeled anti-S2 peptide with tannic acid was injected into live mice by the collaborators. The mice's hearts were extracted either after one day or seven days from the injection. The hearts were sectioned and imaged using fluorescent microscope to check if the peptides succeeded in reaching into the cardiomyocyte. The whole slices from the hearts with the labeled peptide were imaged as tiles, normalized, and stitched. Then, they were analyzed to study the distribution of the peptides within the heart depending on the fluorescence intensity. Also, the ratio of the fluorescence intensity amount to the area of each slice was estimated for a better perception of the distribution of the peptides within the heart.

In addition to that, the sarcomere lengths were measured in the cardiac myofibrils from the mice hearts after injecting tannic acid alone, labeled anti-S2 peptide, and unlabeled anti-S2 peptide. The measured sarcomere lengths tested if the peptides were able to alter muscle contraction by changing the sarcomere length compared to the control (tannic acid alone).

Hypothesis: **Both the anti-S2 peptides and antibodies bind to myosin S2 with high affinity, compete with MyBPC, and possibly interact with titin, in which case the anti-S2 peptides have further impact on myosin helicity and reach the heart with the aid of tannic acid to modulate cardiomyocytes' contraction in live mice.**

First aim:

- **Confirm that anti-S2 peptide binds to myosin S2 through anisotropy.**
- **Study the effect of anti-S2 peptide binding on myosin helicity.**
- **Measure anti-S2 peptide /antibody affinity to myosin S2.**

Second aim:

Using expansion microscopy:

- **Determine the competition between anti-S2 peptide/antibody and MyBPC.**
- **Test possible interaction between anti-S2 peptide/antibody and titin.**

Third aim:

Testing if tannylated anti-S2 peptide is able to reach the heart of live mice and alter cardiomyocyte contraction.

CHAPTER 2

MATERIALS AND METHODS

2.1 Materials

2.1.1 Skeletal Myofibril Preparation

Rabbit skeletal myofibril was prepared and purified as described by Schick and Hass (60) with slight modification. Approximately 20 g of rabbit skeletal muscle was chopped into thin slices and placed into 200 ml of well stirred cold buffer containing 20 mM potassium chloride, 10 mM potassium phosphate, and 4 mM EDTA at pH 6.8. This procedure was undertaken in a cold environment to keep the myofibril in a freezing condition and prevent their shortening (61). The myofibrils were homogenized for 15 seconds in a chilled Waring blender and then centrifuged at 1500 xg at 0 ºC three times in a cold buffer. The final pellet was re-suspended in 50% glycerol and stored at -20 ºC.

2.1.2 Cardiac Myofibril

All procedures were approved by the Institutional Animal Care and Use Committee at University of Wisconsin-Madison and complied with the National Institutes of Health Guide for the Use and Care of Laboratory Animals. cMyBPC KO animals were produced by the laboratory of Dr. Richard L. Moss as described in (Harris et al., 2002) (62). Solution recipes were calculated and prepared as in (Godt and Lindley, 1982) (63).

2.1.3 Myosin Preparation

Myosin was extracted from rabbit skeletal muscles as described by Godfrey and Harrington (64). After the rabbit was euthanized and sacrificed, back and thigh skeletal muscles were derived, and connective and fat tissues were removed. About 400 g of the meat was ground with Krupps meat grinder, then 3X of extraction buffer composed of 0.3 M KCl, 0.072 M NaH_2PO_4, 0.063 M

K_2HPO_4, and 0.001 M EDTA at pH 6.5 was added to the meat (1 g = 1 ml). The meat in the extraction buffer was 10X diluted with distilled water and stirred for 20 min. The mixture was filtered through 4 layers of cheese cloth. The filtrate was saved and diluted 15X the meat weight and left overnight to allow the myosin to polymerize and precipitate. On the next day, the filtrate was decanted, and the precipitate was centrifuged at 7000 RPM for 10 min. The pellet was dissolved in 2 M KCl to depolymerize the myosin, the final concentration of KCl was 0.5 M. Then it was diluted till KCl concentration reached 0.3 M and centrifuged at 9000 RPM for 45 min to precipitate all the contaminant. After that, cold distilled water was added to the supernatant to make the final concentration of KCl 0.033 M to allow the myosin to repolymerize and all the contaminant precipitate again. The last 3 steps were repeated 2 more times for further myosin purification. Myosin was frozen with liquid nitrogen and stored at -70˚C freezer till needed. Myosin concentration was 14.4 mg/ml calculated from absorbance spectrum at 280 nm after background subtracting. Myosin purity was 90% calculated from SDS gel when the myosin loaded was 0.13 µg (Figure 4).

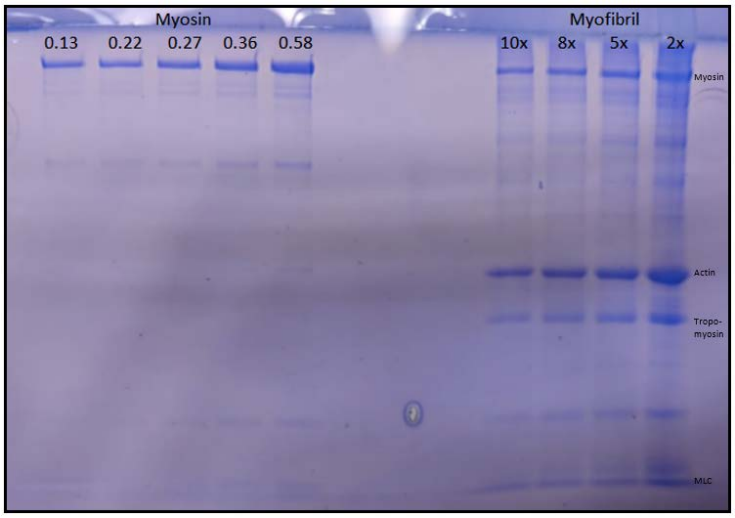

Figure 4: **SDS gel for different concentrations of myofibril (control) and myosin to determine myosin purity. Myosin purity was calculated 90% when the loaded myosin amount was 0.13 µg, actin band was absent at this concentration.**

2.1.4 Synthetic Peptides

The stabilizer peptide is a synthetic peptide that was designed in our lab. It is composed of 17 amino acids, most of them are lysine and was modified by the addition of phenylalanine and alanine. Simulation testing for this peptide, when it interacts with myosin S2 coiled coil, showed that the positively charged amino acids of the peptide interact with the negatively charged glutamate rich region within myosin S2. This electrostatic interaction allows the peptide to wrap around myosin S2 dimer and stabilize it (Figure 5A). However, the destabilizer peptide was designed to destabilize myosin S2 coiled coil by disrupting the dimer formation. This peptide is composed of 19 amino acids that are similar to the myosin S2 amino acids sequence except for a few amino acids. The amino acids that were substituted are expected to allow the peptide to bind stronger to the myosin monomer and prevent dimer formation leaving S2 unstable (Figure 5B). Both synthetic peptides were synthesized in Bio-synthesis Inc. (BSI), Lewisville, Texas, United States.

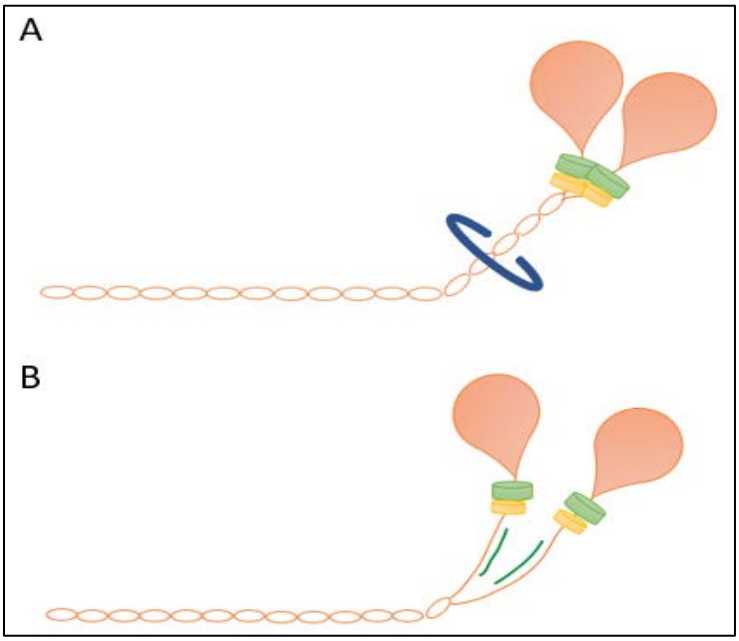

Figure 5: Anti-S2 synthetic peptides bind to myosin filaments diagrams. A: The stabilizer peptide wraps around myosin S2 and stabilizes it. B: Two destabilizer peptides bind to myosin S2, one on each monomer preventing dimer formation.

2.1.5 Monoclonal Antibodies

MF30, which binds to myosin sub-fragment 2, and MF20, which binds to light meromyosin, were obtained from the Developmental Studies Hybridoma Bank. α-MyBPC1 antibody that binds to MyBPC and E-2 anti-titin that binds to the C-terminus of titin were obtained from Thermo-Fisher Scientific (Figure 6).

2.1.6 Polyclonal Antibody

This antibody was raised in guinea pig against a specific site on myosin S2 which is the same site where the synthetic destabilizer peptide was designed to bind (Figure 6). This antibody was produced by Bio-synthesis Inc., Lewisville, Texas, United State.

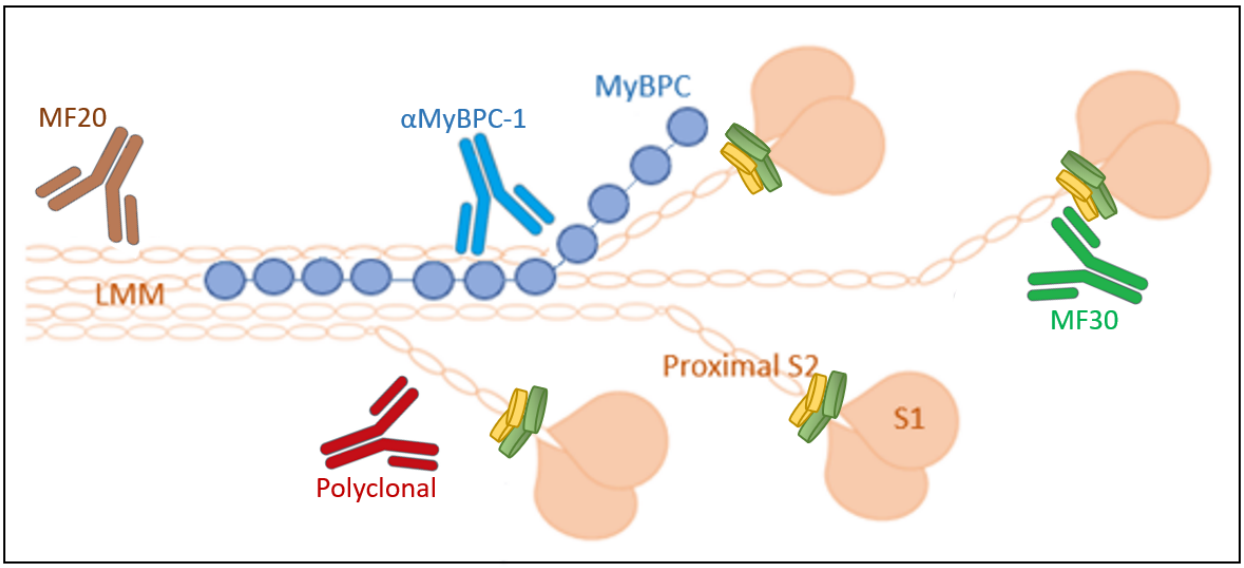

Figure 6: **Myosin thick filament with antibodies diagram**. **The binding sites of different antibodies are illustrated in this diagram.**

2.2 Methods

2.2.1 Antibody Conjugation and Purification

The antibody was conjugated either to Fluorescein isothiocyanate (FITC) or Tetramethylrhodamine-isothiocyanate (TRITC). The fluorophore has a thiocyanate group that is

very reactive to the amine group of the IgG/peptide at the N-terminus, the reaction will result in forming thiourea linkage between the fluorophore and the IgG/peptide.

The fluorophore was dissolved in dimethyl formamide (DMF) to 10 mg/ml, then 10 µl of FITC/TRITC was added to 100 µl of 2 µg of IgG in 20 mM in HEPES at pH 8 and left to react for 1 hour at room temperature with continuous shaking on the vortex.

The conjugated IgG was purified using Micro Bio-Spin 6 chromatography pre-packed column (BIO RAD). First, the column was washed with the buffer 3 times at 1000 RCF for 5 min using IEC Micromax microcentrifuge. The sample was loaded on the column and centrifuged at 1000 RCF for 30 seconds to elute the conjugated antibody first, then the column was washed to elute the free dye to be discarded.

An Agilent 8453 UV-Vis spectrophotometer was utilized to measure the absorbance spectra of the conjugated antibodies to determine their concentration using Beer-Lambert law equation:

$$A = \lambda \cdot e \cdot l \cdot c$$

where A is the measured absorbance, λ is the wavelength in nm, e is the extinction coefficient at that wavelength in $M^{-1}cm^{-1}$, l is the path length in cm, and c is the analytic concentration.

The conjugation efficiency was calculated to estimate the actual number of fluorophores per antibody depending on the conjugated antibody and fluorophore alone spectra as follows:

> Net A of Ab at 280 nm = A of conjugated Ab at 280 nm – ((A of F at 280 nm) / (A of F at 495 nm) * (A of conjugated Ab at 495 nm))

where A is absorbance, Ab is an antibody, F is fluorophore (FITC in the above equation). Antibody and fluorophore concentrations are calculated based on the net antibody absorbance at 280 nm and fluorophore absorbance at 495 nm for FITC and 540 nm for TRITC, respectively, considering the extinction coefficients are 70,000 $M^{-1}cm^{-1}$ for FITC and 100,000 $M^{-1}cm^{-1}$ for TRITC. The

calculated concentrations are applied in the following equation to calculate the conjugation efficiency:

Conjugation efficiency= F concentration/Ab concentration.

The conjugation efficiencies were 3, 8, 5, and 3.5 fluorophores/IgG for MF30, MF20, αMyBPC-1, and anti-titin antibodies, respectively calculated as explained in the statistical section.

2.2.2 Synthetic Peptide Conjugation and Purification

The synthetic peptides, the stabilizer and destabilizer peptides were labeled with TRITC and FITC, respectively. 1 µMole of the peptide was dissolved in 650 µl phosphate buffer saline (PBS) composed of: 0.14 M sodium chloride, 2.7 mM potassium chloride, 1.5 mM potassium phosphate monobasic, and 8.1 mM sodium phosphate dibasic at pH 7.4. The fluorophore was dissolved in DMF to 10 mg/ml. To ensure labeling of the amine group at the N-terminus of the peptide, an equal amount of moles from the synthetic peptide and the fluorophore were mixed in 1:1 ratio, resulting in 1 fluorophore per peptide. After mixing, they were left to react for 1 hour at room temperature with continuous shaking on the vortex.

The conjugated peptides were separated from the extra-free dye using reverse phase chromatography (RPC). This purification was performed in two steps: The first separated the conjugated peptides from the free dye, and the second exchanged the buffer from the first step. First, the Pep RPC column was used with 0.05% Trifluoroacetic acid (TFA) in water as buffer A and 0.05% TFA in acetonitrile as buffer B. After sample injection, the linear gradient increased in buffer B concentration from 0-100% at 0.5 ml/min flow rate. The elute was monitored at 280 nm with UV detector, free dye eluted first when the concentration of buffer B was around 50%, and the conjugated peptide eluted from the column later when buffer B concentration was 100%. Second, to get rid of acetonitrile in the sample, a second run of RPC using divinylbenzene column

(DVB) was undertaken to exchange the acetonitrile with methanol; buffer A was water, and buffer B was methanol that easily evaporated from the sample leaving the conjugated peptide only. The flow rate was 1 ml/min, and buffer B concentration increased linearly from 0-100%. The conjugated peptide eluted when the concentration of buffer B was above 70%. The methanol was evaporated leaving the conjugated peptides that were stored in -20℃ freezer till needed.

The concentrations of the conjugated peptides were calculated based on the absorbance spectrums in a similar manner to antibodies as explained in 2.2.7.

2.2.3 Protein Detection and Identification

2.2.3.1 SDS-PAGE

Sodium dodecyl sulfate (SDS) polyacrylamide gel electrophoresis (PAGE) was utilized to separate the different proteins in the cardiac and skeletal myofibrils based on the molecular weight. In this technique, SDS is used to break the disulfide bond in the tertiary structure of the proteins leaving the proteins as polypeptides, therefore, it eliminates the charge and structure impact on protein migration (65). The smaller proteins migrate faster in the gel with less resistant, and the heavier proteins tend to migrate slower with higher resistance (66).

The 10% polyacrylamide gel was prepared as follows: for the 10% resolving gel: 5 ml of 40% acrylamide-bisacrylamide 19:1, 5 ml of 3 M TRIS pH 8.8, 200 µl 10% SDS, 150 µl 10% ammonium persulfate (APS) initiator fresh prepared, 10 µl of 10% of TEMED (Tetramethylethylenediamine) accelerator, and 9.64 ml of distilled water to make up 20 ml. The 5% stacking gel composed of 1 ml of 40% acrylamide-bisacrylamide 19:1, 2.5 ml of 0.5 M TRIS pH 6.8, 100 µl 10% SDS, 75 µl 10% APS, 8 µl of 10% of TEMED, and 6.318 ml distilled water to make up 10 ml. 400 µl of the sample was added to 100 µl from 5X loading buffer composed of: 5% β-Mercaptoethanol, 0.02% Coomassie Blue, 30% glycerol, 10% SDS, and 250 mM TRIS pH

6.8. The samples were boiled in a water bath for 15 min before loading into the wells. Bio-Rad mini-trans blot cell was used to run the SDS-PAGE, the chamber was filled with 900 ml distilled water and 100 ml of 10X running buffer composed of 250 mM TRIS, 1.92 M glycine, 1% SDS, and distilled water to a total volume 1 L. 10 µl of the samples were loaded in each well of the gel and the machine run for 40 min at 190 volts.

The gel was stained with a staining buffer composed of 0.5% Coomassie Blue in 50% methanol and 10% acetic acid for 15 min on a shaker. Then the gel was moved into a de-staining buffer composed of 40% methanol and 10% acetic acid in distilled water, the destaining buffer was changed every 15-30 min until all the bands were clear.

2.2.3.2 Western Blot

Western blot or protein immunoblot is used to identify protein in a specific sample. It depends on proteins separation based on their molecular weight using electrophoresis, then transferring the proteins into a solid membrane. Specific protein is detected through binding to primary and secondary antibodies (67, 68).

In this experiment, cardiac and skeletal myofibrils were run on 10% polyacrylamide gel in SDS electrophoresis for 40 min at 190 volts with Bio-Rad. The gel was stained with Coomassie blue for 15 minutes and then de-stained by soaking in de-stain solution for at least 2 hours. The proteins on the gel were transferred into a 0.45 mm nitrocellulose for 1 hour at 100 volts in transfer buffer composed of 100 ml ethanol, 800 ml distilled water, and 100 ml of 10X transfer buffer (144 g glycine, 30.3 g TRIS base, 2 g SDS to make 1 L). Half of the nitrocellulose was stained with cooper iodide stain to confirm protein transfer to the membrane using Dr. Root protocol described in (69). The second half of the nitrocellulose was blocked with 3% milk in PBS for 30 min, then it was incubated in 3 ml of MF30 (39 µg/ml) for 2 hours. The MF30 was washed with PBS for 5

minutes, and the nitrocellulose was incubated in 3 ml of 1:5000 anti-mouse IgG conjugated with peroxidase for 30 min. The nitrocellulose was washed with PBS-1% Triton then followed by washing with 0.2 M sodium acetate before incubation with DAB peroxidase substrate metal enhanced for another 30 min. The nitrocellulose was washed with distilled water to stop the reaction and stored in the dark.

2.2.4 Spectroscopic Assays

Spectroscopy is a wide field of science that exploits light properties to study molecule characteristics and interactions. The UV-visible absorbance spectrum can detect the presence of specific amino acid residues in a solution, estimate the concentration of a molecule, and detect the conformational change in its structure (70, 71).

The molecules also can be attached to a fluorophore to be further studied by tracking that fluorophore using a spectrofluorometer (72). When the fluorophore is excited at a specific wavelength by light or polarized light, it emits light at a longer wavelength. The emitted light is recorded by a detector. The emission signals detect molecules interaction, binding affinity, and many other analyses (73).

2.2.4.1 Absorbance Spectroscopy

The peptide bonds in a polypeptide/protein absorb light at a specific wavelength (between 180-200 nm) (74). Polypeptides or proteins interactions cause conformational changes in the structure that alter the absorbance spectra. Regarding the changes in the absorbance spectrum before and after adding a specific molecule using different concentrations, the change in the α-helix, β-sheets, and random coils can be estimated through absorbance spectroscopy (75). This estimation is not as accurate as using X-ray crystallography or nuclear magnetic resonance (NMR; however, using absorbance spectra could be an alternative for these techniques when it is hard to

apply them (76).

In this experiment, an Agilent 8453 UV-Vis Spectrophotometer was utilized to measure the absorbance changes when 19 synthetic residues of skeletal wt myosin S2, 35 residues of cardiac wt myosin S2, and 19 residues of cardiac E930del myosin S2 were titrated with either stabilizer or destabilizer peptide. A 1 cm glass cuvette was filled with water to acquire the experiment's blank. The starting concentration of skeletal wt, cardiac wt, and cardiac E930del myosin were 216 µM in 500 µl, 50 µM in 200 µl, and 157 µM in 300 µl respectively. The skeletal wt and cardiac E 930del synthetic myosin were titrated from 150 µM stabilizer peptide stock solution, and the cardiac wt was titrated from 120 µM destabilizer peptide stock solution. The titrations continued until the ratio between the synthetic peptide to the synthetic myosin was about 1.6. The same experiment was repeated without using myosin as a control by measuring the absorbance spectra of the synthetic peptide at the same concentrations used previously. The net absorbance of wt/mutated myosin at a specific concentration was calculated by subtracting the absorbance of the synthetic peptide from the absorbance of the wt/mutated myosin with the synthetic peptide at that concentration. All the net absorbance spectra were normalized to intercept at 214 nm and plotted along with the standard random coil and alpha helical graphs from previously published data (77). The alpha helical percentage for each net myosin curve was calculated using the following equation:

$$\alpha\% = 100 - (\text{area under myosin curve} - \text{area under 100\% } \alpha \text{ coiled coil}) / (\text{area under 100\% random coil} - \text{area under 100\% } \alpha \text{ coiled coil}) \times 100\%$$

Finally, the relative concentration (peptide concentration/myosin concentration) was plotted against the calculated alpha helical percentage for each titration. The data was fitted using the WinCurveFit program using the binding helix equation.

UV absorbance spectrophotometer was utilized to determine the concentration of

peptide/protein used in different experiments depending on the absorbance spectrum at a specific wavelength using the extinction coefficient of that peptide/protein at that wavelength.

2.2.4.2 Fluorescence Anisotropy

To study protein-protein/peptide interaction, fluorescence anisotropy is an accurate experiment to study this binding depending on the changes in the anisotropy reading. The protein or peptide of interest should be conjugated with a suitable fluorophore (78). It is preferable that the fluorophore has a high extinction coefficient, high quantum yield, high stability, suitable lifetime to the type of experiment, and low photobleaching properties (79, 80). In fluorescence anisotropy, the fluorophores rotate in a solution, and a polarized light photo-selects the fluorophore with a dipole parallel to the photons field. The exited fluorophore will emit a fluorescent signal that is recorded by a detector with a polarization filter either vertically or horizontally to the polarized light. The fluorophore with a lifetime suitable to the rotational correlation time of the peptide of interest records a good anisotropy signal-to-noise reading (81, 82).

Anisotropy signal is sensitive to the molecular size and rotation of the fluorophore either alone or bound to a peptide as a complex (83). According to the following equation:

$$\text{Anisotropy } (r) = (I_{VV} - I_{VH}) / (I_{VV} + 2I_{VH})$$

where I is the fluorescence intensity, vertically I_{VV} or horizontally I_{VH} (84).

If there is a big or slowly rotating molecule, the changes in the fluorophore dipole will be slow, meaning that the difference between I_{VV} and I_{VH} is large (I_{VH} could be close to zero), resulting in an anisotropy closer to 1 or an increase in the anisotropy reading. On the other hand, if the molecule is small or fast rotating, the fluorophore dipole rotates faster increasing the I_{VH} reading, so the difference between I_{VV} and I_{VH} is narrow leading to a decrease in the anisotropy value (85). Therefore, it is important for the fluorophore to have a lifetime consistent with the

rotational correlation time of the molecules in order to detect the changes in their rotation. For molecules larger than 100 kDa, fluorophore with a long lifetime is preferable, and if the molecules are smaller than 10 kDa, a fluorophore with a shorter lifetime is preferable (79, 86).

To ensure accurate results, careful fluorophore selection with the optimal lifetime to the peptide/protein molecular weight. The experimental temperature must be controlled, high temperature decreases the rotational correlation time that decreases the anisotropy reading. Also optimal concentration from the fluorophore is required to reduce light scattering (79).

2.2.4.2.1 Fluorescence Anisotropy for Determining Molecules Binding

Fluorescence anisotropy is a precise tool that detects structural alteration when two molecules interact with each other as explained previously (87, 88). The peptide's rotation in a solution is affected by binding to the heavy myosin; this binding slows the peptides' rotation. The change in the peptide's rotation causes an increase in anisotropy reading upon peptide binding to myosin.

For this experiment, SLM Aminco Bowman II luminescence spectrometer was utilized to record the anisotropy before and after myosin addition to the fluorescently labeled anti-S2 peptide. The excitation and emission wavelengths were fixed according to the fluorophore used; 490 nm and 520 nm for FITC and 540 nm and 570 nm for TRITC. A plastic semi-micro cuvette was filled with 0.5 ml PBS to acquire the blank. Then 3 anisotropy readings were recorded using 150 nM of stabilizer or 180 nM of destabilizer in PBS. After that, 5 µl from 4.6 µg/ml (0.23 mg) of myosin was added, and 3 anisotropy readings were recorded again.

2.2.4.2.2 Fluorescence Anisotropy for Determining Molecules Binding Affinity

Molecules' binding affinity indicates the binding strength between two molecules and determines their selectivity and specificity to each other. Affinity can be expressed by the

dissociation constant (Kd) which represents the rate constant at the equilibrium, or when 50% of myosin in this case is occupied by the synthetic peptide or antibody. The unit of Kd is mole/l which is a concentration unit. When the substrate has a low Kd value, it reveals that this substrate is needed in low concentration to cause the desired effect, or it has high affinity to myosin. Contrarily, a high Kd value reveals low binding affinity or higher concentration of the substrate is needed to cause the desired effect (89, 90).

Anisotropy measurement is sensitive to any changes in the association, dissociation, cleavage, and shape of the molecules (79). Binding affinity could be calculated depending on the anisotropy and substrate concentration. Once the substrate concentrations are plotted versus the anisotropy reading, Kd is estimated from the binding graph to be the substrate concentration when half the maximum reading of anisotropy (90).

In this experiment, a spectrofluorometer with automated Glans-Thompson polarizers was utilized to record the anisotropy. A 1 cm glass cuvette was filled with a buffer composed of 50 mM of phosphate and 0.15 M of sodium chloride at pH 7. The excitation and emission wavelength were set at 490 nm and 520 nm, respectively. A 140 nM of destabilizer peptide labeled with FITC was placed in a cuvette filled with 2 ml of the buffer, and the anisotropy reading was recorded. Then the destabilizer was titrated with 9.2 µM of myosin dimer till myosin concentration reached 600 nM. The same experiment was repeated without myosin addition as a control. 120 nM of MF20-FITC and MF30-TRITC were titrated with 9.2 µM of myosin dimer until myosin concentration reached 300 nM.

The fluorescence anisotropy was plotted versus myosin concentrations and fitted using WinCurve Fit by applying the hyperbolic and sigmoidal equations:

$$Y=Bmax*x/(Kd + x)+c$$ Hyperbolic model

Y=Bottom + (Top-Bottom)/(1+(x/EC50)^Hill coefficient)) .Sigmoidal model

In fluorescence anisotropy: Y is the anisotropy at a specific concentration, x is myosin dimer concentration (nM), Bmax is the anisotropy at the maximum binding, Kd is the concentration of myosin dimer needed to achieve half-maximum binding at equilibrium, c is background signal in the absence of binding, Bottom and Top are plateaus of anisotropy at the bottom and the top respectively, EC50 is the concentration of myosin dimer when the anisotropy is halfway between Bottom and Top, Hill coefficient represents the steepness of the curve.

2.2.4.3 Total Internal Reflection Fluorescence Spectroscopy (TIRFS)

Applying the properties of the light for studying the molecular interaction is considered a successful method of detecting molecule binding. In this technique, the light excites the fluorophore bound on a specific surface. The media that the light passes through and the angle of the surface where the light is totally reflected are determined by Snell's law:

$n_i \sin\Theta_i = n_r \sin\Theta_r$

where n is the refractive index, Θ is the angle of incidence i, or refraction r (95).

A glass coverslip was cut and glued vertically inside a plastic cuvette at 25º calculated according to the above equation. The glued coverslip divided the cuvette into 2 chambers A and B (Figure 7). Glycerol with a refractive index equals 1.47 was chosen for the light to pass through without diffraction in chamber B, and PBS at pH 7 for chamber A, which has a lower refractive index (1.33) than glycerol. When the light travels from the higher to lower refractive index media with 25º surface in between, it is totally reflected from the coverslip at this specific angle (91). The coverslip was coated with 0.2% nitrocellulose in amyl acetate on the side facing chamber A and left to dry. Then 100 µl of 9.7 µg/ml of myosin was distributed on the nitrocellulose followed by washing with 5% non-fat dried milk (protein). This washing blocked unattached nitrocellulose

with myosin from binding to the synthetic peptide/antibody during the titration. The coated side of the chamber was filled with 0.6 ml of PBS, and the other chamber was filled with glycerol. The excitation and emission lights were fixed according to the fluorophore used. The excitation beam passed through the cuvette and continued straight inside the glycerol chamber until it hit the coverslip and was totally reflected. The emission signal represented the binding of the conjugated peptide/antibody to the myosin fixed on the coverslip (the free conjugated peptide/antibody in the buffer was not excited). The myosin bound to the coverslip was titrated with different concentrations of conjugated peptide/antibody, and the emission signal was recorded at each titration. The titration continued till reaching saturation.

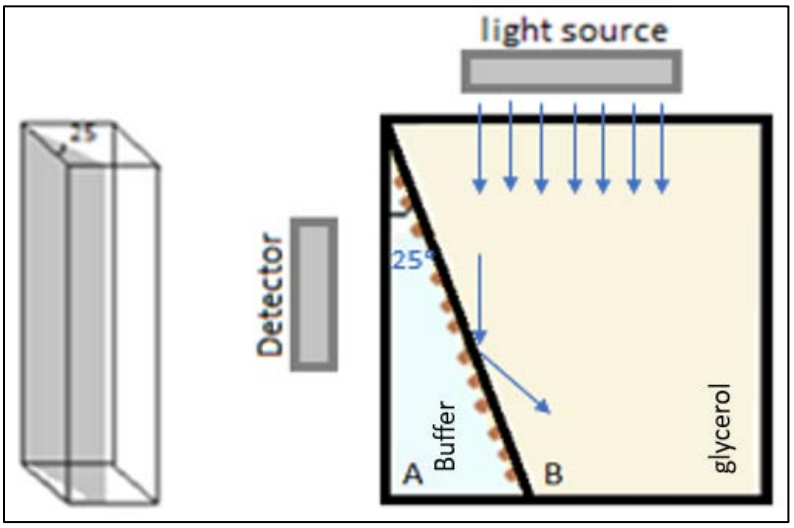

Figure 7: Cuvette design used in TIRFS.

The glass coverslip was cut and glued at 25º inside the cuvette forming 2 chambers. Chamber A was smaller and filled with the buffer. Chamber B was larger and filled with glycerol. The light excited the conjugated peptide/antibody that was bound to the myosin on the coverslip. The blue arrows illustrate the light path.

The same experiment was repeated without fixing myosin on the coverslip as a control to detect any non-specific binding. The nitrocellulose in the control experiment was blocked with 5% non-fat milk and then was titrated with the same concentrations of the conjugated peptide/antibody. The signals collected from the control were subtracted from the corresponding experiment signals to calculate the net signal of the peptide/antibody when it is bound to myosin.

The fluorescence signal versus anti-myosin concentrations were fitted using GraphPad Prism 8.1.2 program by applying the hyperbolic and the sigmoidal equations explained in 2.2.4.2 except that:

Y is the fluorescence signal at specific concentration, x is anti-myosin concentration (nM), Bmax is the fluorescence signal at the maximum binding, Kd is the concentration of anti-myosin needed to achieve half- maximum binding at equilibrium, c is background signal in the absence of binding, Bottom and Top are plateaus of fluorescence signal at the bottom and the top respectively, EC50 is the concentration of anti-myosin when the fluorescence signal is halfway between Bottom and Top, Hill coefficient represents the steepness of the curve.

The binding graphs were used to calculate peptide/antibody affinity to myosin and predict the binding mechanism. In addition to that, binding cooperativity was inspected using the concerted and sequential models. The fraction bound, which is defined as the number of myosin S2 coiled-coil binding sites that are occupied by antibody/peptide with a maximum value of 2, was calculated from the binding graphs depending on the Bmax from the sigmoidal equation, and it was plotted against antibody/peptide concentrations. The graphs were fitted with the concerted and sequential equations below to detect if there is positive cooperative binding between the antibody/peptide and myosin:

Fraction bound = 2*a*[A](1+a*[A])/((1/b)+(1+a*[A])^2) Concerted model

where 2 is the number of binding sites, a is the microscopic binding constant, [A] is the antibody/peptide concentration, b=[T]/[R], T state is the folded myosin no antibody/peptide bound state and R state is the unfolded myosin when antibody/peptide in the bound state. If b is significantly less than 1, it means positive cooperativity (97).

Fraction bound = ([A] + 2*b*[A]^2)/((1/a)+2*[A]+b*[A]^2) sequential model

where 2 is the number of binding sites, [A] is the antibody/peptide concentration, a is the association binding constant of the first myosin strand, b is the association binding constant of the second myosin strand. If b is significantly greater than a, it means positive cooperativity (98, 99)

2.2.4.4 Competitive TIRF Spectroscopy

In this technique, a modification for the TIRFS experiment explained above was undertaken to allow measuring the binding affinity of the destabilizer peptide in a solution. A modified plastic cuvette, as shown in (Figure 7) was used in this experiment. The coverslip was treated with 0.2% nitrocellulose in amyl acetate on the side facing chamber A and left to dry. Then 100 µl of 9.7 µg/ml of myosin was distributed on the nitrocellulose, followed by washing with 5% non-fat dried milk (protein). The immobilized myosin on the coverslip was titrated with the destabilizer peptide till reaching a concentration close to the Kd, and the signal was recorded. After that, titration with myosin was undertaken, and the signal was recorded after each addition. The same experiment was repeated using 40, 80, and 100 nM of the destabilizer peptide. The fluorescence signal versus myosin concentration were plotted and fitted using the following equation:

y= bottom+ (top-bottom)/(1+(x/IC50)^Hill)

y is the fluorescent signal at a specific concentration, x is the myosin concentration (nM), bottom and top are plateaus of fluorescence signal at the bottom and top respectively, IC50 is the concentration of myosin at 50% of the signal reduced, Hill is the steepness of the curve.

IC50 was calculated at each concentration and plotted against the peptide concentration, and the data was fitted using the linear equation. The destabilizer Kd was estimated depending on the following equation where peptide concentration [L] is close to zero, then Ki= Kd=IC50:

Ki=IC50/(1+([L]/Kd)

Ki is the inhibition constant, IC50 is 50% of the maximum signal, [L] is the destabilizer peptide concentration, Kd is the dissociation constant.

2.2.5 Microscopy

Microscopy is a useful tool that magnifies objects not seen by the naked eye. It was used in this research to detect the exact binding site of anti-S2 peptide/antibody on myosin when conjugated to a probe, and it was used to detect the competition between anti-S2 and MyBPC as both bind to myosin S2. Microscopic images can reveal possible interaction between the peptides and titin.

2.2.5.1 Regular Confocal Images

Skeletal rabbit myofibrils were washed with PBS twice to get rid of the glycerol storage liquid. Then they were incubated overnight with conjugated antibody/peptide ~0.7 µM at 4 ºC. Labeled myofibrils were distributed on a microscopic slide, then 50 µl of 10% ascorbic acid and 50 µl of 50% glycerol were added, the coverslip was sealed with transparent nail polish and left to dry. The images were acquired using the Yokogawa spinning disk confocal microscope, LCI Plan-Neofluar 63X 1.3 NA glycerol immersed lens or 40X 1.3 NA water immersed lens and 1.6X tube lens. Argon Laser 488-35 and/or 568-45 lasers were used in acquiring the images with T405/488/568/647 filter. All the images were processed using ImageJ processing software developed by the National Institutes of Health (NIH).

2.2.5.2 Expansion Microscopy

The new arising expansion microscopy technique uses the confocal or light microscope for acquiring super-resolution images by specimen modification rather than microscope improvement. It improves specimen resolution and overcomes the diffraction limit of the microscope by the

physical expansion of the specimen in all dimensions. The fluorophores within a specimen anchor to a swellable gel; therefore, when the gel expands, the fluorophores move apart in all dimensions preserving the specimen detail (92, 93).

Skeletal rabbit or cardiac mouse myofibrils were washed with PBS twice to get rid of the glycerol storage liquid; then they were incubated with conjugated antibody or anti-S2 peptide (concentration range from 700 nM to 20 μM depending on the tissue) at 4 °C for 3 nights. Myofibrils were fixed with 0.1% glutaraldehyde in PBS for 1 hour at room temperature (94), followed by 3 washes with PBS. Fixed myofibrils were incubated in monomer solution (Table 1) for 30 min at 4 ºC prior to gelation. Then, myofibrils were spread on a specially constructed chamber from a microscopic slide, and coverslips were cut on the sides to create a chamber. A polymer gel solution composed of 188 μl of fresh monomer, 4 μl of 0.5% TEMPO (2,2,6,6-Tetramethylpiperidin-1-yl)oxyl or (2,2,6,6-tetramethylpiperidin-1-yl)oxidanyl, 4 μl of 10% of TEMED accelerator, and 4 μl of 10% APS initiator fresh prepared. The polymer was poured over the myofibril, and a coverslip was placed over the chamber and left to polymerize for 3 hours at room temperature. After incubation, the coverslip over the gel chamber was taken off, and the gel was placed in a digestion buffer (Table 2) containing 8 units/ml of proteinase K (1:100, final concentration) at 39 ºC overnight. The next day the gel was removed from the digestion buffer and washed 3-5 times with distilled water for 20 min each wash. The gel was cut and placed between 2 coverslips coated with polylysine to immobilize the gel and prevent drift during imaging. Figure 8 summarizes the expansion protocol. The gel was imaged using the spinning disk confocal microscope and Zeiss LMM 710 confocal scanning microscope, and the images were processed using ImageJ.

Table 1: Components of monomer solution used for expansion microscopy

Components	Amount (ml)	Final concentration*
Sodium acrylate	2.25	8.6
Acrylamide	0.5	2.5
N,N'-Methylenebisacrylamide	0.75	0.15
Sodium chloride	4	11.7
PBS	1	1X
Water	0.9	-
Total	9.4	-

*All concentrations in g/100ml except PBS

Table 2: Components of digestion buffer

Components	Working concentration
TRIS *	50mM
EDTA**	1mM
Urea	4M
Calcium chloride	2mM
Guanidine HCL	0.8M
Triton X-100	0.5%

* Tris(hydroxymethyl)aminomethane
** EDTA Ethylenediaminetetraacetic acid

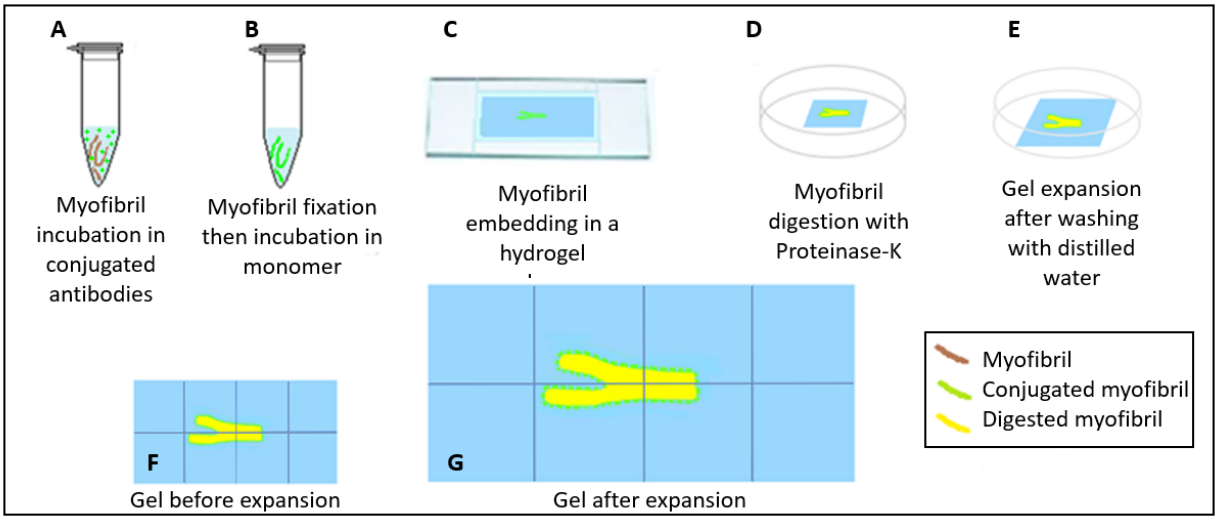

Figure 8: **Expansion microscopy protocol.**

A: Myofibril previously prepared was incubated in conjugated antibody/peptide. B: Myofibril was fixed with glutaraldehyde, then prepared for fluorophore crosslinking with the gel by incubation in the monomer.

C: Myofibril was embedded within a hydrogel. Fluorophores crosslinked with the gel. D: Myofibril was digested by soaking the gel in a digestion buffer with Proteinase-K. E: Gel expanded after washing with distilled water. F: Gel size before expansion. G: Gel size after expansion in all dimensions. The crosslinked fluorophores with the gel retained attached to the gel after the expansion.

The steps explained above were repeated using skeletal rabbit myofibrils alone without any conjugated peptide/antibody as a control for this experiment. Also, the myofibrils were incubated in single, double, or triple reagent/s at the same time as following:

Single labeling: MF30, MF20, polyclonal, stabilizer peptide, destabilizer peptide, α-MyBPC1, anti-titin.

Dual labeling: MF30 and MF20; stabilizer and MF20; destabilizer and MF30; stabilizer and destabilizer peptides; anti-titin and MF30; anti-titin and Stabilizer; anti-titin and destabilizer

Triple labeling: MF30, MF20, and polyclonal.

2.2.5.3 MyBPC Knockout Tissue from Live Animals

The cardiac tissues were extracted from wild type and MyBPC knocked-out hearts from live mice prepared in Dr. Richard L. Moss's laboratory at Washington State University. The preparation was based on the techniques described by Harris et al., 2002 (62), and the solution recipes were calculated and prepared as (Godt and Lindley, 1982) protocol (63).

2.2.6 Live Animal Model Experiment

In an attempt to check if the anti-S2 peptides with the aid of tannic acid can reach cardiac myocytes and interfere with heart contraction, Dr. Douglas Root's laboratory collaborated with Dr. Kenneth S. Campbell from the University of Kentucky to inject live mice with 0.1 mM or 1 mM of tannic acid alone, destabilizer-TA, stabilizer-TA, labeled destabilizer-TA, or labeled stabilizer-TA. The physiological functions of the heart: cardiac output, stroke volume, and heart rate, were carefully monitored during the first 24, 48 hours, and 7 days of the injection.

2.2.6.1 Mouse Heart Sectioning

Once the hearts were excised, some were flash-frozen immediately with liquid nitrogen; others were washed and stored in a fixative solution. The hearts were sectioned using Leica CM1950 Cryostat. First, the heart was attached to the cryostat disk after precooling and covered with the Optimal Cutting Temperature compound (O.P.T.). The heart was cooled down to -20 ºC inside the cryostat, and then it was seated and oriented in the optimal direction for the cutting. The trimming mode was activated, and the slice thickness was set to 1 micron. Manual trimming was performed, and each slice was placed on a microscopic slide. The slices on the microscopic slides were fixed by 2.5% paraformaldehyde in PBS, then stained with 50 µl of Fluoromount G with DAPI for nucleus visualization. Lastly, the slides were covered with coverslips, sealed with transparent nail polish, and stored in a humidified chamber till imaging.

2.2.6.2 Mouse Heart Slices Imaging

The slices were imaged using the EC Plan neofluar objective with a Yokagawa spinning disk confocal microscope. The destabilizer peptide-FITC heart was imaged using the epi-ultraviolet with a blue filter and the epi-blue with a green filter; the exposure time was 3 and 0.5 seconds, respectively. For the stabilizer peptide-TRITC heart, the slices were imaged using the epi-green with a red filter; the exposure time was 0.03 seconds. Every slice was tiled and corrected for the exposure time and background, then stitched using ImageJ. Some slices were imaged using the 3 filters (blue, green, and red) to detect the autofluorescence and the bleed through between the channels.

Slices from the mid-section of the heart were imaged using a 63X oil objective lens in Zeiss LMM 710 confocal scanning microscope using Airyscan to determine the exact binding sites of anti-S2 peptides within the heart tissues.

2.2.6.3 Sarcomere Length Measuring in Mouse Cardiomyocyte

The hearts of the three mice injected with tannic acid alone, labeled peptides-TA, and unlabeled peptides-TA were imaged using SPOT DIC in a spinning disk confocal microscope using the water immersion Apo-C 40X 1.6X NA. Around (110 -210) sarcomere lengths were measured from each heart tissue using ImageJ and averaged to calculate the sarcomere length for each patch.

2.2.7 Statistical Data Analysis

The fluorescence anisotropy binding graphs were fitted by applying the hyperbolic and sigmoidal equations mentioned in section 2.2.4.2 using WinCurveFit 1.1.3 program (n = 3). The student's t-test was applied to calculate p-values through Microsoft Excel. P-value > 0.05 indicated not significant difference between the hyperbolic and the sigmoidal fitting. Therefore, this binding assay could not predict the binding mechanism of anti-S2 peptides and antibodies to myosin.

The p-values in the TIRFS experiment were calculated in GraphPad Prism 7 software using non-linear regression F-test. When the p-value was less than 0.05, the sigmoidal binding graph significantly differed from the hyperbolic graph. The correlation coefficient determined the favorable binding mechanism; the fitting with the higher correlation coefficient (R^2) was considered more favorable.

In TIRFS, A hill slope of 1 indicates independent binding; if it is greater than 1, it indicates positive cooperativity, which means binding of one antibody/peptide to myosin facilitates binding another antibody/peptide. A slope lower than 1 indicates negative cooperativity (96). Z-test in Excel sheet was applied to the binding graphs' mean and standard deviation to predict binding cooperativity. The p-values for MF30 and destabilizer were less than 0.05, meaning that their hill slopes were significantly different from 1, indicating positive cooperative binding; however, MF20

p-value was > 0.05, which indicated no significant difference between the hill slope and 1 value supporting a simple binding mechanism.

The fluorescent intensity graphs of the stained sarcomeres from the expanded microscopy images were compared using the Student's t-test. P-value < 0.05 indicated a significant difference in the labeling pattern between the compared sarcomeres. However, a p-value > 0.05 suggested that the staining pattern was similar in the compared sarcomeres.

The normal distribution of the measured sarcomere lengths from live animal heart tissue was measured using the Chi-squared test (n of mouse = 1, n of sarcomeres 160-184). The p-value from the stabilizer peptide tissue was higher than 0.05 indicating a normal distribution of the sarcomere lengths. The sarcomere lengths from the control and the destabilizer peptide cardiac tissue did not show normal distribution, as p-values were less than 0.05.

The error bars in the graphs of this research represent the standard deviation of the collected data.

CHAPTER 3

SPECTROSCOPIC ASSAYS RESULTS

3.1 Determining Anti-S2 Peptide Binding to Myosin by Fluorescence Anisotropy

Fluorescence anisotropy is an accurate tool that can predict the reaction between 2 molecules based on the change in anisotropy reading before and after the reaction (100). The fluorescently labeled molecules' rotation in a solution will be restricted once they react to another molecule; the anisotropy value changes according to the molecular weight of the reactants as a complex and the binding site flexibility (88).

Myosin dimer has a molecular weight of around 223 kDa (7, 101); however, the stabilizer and destabilizer peptides' molecular weights are 2158 and 2322 Da, respectively. The substantial disparity in the molecular weight between the myosin and the peptides predicts if the labeled peptide binds to myosin or not. The binding of the peptide to the heavy myosin leads to a decrease in its rotation in the buffer, increasing the observed anisotropy reading (79, 84).

To verify the binding of the destabilizer and stabilizer peptides bind to myosin, the anisotropy reading of the conjugated peptide was initially measured. Subsequently, myosin dimer was introduced, and the anisotropy reading was recorded once more. When the small peptide bound to myosin, the rotational motion of the peptide was impeded by the presence of the heavy myosin, resulting in a deceleration of its rotation. This binding was reflected as an increase in anisotropy reading for both peptides; the anisotropy value increased from 0.0069 to 0.01 when myosin was added to the labeled destabilizer peptide and from 0.00889 to 0.013 when myosin was added to the stabilizer peptide. The significant increase in anisotropy value before and after adding

myosin indicates myosin binding to the peptides (p-values calculated from Student's t-test are 0.046 and 0.03 for destabilizer and stabilizer peptides, respectively) (Figure 9).

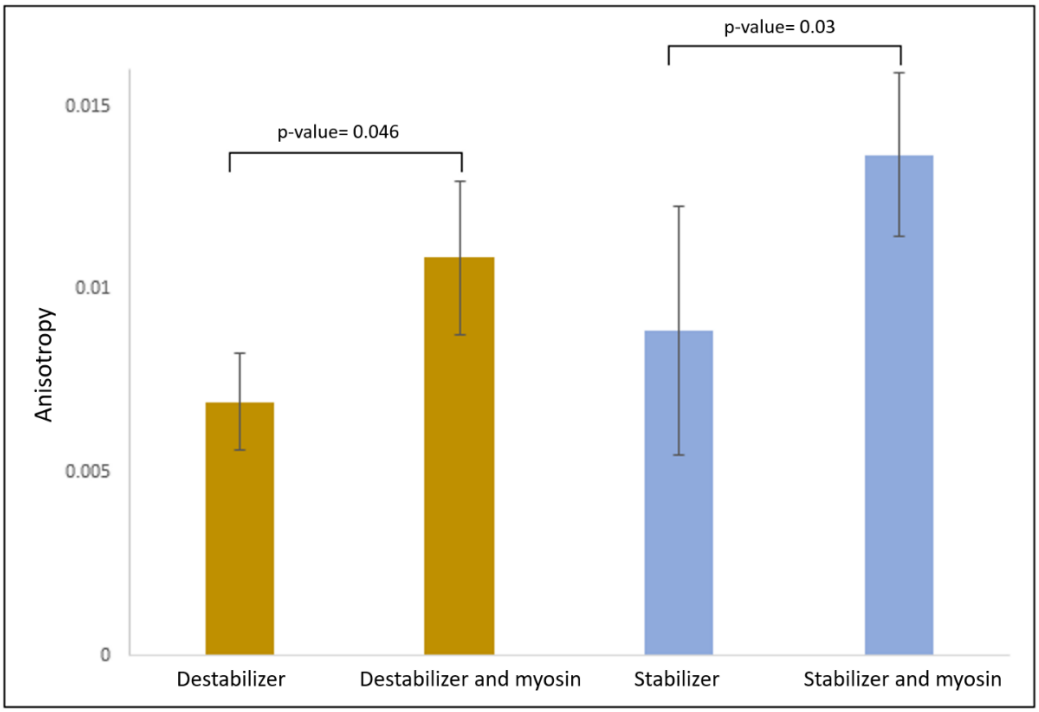

Figure 9: **Anti-S2 peptides anisotropy before and after adding myosin.**

Anisotropy increased after the addition of myosin in both the destabilizer and stabilizer peptide confirming the binding between the peptides and myosin ($p < 0.05$ from Student's t-test).

3.2 Wild Type and E930del Myosin S2 Helicities

The function of myosin S2, which plays a crucial role in muscle contraction, can be influenced by alternation in its coiled-coil structure (4). The interaction between myosin S2 and anti-S2 peptides can potentially affect the α-helical coiled-coil within this region, consequently interfering with muscle contraction.

3.2.1 Stabilizer Peptide Improved Alpha-Helical Content of Wild Type Skeletal Myosin

To identify alternations in the helical content of the synthetic myosin upon adding a stabilizer peptide, UV-Vis Spectrophotometer was employed to measure the absorbance spectra of myosin-stabilizer complexes at various concentrations. In this experiment, synthetic myosin in

water was titrated with different concentrations of stabilizer peptide until saturation was reached. The absorbance spectrum at each concentration was recorded and subtracted from the absorbance spectrum of the stabilizer peptide alone at that concentration. All the net absorbance spectra were plotted along with the 100% alpha-helical and 100% random coil graphs from the literature (77). The alpha-helical percentages were calculated between 190-197 nm and plotted versus the stabilizer/myosin concentrations ratio. It was found that the stabilizer peptide improved wild type skeletal myosin helicity by increasing the alpha-helical content by 24.2 ± 7.8% at a low concentration of the peptide, and it reached saturation when the ratio of the stabilizer to myosin monomer was 0.5 ± 0.1. The ratio implies that 1 stabilizer peptide binds to one myosin dimer probably by wrapping around the dimer and stabilizing it (Figure 10).

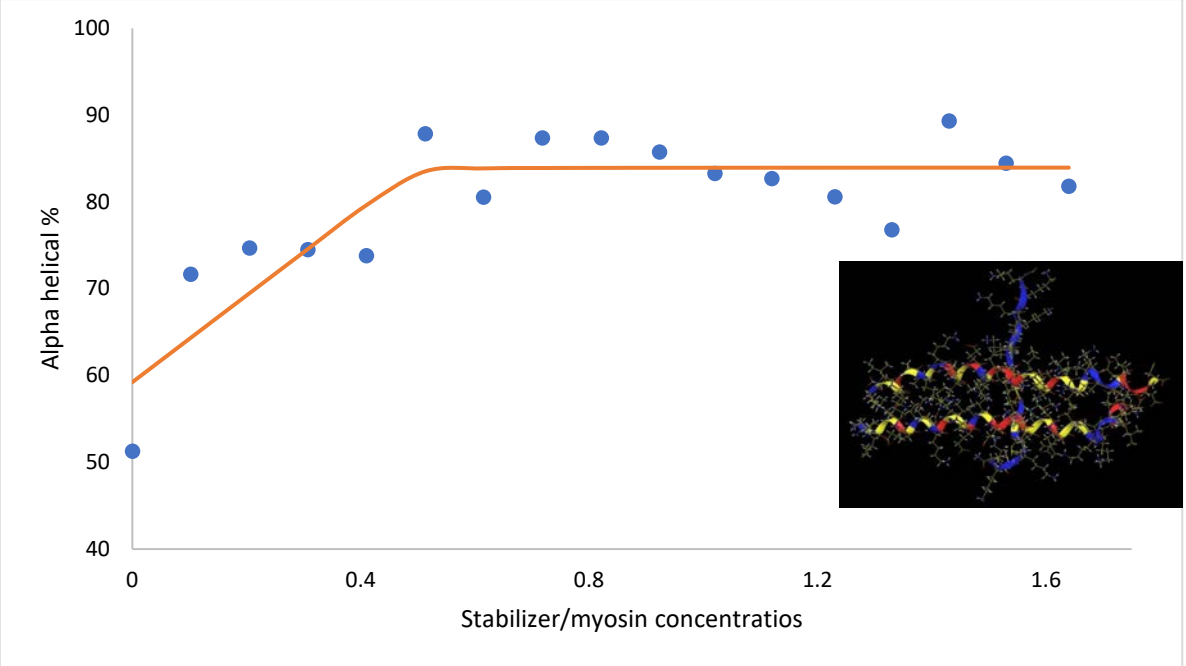

Figure 10: **Alpha-helical percentages graph of the stabilizer peptide in wild type skeletal myosin.**

The alpha-helical percentage increased by 24.2 ±7.8% at low concentrations of the peptide. The molecular model to the right from Qadan, M.M. 2021 (102) illustrates that one stabilizer peptide wrapping around synthetic wt myosin to stabilize it and improve its helicity.

3.2.2 Stabilizer Peptide Improved Alpha-Helical Content of E930del Cardiac Myosin

To investigate the impact of the stabilizer peptide on mutated myosin, the same experimental procedure described earlier was applied to synthetic E930del cardiac myosin. The results revealed that the stabilizer peptide enhanced the helicity of the mutated myosin helicity by approximately 9.3 ± 3%, which was significantly lower than the improvement observed in wild type myosin (p-value <0.001 from Student's t-test). Meanwhile, a higher concentration of the stabilizer peptide was required to reach saturation with myosin, approximately 1.3 ± 0.3. Based on this ratio, it was estimated that two stabilizer peptides were necessary to wrap around the mutated myosin dimer, thereby stabilizing it and enhancing its helicity (Figure 11).

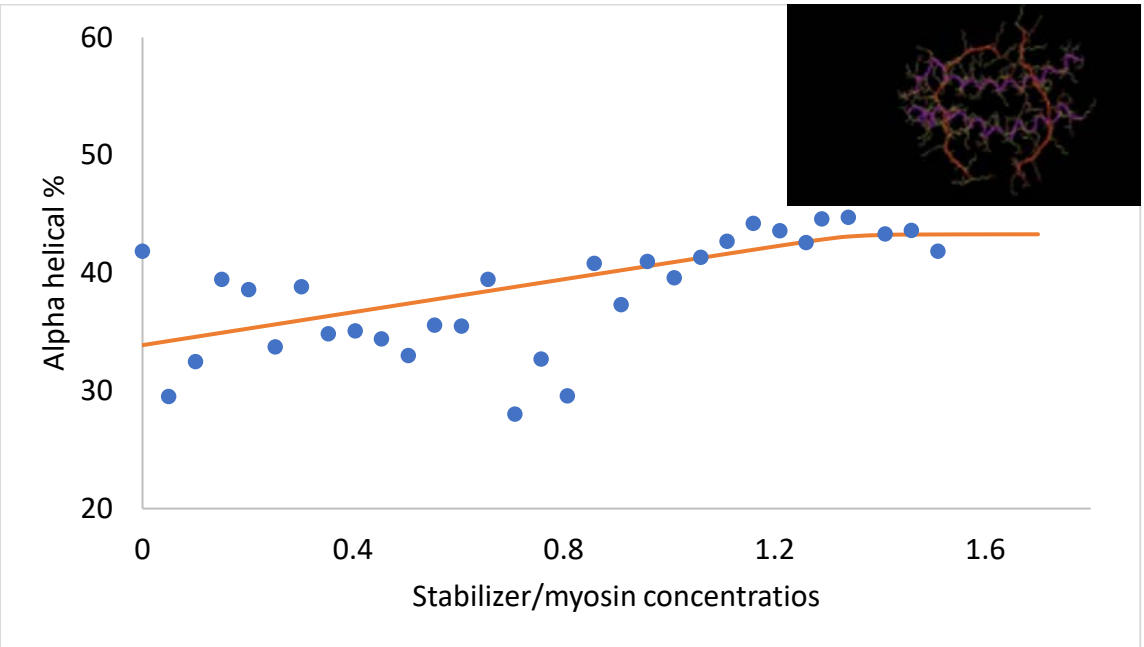

Figure 11: **Alpha-helical percentages graph of the stabilizer peptide in E930del cardiac myosin.**

The alpha-helical percentage increased by increasing the stabilizer peptide concentration by 9.3 ± 3% and reached saturation when the stabilizer to myosin ratio was 1.3 ± 0.3. The molecular model to the right from Qadan, M.M. 2021 (102) illustrates that two stabilizer peptides are wrapping around synthetic E930del myosin to stabilize it and improve its helicity.

3.2.3 Destabilizer Peptide Decreased Alpha-Helical Content in Cardiac Myosin

Through titration of synthetic cardiac myosin with varying concentrations of destabilizer

peptide, it was observed that the peptide caused a decrease in the alpha-helical content of cardiac myosin by 14.2 ± 5.5%. This reduction can be attributed to the disruption of the coiled-coil structure of myosin S2, which facilitates the binding of the peptide. Saturation of the cardiac myosin with the peptide occurred at a ratio of approximately 1.1 ± 0.28 peptide molecule per myosin monomer. This ratio suggests that two peptides are required to bind to the myosin dimer, causing the coiled-coil structure to unravel and rendering the myosin unstable (Figure 12). The effect of the destabilizer peptide on myosin helicity is significantly different from the stabilizer peptide (p-value <0.001 from Student's t-test), as it induces the unzipping of the coiled-coil structure of myosin upon binding, thereby reducing the dimer helicity.

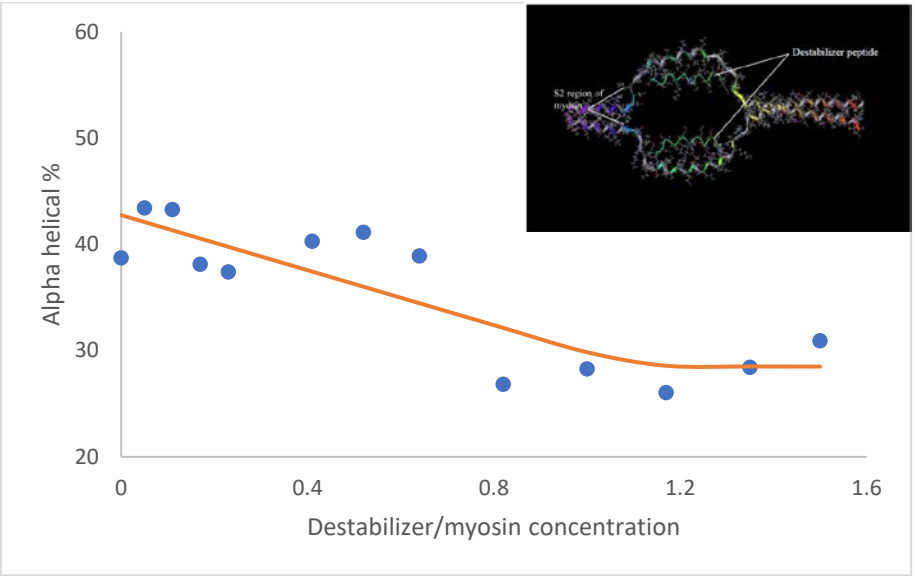

Figure 12: **Alpha-helical percentages graph of the destabilizer peptide in cardiac myosin.**

The alpha-helical percentage decreased by increasing the destabilizer peptide concentration by 14.2 ± 5.5% and reached saturation when the destabilizer to myosin ratio was 1.1. The molecular model to the right from Qadan, M.M. 2021 (102) illustrates that two destabilizer peptides unzip the synthetic cardiac myosin dimer to destabilize it and reduce its helicity.

3.3 Myosin S2 Affinity to Anti S2 Peptide/Antibody

Measuring the binding affinity of the anti-S2 peptides to myosin opens the doors to appointing the optimal concentration that should be tested in myofibril tissue and live animal

model trials to provoke the intended effect. The anti-S2 peptide/antibody affinity was measured using 3 different fluorescence spectroscopic experiments. It was calculated depending on fluorescence anisotropy, total internal reflectance spectroscopy (TIRFS), or competitive TIRFS.

In fluorescence anisotropy, Kd was measured based on an in-solution binding assay (90). Conjugated anti-S2 peptide/antibody at specific concentrations was titrated with myosin dimer till saturation. Anisotropy reading was recorded at each concentration, and the background was subtracted (Figure 13). Anisotropy readings against myosin concentrations were plotted and fitted using the hyperbolic and sigmoidal equations that support the simple and the positive cooperative binding models, respectively (103). This experiment was applied to MF20, MF30, and destabilizer peptides (Figure 14). There was a significant light scattering with the stabilizer peptide producing faulty readings, which was measured with different experiments (TIRFS).

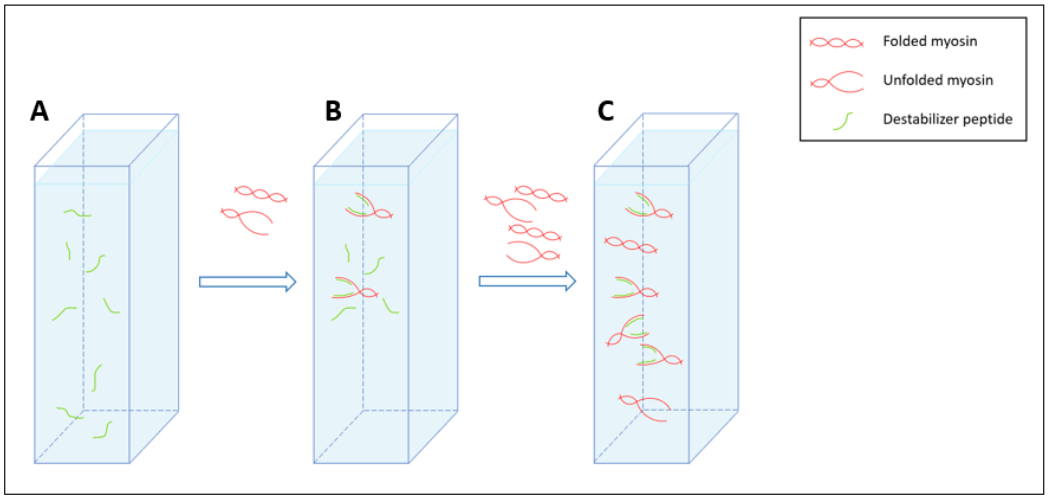

Figure 13: **Diagram explains anisotropy experiment to calculate molecule affinity in solution.**

A: Labeled destabilizer peptide was placed in a buffer in a glass cuvette, and the anisotropy reading was recorded. B: The destabilizer peptide was titrated with myosin dimer, and the anisotropy reading was recorded. C: Adding more myosin dimer till all destabilizer peptides are bound to myosin. Extra unbound folded myosin stayed in equilibrium with the unfolded myosin.

Regarding the positive cooperative binding model, MF20 has the highest affinity to myosin dimer with a Kd equal 100 ± 42 nM, MF30 Kd is 146 ± 110 nM which has a high affinity to

myosin, and the destabilizer peptide also has a high affinity to myosin with a Kd value equals 152 ± 4.5 nM. There is no significant difference between the simple and positive cooperative binding models in this experiment (p-value > 0.05 calculated from Student's t-test), as listed in Table 3. The equilibrium between the folded and unfolded states of myosin dimer did not change; when the ani-S2 peptide or antibody was titrated with myosin dimer, there was no shift in the equilibrium. The stability of equilibrium will not show a difference between the hyperbolic and sigmoidal fittings, as proved by the statistic between these two models.

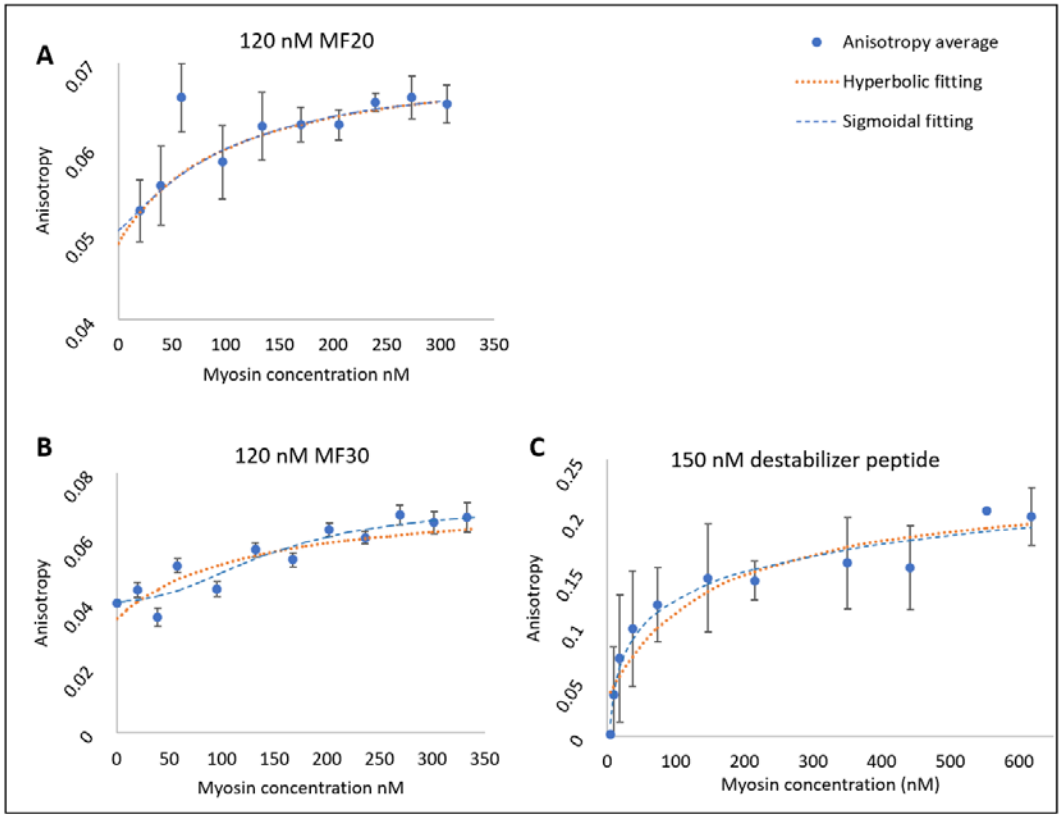

Figure 14: **Anti-S2 peptide/antibody fluorescence anisotropy in solution binding assay to measure the affinity.**

A: 120 nM of conjugated MF20 was titrated with myosin, calculated Kd equals 100 ± 42 nM in the positive cooperative binding model and 101 ± 50 nM in the simple binding model (p-value = 0.12 from t-test). B: 120 nM of conjugated MF30 was titrated with myosin, calculated Kd equals 146 ± 110 nM in the positive cooperative binding model and 121 ± 144 nM in the simple binding model (p-value =0.52 from t-test). C: 140 nM of conjugated destabilizer peptide was titrated with myosin; calculated Kd equals 152 ± 4.5E4 nM in the positive cooperative binding model and 153.2 ± 104 nM in the simple binding model (p-value =0.99 from t-test). MF20, MF30, and destabilizer peptide had high affinity to myosin dimer with no significant difference between the hyperbolic and sigmoidal fitting.

Table 3: Anti-S2 peptide/antibody Kd measured from fluorescence anisotropy

Reagent (Fitting model)	Kd (nM) of myosin dimer	Hill slope	R^2	n	p-value
MF20 (120 nM) (Sigmoidal)	100 ± 42	1.2 ± 1.0	0.96	3	0.12
MF20 (120 nM) (Hyperbolic)	101 ± 50	-	0.96	3	
MF30 (120 nM) (Sigmoidal)	146 ± 110	2.3 ± 2.5	0.82	3	0.52
MF30 (120 nM) (Hyperbolic)	121 ± 144	-	0.74	3	
Destabilizer (150 nM) (Sigmoidal)	152 ± 4.5	0.045 ± 6.1	0.95	3	0.99
Destabilizer (150 nM) (Hyperbolic)	153.2 ± 104	-	0.89	3	

R^2 is the coefficient of determination. n is the number of experiment repetitions. p-values calculated from the Student t-test to compare sigmoidal versus hyperbolic fittings.

TIRFS measured the binding affinity based on a solid-phase binding assay. A specifically designed cuvette with a coverslip glued inside at 25° angle, the coverslip was coated with myosin dimer from one side (Figure 7) and titrated with different concentrations of conjugated MF20/MF30/stabilizer/destabilizer peptide. The conjugated peptide/antibody in the buffer bound to the unfolded myosin dimer on the coverslip at both strands of myosin at the same time. As a result, the unbound folded myosin transformed into the unfolded state to stay in equilibrium with the folded state. The myosin-peptide/antibody complex stabilizes the unbound unfolded myosin. More titrations result in more binding to the unfolded myosin and more shifting in the unbound folded myosin toward the unfolded state to maintain the equilibrium. Then titration continued until myosin was saturated with the peptide/antibody, and the signal was recorded at each titration (Figure 15). Fluorescence signals versus peptide/antibody concentrations were plotted and fitted using the hyperbolic and sigmoidal equations (Figure 16).

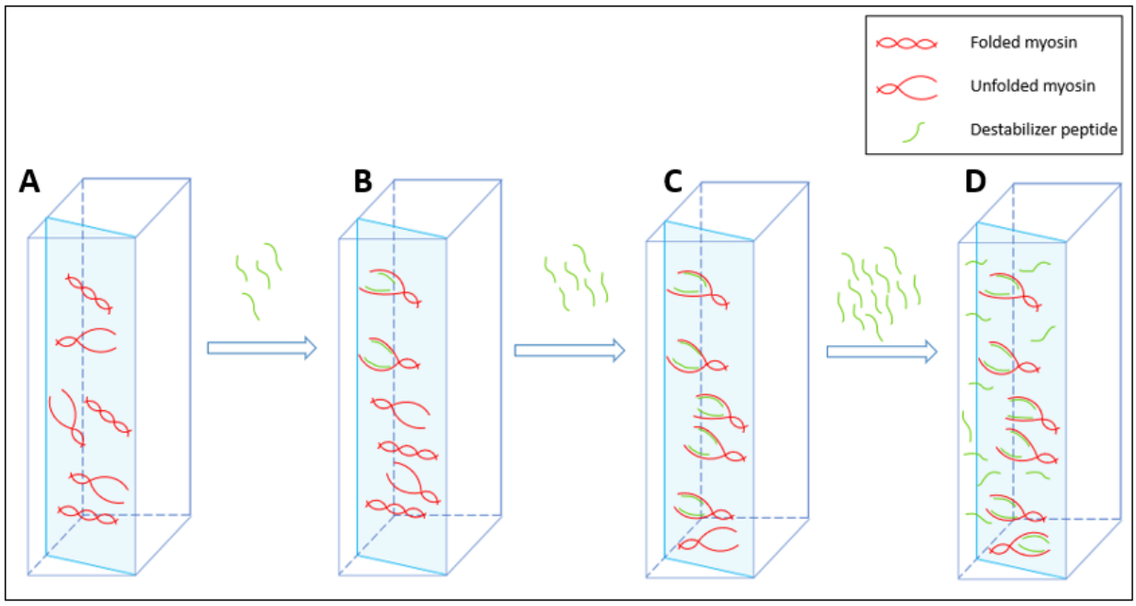

Figure 15: **TIRFS diagram for measuring anti-S2 peptide/ antibody affinity.**

A: Myosin dimers were immobilized on a treated coverslip with 0.2% nitrocellulose. B: Myosin dimers were titrated with labeled destabilizer peptide. Peptide caused unzipping to myosin dimer and bound to the unfolded dimer with high affinity. The signal that was recorded indicated the binding between the myosin dimer and the peptide on the coverslip. C: Increasing the concentration of the labeled destabilizer allowed more of the dimers to bind to the peptide and more shifting of the unbound myosin to the unfolded state to stay in equilibrium with the folded myosin. D: At higher concentrations of the peptide, when all the myosin dimers were saturated, the excess of the peptide stayed in the buffer and did not affect the recorded signal.

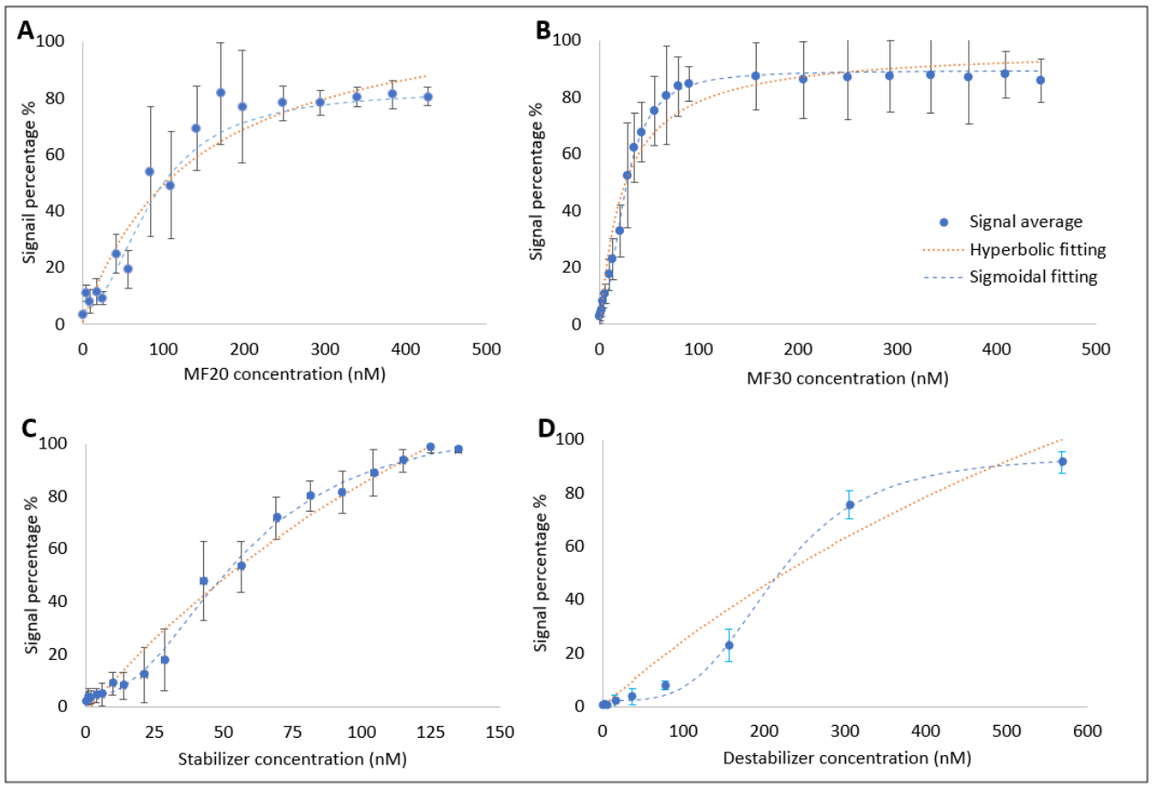

Figure 16: **Anti-S2 peptide/antibody solid-phase binding assay graphs to measure affinity from TIRFS.**

Immobilized myosin dimer on 25° coverslip inside cuvette was titrated with MF20 (A), MF30 (B), stabilizer peptide (C), and destabilizer peptide (D) till saturation. Fluorescence signal percentages were fitted using sigmoidal and hyperbolic equations. (Sigmoidal versus hyperbolic models p-values <0.05 in MF30 and destabilizer, and >0.05 in MF20 and stabilizer peptide calculated from non-linear regression F-test).

According to the sigmoidal fitting, the Kds were 86.4 ±13 nM for MF20, 26.1 ± 0.7 nM for MF30, 55 ± 3.3 nM for stabilizer, and 214 ± 9.18 nM for destabilizer. This solid-phase binding assay indicated the positive cooperative binding mechanism of MF30, stabilizer, and destabilizer peptides to myosin. According to the correlation coefficient R^2 from (Table 4), the sigmoidal fitting was the preferable model, and it significantly differed from the hyperbolic model in MF30 and destabilizer peptide (p-values calculated from non-linear regression F-test are 0.003 and <0.0001, respectively). The hill slope indicates positive cooperativity, if it is greater than 1, in which case MF30, stabilizer, and destabilizer hill slopes are greater than 1 and significantly differ from 1 (p-values < 0.05 from Z-test), except for MF20, the hill slope does not differ significantly from 1 (p-value=0.066 from Z-test) This conclusion supports the idea that MF30 and destabilizer peptide bind cooperatively to myosin dimer and stabilize the unfolded myosin dimer by shifting more folded myosin into the unfolded state to maintain equilibrium. However, the stabilizer peptide and MF20 did not significantly differ between the simple and cooperative binding models, even though the positive cooperativity model was preferable.

Table 4: Anti-S2 peptide/antibody Kd measured from TIRFS

Reagent (Fitting model)	Kd (nM)	Hill slope	R^2	n	p-value
MF20 (Sigmoidal)	86.4 ± 13	2.0 ± 0.63	0.94	9	0.14
MF20 (Hyperbolic)	137 ± 52	-	0.93	9	
MF30 (Sigmoidal)	26.1 ± 0.7	2.2 ± 0.16	0.99	7	0.003
MF30 (Hyperbolic)	23 ± 4	-	0.96	7	
Stabilizer (Sigmoidal)	55 ± 3.3	2.3 ± 0.25	0.99	5	0.53
Stabilizer (Hyperbolic)	239 ± 102	-	0.98	5	
Destabilizer (Sigmoidal)	214 ± 9.18	3.7 ± 0.41	0.99	3	< 0.0001
Destabilizer (Hyperbolic)	1078 ± 1148	-	0.95	3	

R^2 is the coefficient of determination. n is the number of experiment repetitions. p-values calculated from non-linear regression F-test to compare sigmoidal versus hyperbolic fittings.

The concerted model fitting (104) supported the positive cooperative binding

mechanism in MF30 and anti-S2 peptides. MF30 and destabilizer peptide unfolded state (myosin-antibody complex) is higher than the folded state (no binding) from the fraction bound graph, and with stabilizer peptide, the folded (stabilizer-myosin complex) is higher than the unfolded state (no binding) (Table 5).

Table 5: Antibody/peptide parameters from concerted model fitting

Reactant	a*(1/nM)	b**	R^2	n
MF20	0.0848 ± 0.094	0.0189 ± 0.008	0.94	6
MF30	0.28 ± 0.15	2.6E-02 ± 2.9E-2	0.98	4
Stabilizer	320 ± 2.8E+5	3.6E-09 ± 6.5E-6	0.99	5
Destabilizer	29.23 ± 3.1E+4	2.7E-08 ± 6.0E-5	0.96	3

* a is the microscopic binding constant. ** b is [T]/[R], where in MF30 and destabilizer peptide T is folded state (no binding), and R is unfolded state (binding to destabilizer). In the stabilizer, T is unfolded state (no binding), and R is folded state (binding). b<1 indicates positive cooperativity. R^2 is the coefficient of determination. n is the number of experiment repetitions.

Furthermore, the sequential model (104) proved that MF30 and destabilizer peptide bind to myosin cooperatively, as the association constant of the second strand of myosin (b) is higher than the association constant of the first strand (a) (Table 6).

Table 6: Antibody/peptide parameters from sequential model fitting

Reactant	a*	b**	R^2	n
MF20	1.32E-03 ± 2.08E-03	0.113 ± 0.156	0.94	6
MF30	5.7E-03 ± 4.6E-03	0.407 ± 0.278	0.97	4
Stabilizer	9.8E-07 ± 1.0E-03	379.5 ± 3.8E+05	0.99	5
Destabilizer	1.2E-07 ± 8.8E+04	188.3 ± 1.3E+6	0.96	3

* a is the association binding constant of the first myosin strand. ** b is the association binding constant of the second myosin strand. a<b indicates positive cooperativity. R^2 is the coefficient of determination. n is the number of experiment repetitions.

Based on data fitting with different equations to extrapolate the preferable binding model, it is suggested that MF30 and anti-S2 peptides bind cooperatively to myosin. It is postulated that MF30 and destabilizer peptide binding unzips myosin S2 leaving the other monomer available for binding. Yet, when the stabilizer peptide

wraps around myosin heads, it is proposed that the heads are in the OFF state, the bended heads over myosin rod makes other myosin S2 accessible for the stabilizer peptides due to disrupting the interacting heads motif of myosin (105).

Competitive TIRFS was utilized to measure destabilizer Kd differently. In this technique, the regular TIRFS was undertaken by titrating the immobilized myosin on the coverslip with a specific concentration of the destabilizer peptide (40, 80, and 100 nM). Another titration was started using myosin dimer. By increasing the concentration of myosin dimer, the peptide that was bound to the immobilized myosin dimer favored to move into the free myosin in the solution to achieve equilibrium; this shifting in the binding led to a decrease in the fluorescence signal (Figure 17). As shown in the graph in (Figure 18), the fluorescence signal decreased by increasing myosin concentration. Myosin IC50 was estimated from the 40, 80, and 100 nM destabilizer peptide binding graphs when fitted by the Hill equation to be 157, 162, and 160 nM, respectively (Table 7).

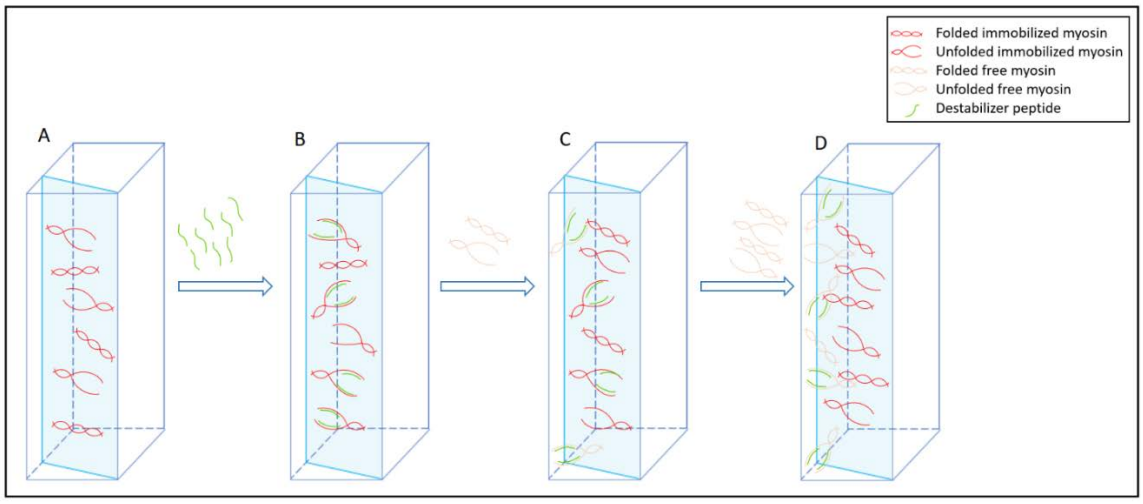

Figure 17: **Competitive TIRFS experiment diagram.**

A: Myosin dimers were immobilized on a treated coverslip with 0.2% nitrocellulose. B: Labeled destabilizer peptides were added and bound to myosin dimers on the coverslip causing an increase in the signal. C: Titrating with myosin dimer caused the labeled peptides to leave the immobilized myosin and bind to the free myosin leading to a decrease in the recorded signal. D: Titrating with more myosin dimer increased the competition; therefore, more peptides moved and bound to the free myosin dimer in the solution causing more decrease in the fluorescence signal.

The following equation was used to calculate destabilizer Kd when the peptide concentration was close to zero (Figure 19):

Ki=IC50/(1+([L]/Kd)

where Ki is the inhibition constant and is used to describe the binding affinity between two reactants, IC50 is half maximum inhibitory concentration, L is the legend concentration representing destabilizer concentration, and Kd is the dissociation constant.

When destabilizer concentration was close to zero Ki= IC50, and according to the graph in (Figure 19) it was 155 ± 4.3 nM, which is very close to the estimated Kd from the anisotropy experiment (152 nM) as both experiments are in-solution binding assays.

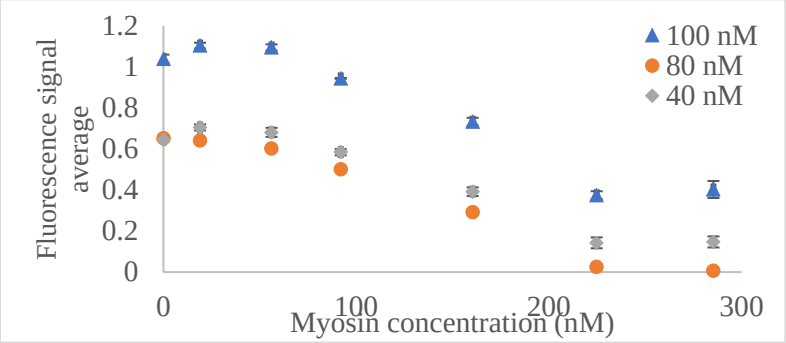

Figure 18: **Fluorescence signal of myosin from competitive TIRFS at different concentrations of the destabilizer peptide.**

Fluorescence signal decreased by increasing myosin concentration due to the detachment of labeled destabilizer from the immobilized myosin on the coverslip to bind to the free myosin in the chamber.

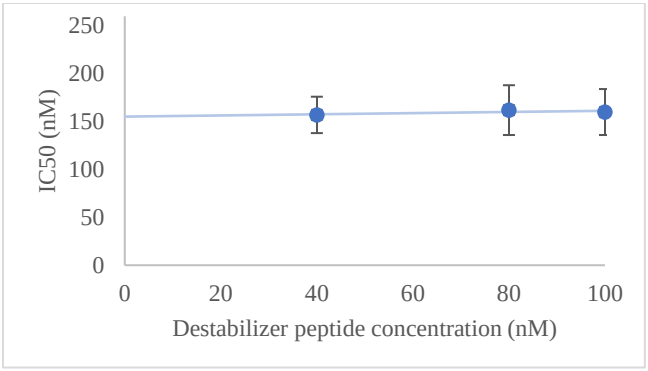

Figure 19: **Myosin IC50 at different destabilizer peptide concentrations.**

Destabilizer Kd equals IC50 when destabilizer peptide concentration was close to zero which was 155 ± 4.3 nM.

Table 7: Myosin IC50 at different concentrations of destabilizer peptide

Destabilizer concentration (nM)	IC50 (nM)	n	R^2
40	157 ± 19	3	0.99
80	162 ± 26	3	0.97
100	160 ± 24	3	0.99

R^2 is the coefficient of determination. n is the number of experiment repetitions.

3.4 Conclusion

Testing the stabilizer and destabilizer peptides at the molecular level using biophysical spectroscopic experiments has a significant contribution to live animal experiments. Binding graphs analysis determined peptides' affinity to myosin, which is crucial for estimating the optimal required concentration for later functional studies.

The stabilizer peptide improved myosin helicity by wrapping around the synthetic wt skeletal myosin dimer; one peptide is required for the wt myosin, while two peptides are necessary for the E930del cardiac myosin dimer. It does so through the positive charges it carries that allow it to wrap around the negatively charged glutamate-rich region in myosin S2. Stabilizer peptide increased myosin helicity by increasing alpha-helical content in skeletal and mutated cardiac myosin.

Myosin dimer required 2 destabilizer peptides to break it (one peptide per strand). The design of the destabilizer peptide favors myosin monomer binding to the peptide rather than binding to the other myosin strand preventing dimer formation. The disruption of myosin dimer reduced the helical content of the synthetic cardiac myosin once it was titrated with the destabilizer peptide.

In solution binding assay using fluorescence anisotropy revealed that MF20, MF30, and destabilizer peptide have high affinity to purified whole myosin. This assay could not predict the antibody or peptide binding mechanism to myosin. Therefore, a solid phase binding assay using

TIRFS was performed and indicated that MF30, stabilizer, and destabilizer peptides bind to myosin cooperatively; this finding was confirmed from the concerted and sequential equations. When MF30 or destabilizer peptides were added to myosin, they bound favorably to the unfolded myosin on both strands of the myosin dimer. The free-folded myosin shifted into the unfolded state to maintain equilibrium and was stabilized by the bound myosin to the MF30 or destabilizer peptide. This shifting resulted in a sigmoidal binding curve that significantly differs from the hyperbolic curve. On the other hand, as the stabilizer peptide wraps around myosin S2 it possibly disrupts the interacting head motifs of other myosin; this disruption makes myosin S2 accessible for other stabilizer peptides to bind. The binding graphs pointed to the high affinity of MF20, MF30, stabilizer, and destabilizer peptide to the whole myosin. The destabilizer peptide affinity that was further estimated from the competitive TIRFS was similar to what was calculated from the fluorescence anisotropy as both are in solution binding assays and denoted the high affinity of myosin to the destabilizer peptide.

CHAPTER 4

ANTI-S2 PEPTIDE/ANTIBODY COMPETITION WITH THE SARCOMERE REGULATORY PROTEINS THROUGH EXPANSION MICROSCOPY

The electron microscope has been an indispensable tool in science for providing high-resolution images that reaches about 0.1 nm (106); however, due to its elaborate sample preparation, microscope cost, special operator training, and other limitations, the need for developing alternatives has been invested (107). The arising expansion microscopy technique implement attaining high-resolution images using the regular confocal microscope. This technique demands special sample preparation by embedding fluorescently conjugated anti-S2 peptide/antibody labeled myofibril in a hydrogel, then the myofibril was digested, and the gel was washed to expand (Figure 8 A-E). The fluorophores crosslinked within the gel preserving the detail of the digested myofibril. When the gel expanded, the fluorophores moved apart and revealed more detail with high resolution (Figure 8 F and G).

Tracing the attached fluorophores to the gel implies the staining pattern of the antibody/anti-S2 peptide in the digested myofibrils. The staining pattern points to the binding sites of the antibody/peptide within the myofibril, in addition to detecting any competition between them and the regulatory proteins.

4.1 Validate Expansion Microscopy Image through super-Resolution Microscopy Images

To validate the expansion microscopy images, expanded myofibril labeled with MF20 was compared with photolocalization, and Airyscan super-resolution microscopic images for MF20 labeled myofibrils. The expansion microscopy image points to strong labeling of the P-zones and a decrease in MF20 labeling at the C-zone (Figure 20B). The photolocalization image that was previously acquired in the lab (108) was mirror-imaged for half a sarcomere, and a gaussian blur

filter radius 20 nm was applied (Figure 20C). Labeling for the P-zones and a remarkable decrease at the C-zone in the photolocalization microscopic image were detected. However, the super-resolution Airyscan image declared intense labeling for the P-zones. Still, it did not detect the drop in MF20 labeling at the C-zone as in the other super-resolution images (Figure 20D).

The fluorescence intensity graphs of the sarcomeres from the expansion and the super-resolution images were very similar (Figure 20A). MF20 labeled the D-zone close to the center of the A-band and depression at the C-zone, where they competed with MyBPC to bind at the LMM. The C-zone was accurately located using α-MyBPC1 antibody (Figure 20E).

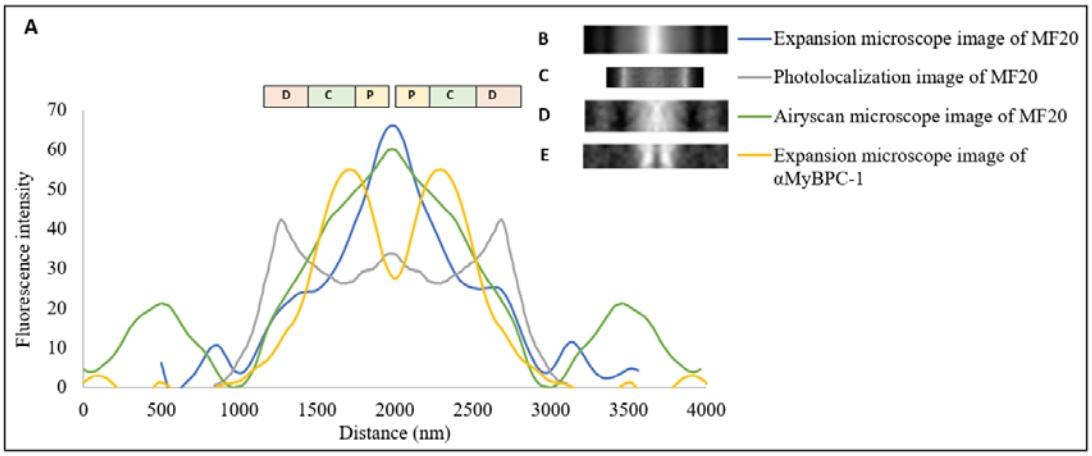

Figure 20: **Expansion microscopy reveals A-band staining pattern is similar to super-resolution images using MF20.**

A: Fluorescence intensity graphs along the A-band from super-resolution images for myofibrils labeled with MF20/α-MyBPC1. In expansion (blue graph), electron (red graph), and photolocalization (grey graph) images of MF20, the M-line was strongly labeled, and a slight decrease in the fluorescent intensity at the C-zone. No decrease at the C-zone was noticed with the Airyscan image (green graph). The C-zone within the A-band was accurately localized using α-MyBPC1 antibody (yellow graph). The expansion microscopy images are corrected for expansion compared to the other microscopy profiles in this panel. B: Expansion microscopic image from averaging 56 sarcomeres. The image width is 10.5 µm. C: Photolocalization image for half a sarcomere from myofibril labeled with MF20; half a sarcomere was mirror imaged and filtered with Gaussian blur radius 20 nm. The image width is 2.64 µm. D: Airyscan microscopic image from averaging 24 sarcomeres revealed shallow details about the A-band staining pattern. The image width is 4 µm. E: Expansion microscopy image from averaging 15 sarcomeres from myofibril labeled with α-MyBPC1 antibody showing the 2 C-zones within the A-band. The image width is 10 µm.

4.2 Expansion Images Declared More Detail about Myofibril Staining

Skeletal rabbit myofibril labeled with conjugated monoclonal antibodies were imaged with

the confocal microscope. The images indicate that the A-band and the Z-disc of the sarcomere were stained (Figure 21A and D); however, the detail of this staining pattern was not as clear with this traditional imaging technique. Therefore, the labeled myofibrils were imaged using the expansion technique to clarify the labeling pattern of the sarcomere. With expansion microscopy, the labeled myofibril with MF20 revealed a strong labeling in the P-zone near the M-line in the middle of the A-band, then a gradual decrease in the fluorescence intensity toward the edges of the A-band with a slight decrease at the C-zone (Figure 21B and C). The same assessment was perceived with MF30; strong labeling for the P-zones, then a gradual decrease in the fluorescence intensity toward the edges of the A-band; however, more obvious depression at the C-zone was detected (Figure 21E and F). It is thought that the MyBPC N-terminal region binds either to the thin filament or alternatively to myosin S2 which could compete with MF30 binding. The C-terminal region of MyBPC may bind with high affinity to LMM which could compete with MF20 binding (23, 109). Therefore, a decrease in the fluorescent intensity was noticed at the C-zone due to blocking this site by MyBPC which competed with the antibodies and prevented them from binding.

As expansion microscopy experiments were performed under rigorous conditions, the number of available heads were reduced due to binding to actin; myosin S2 from the bound heads are sterically blocked and unavailable for the antibodies to bind. In the super-resolution microscopy experiments, it was apparent that MF30 labeling was reduced at the Distal (D)- and C- zones more than the Proximal (P)-zone due to possible steric hindrance when the myosin heads bind to the actin thin filament which overlapped the D- and C-zones but not the P-zones at the sarcomere lengths studied (Figure 21C and F)

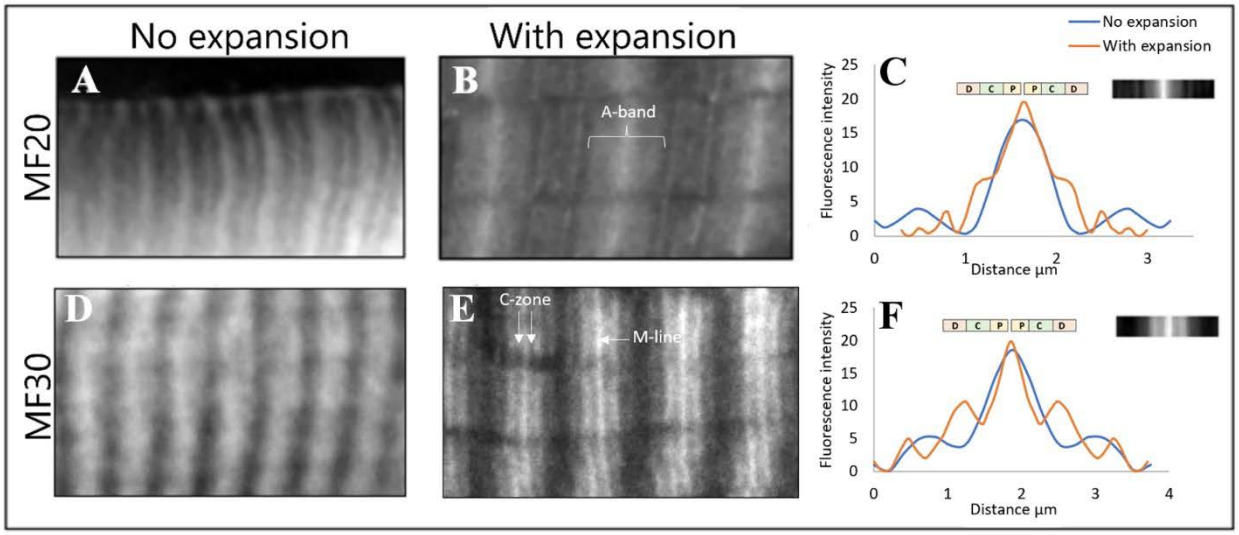

Figure 21: **Staining pattern in myofibril labeled with MF20 and MF30 with and without expansion.**

A: MF20 labeled both the A-band and the Z-disc of the sarcomere in the non-expanded myofibril. B: Expanded myofibril stained with MF20 revealed strong labeling of the P-zones near the M-line, then a gradual decrease in the fluorescence intensity toward the edges of the A-band with a slight decrease in the fluorescence intensity at the C-zone. C: MF20 fluorescence intensity graphs with and without expansion (orange and blue graphs, respectively), the expansion graph reveals depression at the C-zone that is not seen in the graph from the regular confocal images. The sarcomere to the right is from averaging 56 expanded sarcomeres. This C panel has corrected the expansion microscopy image profile for expansion magnification. D: Non-expanded myofibril stained with MF30 labeling the A-band. E: Expanded myofibril stained with MF30 showing the P-zones near the M-line strongly labeled with a more remarkable decrease in the fluorescence intensity at the C-zone compared to the MF20. F: MF30 fluorescence intensity graphs with and without expansion (orange and blue graphs respectively), more accurate detail extrapolated from the expansion graph showing the apparent decrease at the C-zone. The sarcomere to the right is from averaging 50 expanded sarcomeres. The expansion microscopy image profile has been corrected for expansion magnification in this F panel. Images in A, B, D, and E are 28 x 16 µm.

When rabbit skeletal myofibrils were labeled with conjugated destabilizer and stabilizer peptides, regular confocal images showed labeling for the A-band with both anti-S2 peptides (Figure 22A and D). Whereas expansion microscopy images showed that the P-zone near M-line was strongly labeled with a noticeable decrease in the fluorescent intensity at the C-zone (Figure 22B and E). This drop in the fluorescence intensity at the C-zone was due to the competition between the anti-S2 peptides and MyBPC that blocked this zone and prevented the peptides from binding. The stabilizer peptide displayed a slight increase in fluorescence intensity at the edges of

the A-band, yet this increase within the D-zone is still less than the P-zone as shown in the graph (Figure 22F).

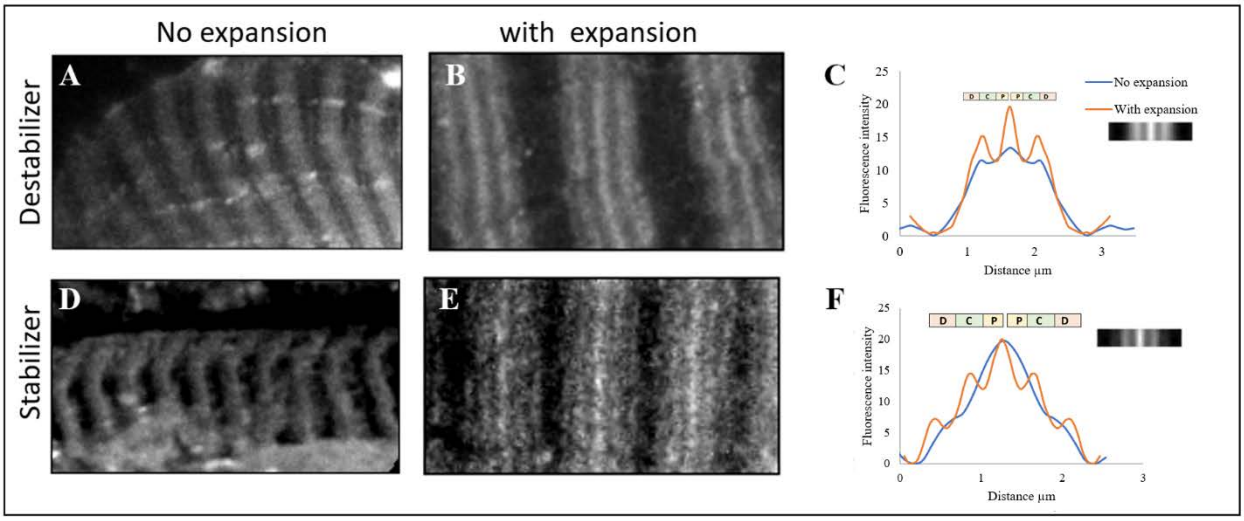

Figure 22: **Staining pattern in myofibril labeled with destabilizer and stabilizer with and without expansion.**

A: Destabilizer peptide labeled the A-band in the non-expanded myofibril. B: Expanded myofibril labeled with destabilizer peptide revealed strong labeling for the P-zones, then a gradual decrease in the fluorescence intensity toward the edges of the A-band. A decreased fluorescence intensity at the C-zone due to the competition between the peptide and MyBPC. C: Destabilizer peptide fluorescence intensity graphs along the sarcomere with and without expansion (orange and blue graphs, respectively). More accurate detail is extrapolated from the expansion graph. The sarcomere to the right is from averaging 60 expanded sarcomeres. This C panel has corrected the expansion microscopy image profile for expansion magnification. D: Stabilizer peptide labeled the A-band in the non-expanded myofibril. E: Expanded myofibril labeled with stabilizer peptide revealed strong labeling for the P-zones, decreased fluorescent intensity at the C-zone but less than the destabilizer peptide, and increased labeling at the edges of the A-band. F: Stabilizer peptide fluorescence intensity graphs along the sarcomere with and without expansion (orange and blue graphs, respectively). More accurate detail extrapolated from the expansion graph showing the trough at the C-zone and the increase in the fluorescence intensity at the edges of the A-band. The expansion microscopy image profile has been corrected for expansion magnification in this F panel. The sarcomere to the right is from averaging 67 expanded sarcomeres. Microscopic images are 27.7 x 15.3 µm.

4.3 MF20 and MF30 Competition with MyBPC were Enhanced in Dual and Triple-Labeled Myofibrils

Single labeling for myofibril with MF20 or MF30 manifested their competition with MyBPC as they share the same binding sites on myosin. MyBPC blocked myosin S2 and prevented MF30 from binding at this site, which was noticed as a depression within the C-zone in the fluorescent intensity graph. Even though the competition with MF20 was not as strong as with

MF30, it was not negligible. As the C-terminus of MyBPC binds to LMM (109), it partially blocked this site from MF20 causing a slight decrease in the fluorescence intensity at the C-zone (Fig. 24A). The amount of depression estimated at the C-zone in relation to the peak at the edge of the A-band in singly labeled myofibril with MF20 and MF30 were 5.5 ± 12.5% and 34.8 ± 12.7% respectively (Table 8).

The competition between the antibodies and MyBPC was more apparent when the myofibril was labeled with 2 or 3 antibodies simultaneously. Dual labeling of the myofibril with MF20 and MF30 demonstrated 20.2 ± 9.2% and 39.3 ± 16.4% depression at the C-zone, respectively (Figure 23B), while triple labeling using MF20, MF30, and polyclonal antibodies caused a 33.9 ± 6.4% and 44.8 ± 9.2% depression at the C-zone in MF20 and MF30 respectively (Figure 23C). The presence of multiple antibodies simultaneously created more competition between the antibodies and MyBPC. This competition was more distinct with MF20, which recessed nearly 6X more at the C-zone in triple labeling than in single labeling. The monoclonal antibodies were clearly sensitive to competitive binding in the C-zone. Furthermore, the depression at the C-zone expressed in MF20 significantly differs from MF30 when the same number of antibodies were used (p-values <0.05 calculated from Student's t-test).

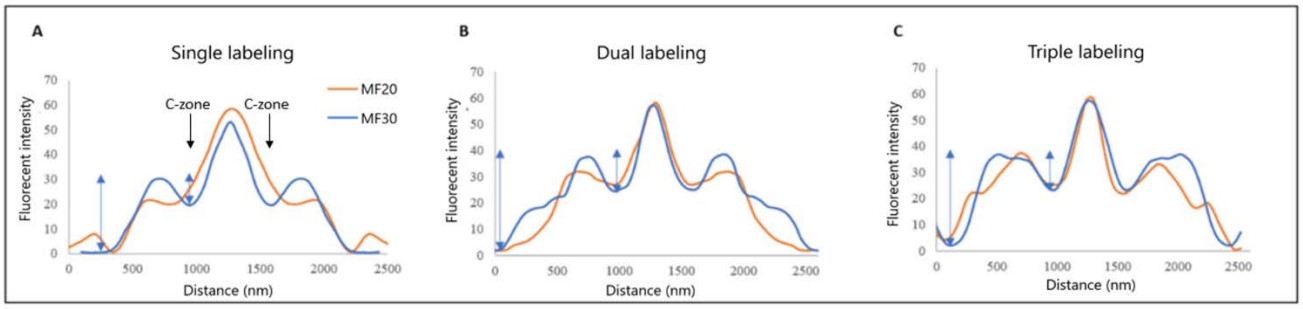

Figure 23: **MF20 and MF30 competition with MyBPC in single, dual, and triple-labeled myofibrils.**

A: Singly labeled myofibril fluorescence intensity graphs with either MF20 (orange) or MF30 (blue) revealed their competition with MyBPC as a decrease in the fluorescence intensity at the C-zone. B: Labeling the myofibril with MF20 and MF30 simultaneously increased the competition with MyBPC, decreasing the fluorescence intensity at the C-zone, especially with MF20. C: Labeling the myofibril with

MF20, MF30, and polyclonal antibodies at the same time declared more competition with MyBPC as the troughs are deeper at the C-zone. This figure has corrected the expansion microscopy image profiles for expansion magnification.

Table 8: MF20/MF30 depression percentages at the C-zone

Number of labeling	MF20 %	MF30 %	Polyclonal %	p-values
Single labeling	5.5 ± 12.5	34.8 ± 12.7	46.8 ± 9.2	3.2E-05
Dual labeling	20.2 ± 9.2	39.3 ± 16.4	-	9E-4
Triple labeling	33.9 ± 6.4	44.8 ± 9.2	49.2 ± 9.2	3E-2

p-values from Student t-test to compare if the depression at C-zone in MF20 is significantly differs from MF30

4.4 MF30 Competition with c-MyBPC was Evident from Mice Cardiac Tissue with c-MyBPC Ablated

Currently, there is no available rabbit skeletal muscle MyBPC knockout as skeletal muscle expresses multiple MyBPC genes; therefore, a mouse cardiac c-MyBPC knockout model was chosen to test the effects of c-MyBPC on MF30 labeling. Western blot detected that MF30 bound to myosin in both cardiac and skeletal myofibril similarly (Figure 24). c-MyBPC knockout cardiac myofibrils labeled with MF30-FITC were imaged using the super-resolution expansion microscopy technique to observe the c-MyBPC role in blocking the C-zone. Intense labeling for the whole A-band, including the C-zone, was detected in the expansion images. The fluorescent intensity of the A-band in the KO tissue was 3.5X more than the wild type (control), assigning the relative fluorescent intensity of the wild type to 100% (Figure 25). The c-MyBPC presence, as detected from the control images, reduced MF30 labeling at the C-zone and increased non-muscle myosin binding at the Z-disc (Figure 26A and C). Non-muscle myosin II in the cardiac tissue is 83% identical to the MF30 antigenic residues binding site within the muscle myosin sarcomere; therefore, when MyBPC is present, it blocks MF30 binding sites on myosin S2 driving the antibody to bind to the Z-disc where non-muscle myosin II usually resides after myofibrillogenesis. Meanwhile, there was no reduction in the fluorescent intensity at the P- and D-zones when MyBPC

was absent (5). It has been reported that the lack of MyBPC inhibits the migration of non-muscle myosin IIB to the Z-disc from the A-band after myofibrillogenesis (60), which might contribute to the higher relative intensity of Z-disc immunostaining observed in wild type than in the MyBPC KO.

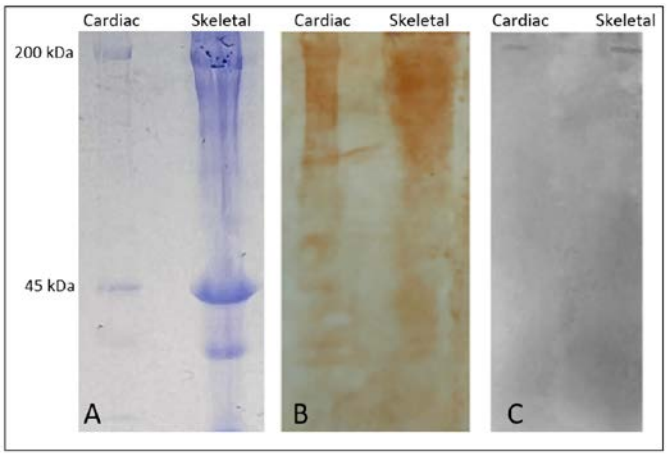

Figure 24: **MF30 binds myosin in both the cardiac and skeletal myofibrils.**

A: SDS-PAGE for the myofibrils in 10% acrylamide gel demonstrates protein separation. B: Nitrocellulose stained with copper iodide to illustrate protein binding after the transfer. C: Western blot endorses MF30 binding to myosin in cardiac and skeletal myofibrils

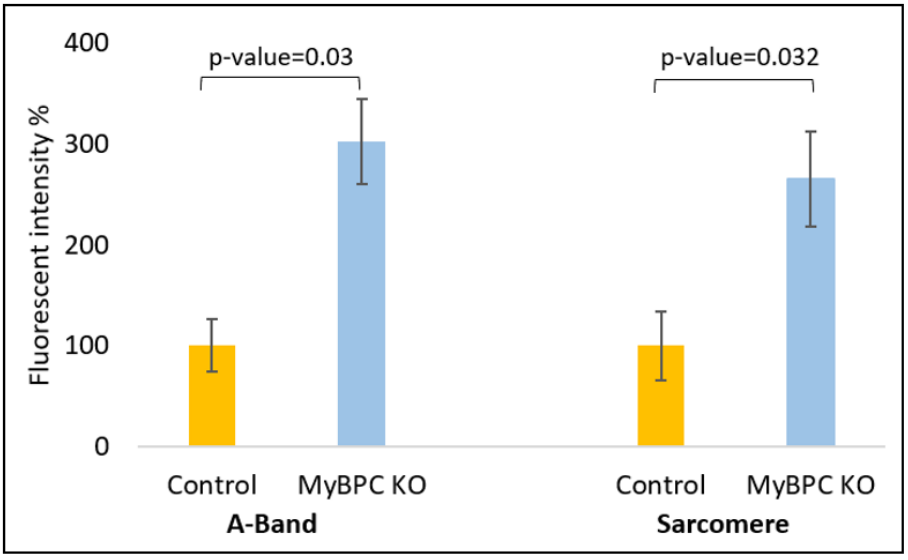

Figure 25: **MF30 labeled MyBPC KO myofibril has higher fluorescent intensity percentages than the control.**

Considering the fluorescent intensity percentage of the control is 100%, MyBPC KO fluorescent intensity percentages are 3X higher in the A-band and 2.6x in the sarcomere (p-values <0.05 calculated from Student's t-test, n=4).

The MyBPC KO myofibril labeled with MF30 revealed stronger labeling for the A-band, including the C-zone, than the wild type. This finding supports that MyPBC presence competes with MF30 and prevents MF30 from binding at the C-zone (Figure 26B and D) (110). Despite staining the whole A-band with MF30, the P-zone was more stained than the D-zone, which might be explained by the binding of myosin heads to actin thin filament at the D- and C-zones in contracted myofibrils, this binding leaves fewer myosin S2 available for MF30 to bind, while the P-zone is more accessible.

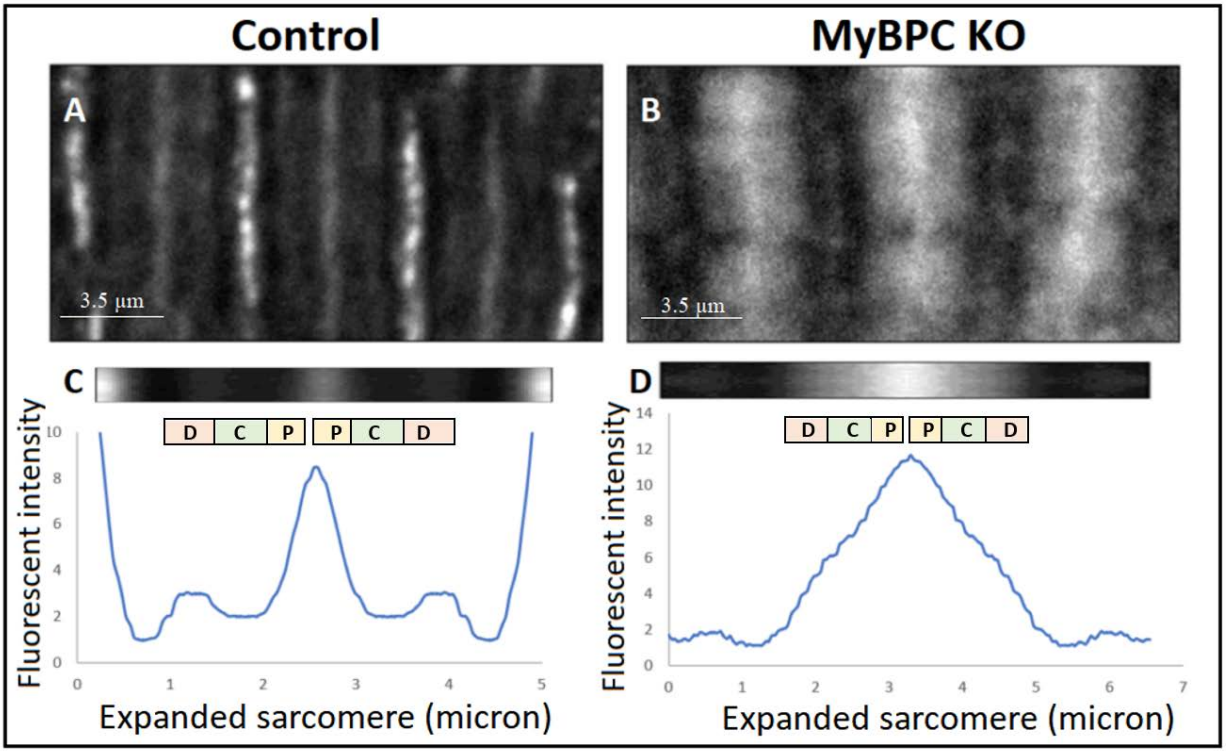

Figure 26: **Absence of MyBPC increased MF30 labeling at the A-band and reduced it at the Z-disc in cardiac mice tissue.**

A: Wild type cardiac tissue (control) revealed weak labeling of the A-band with reduced labeling at the C-zone due to the competition with MyBPC that bound to the non-muscle myosin at the Z-disc (Image dimensions are 17.4x8.7 microns). B: MF30 antibody in MyBPC KO cardiac tissue strongly labeled the A-band and weakly labeled the Z-disc (Image dimensions are 17.4x8.7 microns). C: Fluorescent intensity graph from averaging control sarcomeres indicating drop in fluorescent intensity at the C-zone and increase in Z-disc labeling. At the top of the graph is the image of the averaged sarcomeres 5.5x0.66 microns. D: Fluorescent intensity graph from averaging MyBPC KO sarcomeres indicating A-band labeling. At the top of the graph is the image of the averaged sarcomeres 6.6x1.5 microns. This figure has corrected the expansion microscopy image profiles for expansion magnification.

4.5 Dual Labeling Affected the Anti-S2 Labeling Pattern

In order to study the interaction of the anti-S2 peptide with titin and with each other, skeletal rabbit myofibrils were incubated with stabilizer and destabilizer, destabilizer and anti-titin, stabilizer and anti-titin, and stabilizer and MF20. The fluorescence intensity graph of a singly labeled myofibril with the anti-S2 peptide was compared to the anti-S2 peptide graphs from dual-labeling.

The staining pattern of the destabilizer peptide did not significantly differ after adding the stabilizer peptide or anti-titin (p-values are more than 0.05 calculated from Student's t-test) as shown in Table 9 (Figure 27A). On the other hand, the stabilizer peptide's staining pattern significantly differed after adding the destabilizer peptide or anti-titin (Table 9). Dual labeling of the stabilizer peptide with the destabilizer or anti-titin affected the amount of labeling at the P-zone near the M-line, the depression at the C-zone, and the labeling band length (Figure 27B).

Table 9: Anti-S2 peptides labeling pattern significance alternation after dual labeling

Compared samples	p-value (t-test)
Destabilizer alone and dual labeling with stabilizer	0.17
Destabilizer alone and dual labeling with anti-titin	0.48
Stabilizer alone and dual labeling with MF20	0.06
Stabilizer alone and dual labeling with destabilizer	0.013
Stabilizer alone and dual labeling with anti-titin	0.018

The presence of the destabilizer peptide along with the stabilizer increased stabilizer peptide labeling at the P- and D-zones. It is possible that the destabilizer peptide facilitates stabilizer peptide binding by making the glutamate-rich area on myosin S2 accessible to the stabilizer peptide. Also, the addition of the anti-titin to the stabilizer peptide shed light on the possible interaction between the stabilizer peptide and titin; therefore, when anti-titin was added, it blocked titin from the peptide-reducing stabilizer labeling to titin within the A-band. On the

contrary, the addition of MF20 to the stabilizer peptide did not cause a significant change in the fluorescent intensity graph (p-value > 0.05 calculated from Student's t-test) as both bind to different antigenic locations on myosin (Figure 27B).

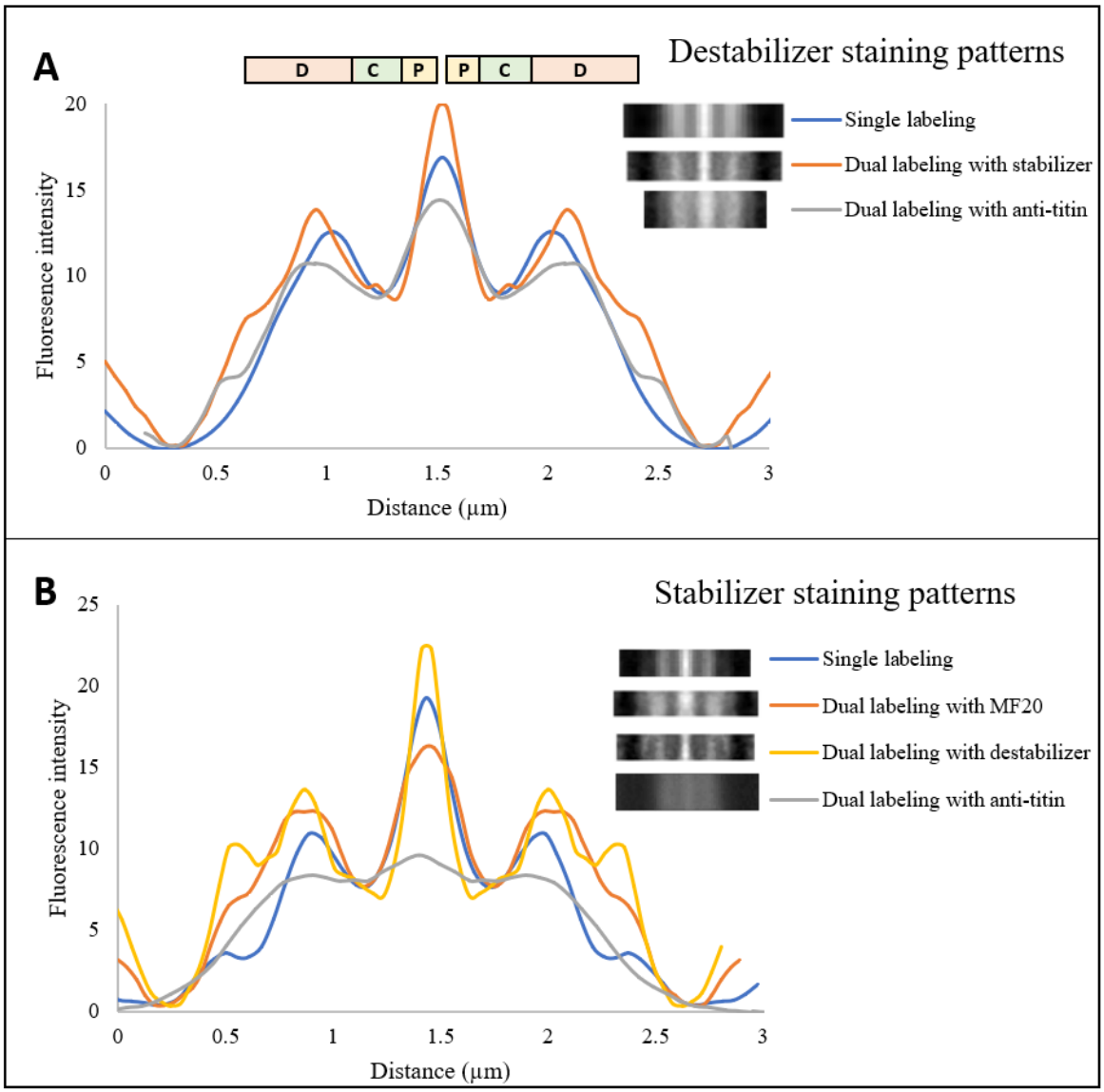

Figure 27: **Singly labeled myofibrils with destabilizer and stabilizer compared to dual-labeled myofibrils.**

A: Destabilizer peptide fluorescent intensity graph (blue graph) does not significantly differ from dual labeled graphs of stabilizer peptide (orange graph) and anti-titin antibody (grey graph). B: The stabilizer peptide fluorescent intensity graph (blue graph) significantly differs from dual labeled graphs with destabilizer peptide (yellow graph) and anti-titin (grey graph). However, the stabilizer peptide fluorescent intensity graph (orange graph) does not significantly differ from the dual-labeled graph with MF20. The sarcomeres on the right were obtained by averaging 24-42 expanded sarcomeres ~ (11x2 microns). This figure has corrected the expansion microscopy image profiles for expansion magnification.

4.6 Anti-Titin Labeling Band Increased by Increasing Sarcomere Length and Altered by the Addition of MF30 and Anti-S2 Peptides

E2 anti-titin monoclonal antibody is designed to bind at the C-terminus of titin, so it is used to locate titin within the sarcomere around the M-line. To determine the relationship between the anti-titin labeling band and the sarcomere length, skeletal rabbit myofibrils were labeled with anti-titin alone (single labeling) or dual labeling with MF30, stabilizer, or destabilizer peptides. The myofibrils were imaged with expansion microscopy. The anti-titin labeling bands were measured using Image J software and plotted versus the sarcomere lengths taking into consideration the amount of expansion in each.

Table 10: P-values from comparing single and dual labeled myofibrils in regard to anti-titin labeling band length and staining pattern

Anti-titin labeling band lengths in dual labeling with:	p-value (t.tst) (Anti-titin in single labeling versus dual labeling)
MF30	0.001
Stabilizer	9.6E-07
Destabilizer	0.69
Staining pattern in dual labeling with:	
MF30	0.09
Stabilizer	0.02
Destabilizer	0.97

The anti-titin labeling band was increased when the sarcomere length increased in single and dual-labeled myofibril (Figure 28 A-D). Anti-titin labeling band to sarcomere length in myofibril labeled with anti-titin significantly differ from the dual-labeled myofibrils with MF30 and stabilizer peptide ($p < 0.05$ calculated from Student's t-test). Meanwhile, the destabilizer peptide did not cause a significant difference in the anti-titin band length (Table 10). In other words, adding MF30 and stabilizer peptide to the anti-titin antibody reduced the anti-titin labeling band length compared to the singly labeled myofibril with anti-titin. At the same time, they

increased the anti-titin labeling band by increasing the sarcomere length. The stabilizer peptide altered the staining pattern of the anti-titin by causing a decrease in the fluorescent intensity at the M-line along with the change in the labeling band length. This observation provides another insight about stabilizer peptide and anti-titin antibody competition for binding to titin within the sarcomere (Figure 29 E).

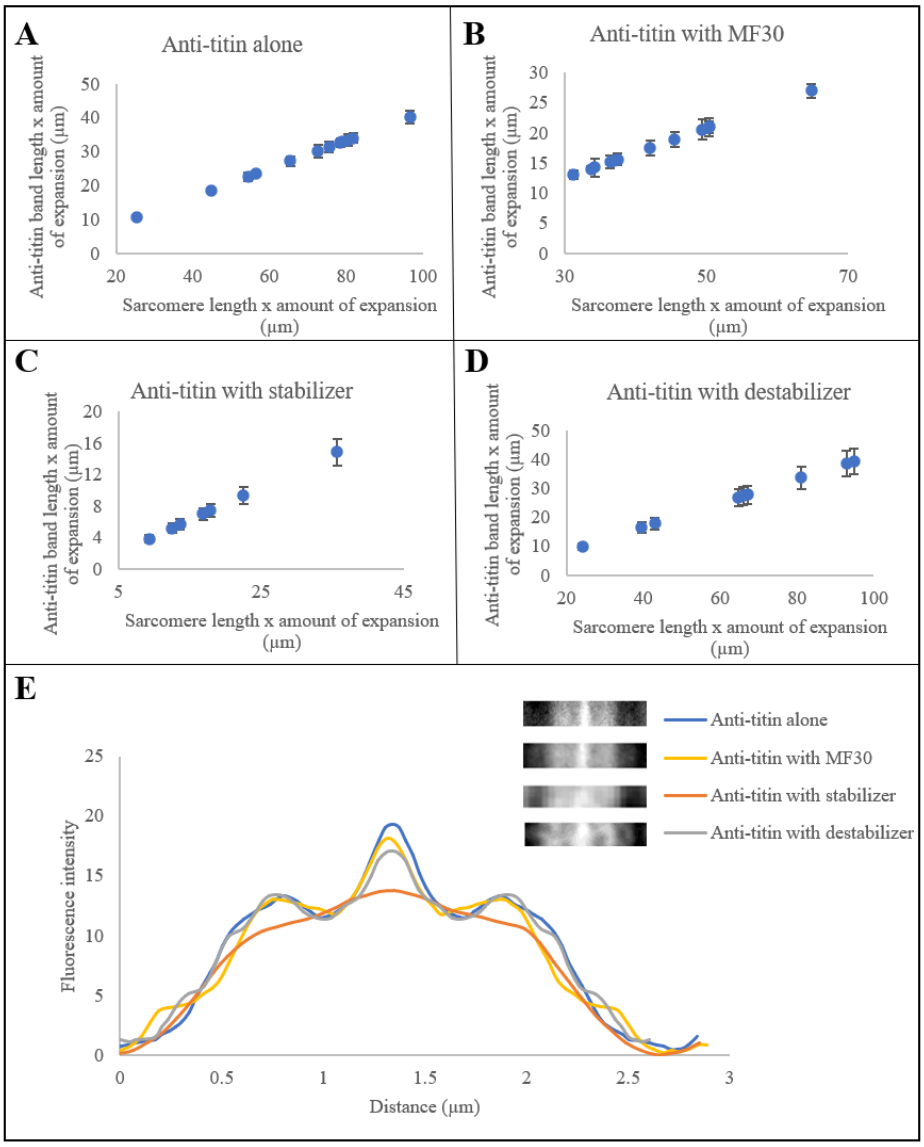

Figure 28: **Anti-titin labeling bands increased by increasing sarcomere length and altered by adding MF30 and stabilizer peptide.**

A: Singly labeled myofibril with anti-titin denoted the increase in the labeling band by sarcomere elongation. B, C, and D: Dual-labeled myofibrils with anti-titin and MF30, stabilizer, or destabilizer, respectively, pointed to the increase in the anti-titin labeling band when sarcomere length increased.

Significant difference in the anti-titin band to sarcomere length was noticed between the single and double-labeled myofibrils with MF30 and stabilizer peptide ($p<0.05$). E: Dual labeling with the stabilizer peptide caused a decrease in the anti-titin labeling at the M-line that significantly differed from the staining pattern of the singly labeled myofibril. The sarcomeres on the right are from averaging 20-40 expanded sarcomeres. The expansion microscopy image profiles have been corrected for expansion magnification in this panel.

4.7 Conclusion

The field of expansion microscopy opened the door for acquiring high-resolution images using the regular confocal microscope and the physical expansion of the sample. Labeled myofibril with MF20 monoclonal antibody validated the expansion protocol by comparing it with known super-resolution microscopic images. Expansion microscopy image for MF20 labeled myofibril revealed a similar staining pattern to the photolocalization image. However, the Airyscan image had diminished staining pattern detail compared to the expansion microscopy image.

Expansion microscopy revealed a detailed staining pattern for myofibrils labeled with MF20, MF30, stabilizer, and destabilizer peptides. It was apparent that the P-zone near the M-line was strongly labeled in all of them, with a gradual decrease in the fluorescence intensity toward the edges of the A-band. However, there was a variant reduction in the fluorescent intensity at the C-zone. Since the imaged myofibrils were in a rigorous condition, the interdigitated thick and thin filaments extended through the D- and C-zones and parts of the P-zone. In the overlapped region, some of the myosin heads are in contact with actin; therefore, myosin S2 was inaccessible to the anti-S2 antibodies or peptides to bind, and this blockage caused a reduction in D- and C- zones labeling.

It is thought that the MyBPC N-terminal region binds either to the thin filament or alternatively to myosin S2 which could compete with MF30 or anti-S2 peptides binding. The C-terminal region of MyBPC may bind with high affinity to LMM, which could compete with MF20 binding (23, 109). Therefore, the fluorescent intensity was decreased at the C-zone due to blocking

this site by MyBPC and preventing the antibodies and peptides from binding to myosin. Myofibril labeling with multiple antibodies at the same time clarified this competition with MyBPC as more decrease in the C-zone labeling when more antibodies were used simultaneously.

This competition was further confirmed by comparing MF30-labeled cardiac tissue in the presence and absence of MyBPC. MF30 labeled the non-muscle myosin within the Z-disc in wt cardiac tissue as opposed to the c-MyBPC ablated cardiac tissue. Since the antigenic site on myosin S2 resembles that on the non-muscle myosin, S2 blockage with MyBPC caused MF30 binding to the Z-disc non-muscle myosin. However, higher amounts of MF30 labeled the C-zone rather than the Z-disc when c-MyBPC was knocked-out.

As for the destabilizer peptide's staining pattern did not change when the myofibrils were dual labeled with the stabilizer and/or anti-titin. However, the stabilizer peptide staining pattern changed with the destabilizer or anti-titin presence. Suggesting that the stabilizer peptide competed with the destabilizer to bind at myosin S2 and with anti-titin to bind at titin. Contrary to that, the addition of MF20 did not affect the staining pattern of the stabilizer peptide since they bind to a different location on myosin.

Lastly, the anti-titin labeling band increased by increasing sarcomere length. It differed from the dual-labeled myofibrils with anti-titin and MF30 or stabilizer peptide but not with destabilizer peptide. Moreover, dual-labeling with anti-titin and stabilizer peptide caused a significant change in the staining pattern of the anti-titin. In contrast, the MF30 or the destabilizer peptide did not affect the staining pattern of the anti-titin. This finding suggests possible non-specific binding of the stabilizer peptide to titin that might affect its intended function.

CHAPTER 5

STABILIZER AND DESTABILIZER PEPTIDES IN LIVE MICE

5.1 The Labeled Peptides Reached the Mice's Hearts

As the anti-S2 peptides displayed a promising result at the molecular and tissue levels experiments, it was time to try their effect in vivo. The mouse was chosen to test the peptides since it has genetic and physiological similarities with humans and is easy to raise and breed in the laboratory (111). Injecting the peptides bound to the guiding molecule "tannic acid" into live mice was crucial to know if the peptides could reach the cardiomyocytes and impact the cardiac function.

Live mice were injected intravenously with 200 µl of 0.1 mM or 1 mM of labeled/unlabeled anti-S2 bound to tannic acid. The heart's physiological functions of heart rate, stroke volume, and cardiac output were carefully monitored after the injection and compared with the results before the injection. Some hearts were excised after 24 hours and others after 7 days from the injection for further histological assessment. The hearts were stored either with immediate freezing in liquid nitrogen or fixed in a solution after washing. The extracted hearts were sliced in the cryostat and stained with Fluoromount G with DAPI to visualize myocyte nuclei.

In order to confirm that the labeled peptides reached the heart, each slice from the sectioned heart was imaged with the epifluorescence microscope. The fluorescence amount in the slices were estimated and compared to the control heart slices (injected with tannic acid only) to estimate the amount of auto-fluorescence. The epi-ultraviolet light excited the DAPI stain and detected the cardiomyocyte nuclei through the blue filter, the epi-blue light excited FITC in the labeled destabilizer that was detected through the green filter, and the epi-green light excited TRITC in the labeled stabilizer and was detected through the red filter.

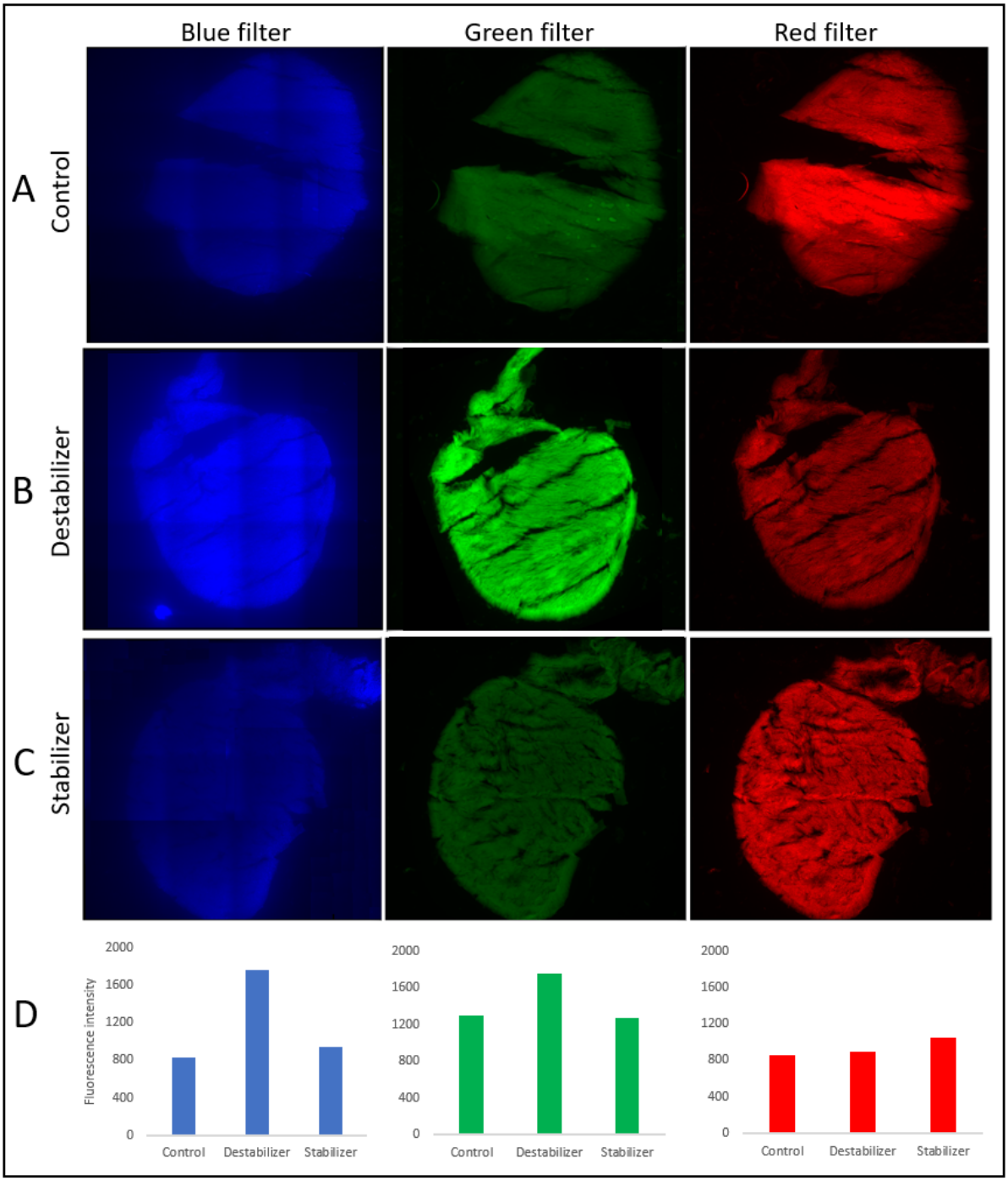

Figure 29: **Epi-fluorescence microscopic images for heart slices from mice injected with tannic acid (control), FITC labeled destabilizer, and TRITC labeled stabilizer using blue, green, and red filters.**

A: Control images estimated the amount of auto-fluorescence in the mouse heart. B: Labeled destabilizer fluorescence with the 3 filters. C: Labeled stabilizer fluorescence with the 3 filters. D: The fluorescence intensity for the labeled destabilizer was the most with the blue and green filters; however, the labeled stabilizer had the most fluorescent intensity with the red filter. Images dimension ~4.9 X 4.9 mm.

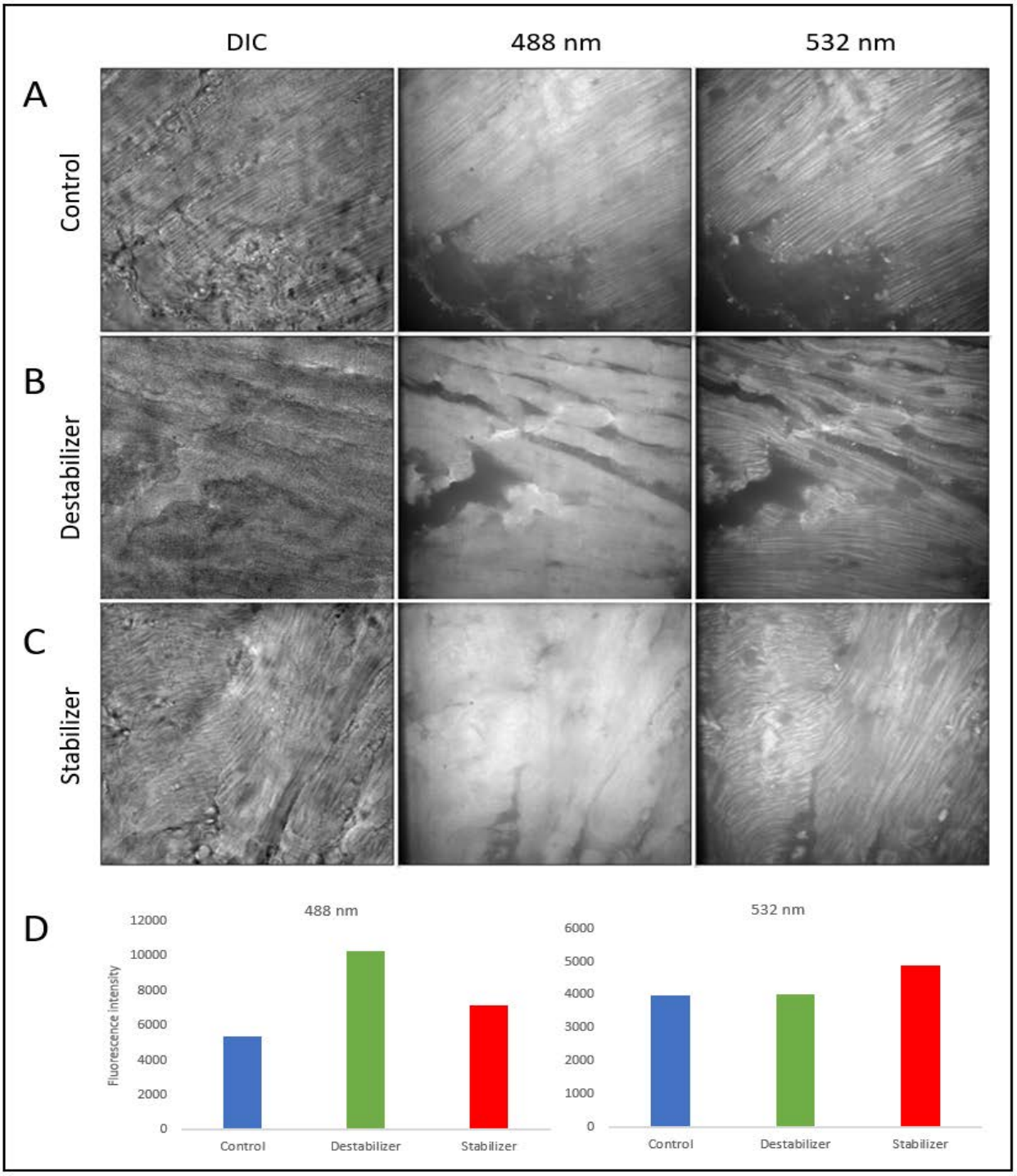

Figure 30: **Confocal microscopy images from mice hearts injected with tannic acid (control), FITC labeled destabilizer, and TRITC labeled stabilizer using 488 and 532 nm lasers.**

A, B, and C: Images for control, labeled destabilizer, and labeled stabilizer, respectively, were imaged with DIC, 488 nm, and 532 nm lasers. D: FITC labeled destabilizer was detected with the 488 nm laser and a slight bleed-through was noticed with TRITC labeled stabilizer at 488 nm, which was detected with the 532 nm laser. Images dimension 0.11 X 0.11 mm.

The heart slices were imaged using the same conditions to detect if the labeled peptides reached the hearts. Figure 29A represents the auto-fluorescence detected in the control heart using 3 filters. The labeled destabilizer and stabilizer heart slices were imaged using the same conditions of the control with the 3 filters (Figure 29 B and C). The fluorescent intensities for the control, stabilizer, and destabilizer in each channel used were compared in (Figure 29D). The labeled destabilizer peptide was detected with the blue and green filters; the fluorescence intensities were 52% and 25% higher than the control, respectively. However, the stabilizer peptide had a 19% increase in the fluorescent intensity than the control detected in the red filter. According to the previous results, the fluorescently labeled anti-S2 peptides were able to reach the heart after IV injection into the mice.

The previous result from the epi-fluorescence microscopy images indicated that some of the injected labeled peptides were able to reach the heart, which was further confirmed when the fluorescence intensities were estimated using the confocal microscope with the 488 and 532 nm lasers to find if the labeled peptides existed in the heart (Figure 30). The destabilizer peptide had a 48% increase in fluorescence intensity compared to the control with the 488 nm laser that excited FITC. Meanwhile, the stabilizer peptide had an 18% increase in fluorescence intensity compared to the control with the 532 nm laser that excited TRITC (Figure 30D).

Both methods of imaging support that the peptides reached the heart and were detected even after 24 hours of intravenous injection. But the destabilizer peptide reached the heart at a higher concentration than the stabilizer, even though the injected amount was the same in both.

5.2 Estimating the Amount of Labeled Peptides in Mice Hearts

To assist the amount of the labeled peptides reached the heart after 24 hours of the injection, a normal mouse heart was sliced and stained with different concentrations of FITC or TRITC. The

slices were imaged with an epi-fluorescence microscope using the same conditions to image the peptides. The fluorescence intensities of the control were used to formulate a standard curve to calculate the peptides concentrations accordingly.

The fluorescent intensity of the labeled destabilizer acquired from averaging the 50 slices of the heart is 2212, corresponding to 2.05 nMole in the FITC standard graph (Figure 31A). Meanwhile, the stabilizer peptide fluorescent intensity from averaging the 47 slices of the heart is 1207, corresponding to the 0.31 nMole in the TRITC standard graph (Figure 31B). According to the previous calculations, the destabilizer peptide concentration in the heart after 24 hours from the injection was 6X higher than the stabilizer peptide. It is possible that some of the stabilizer peptide was degraded in the blood before reaching the heart; therefore, it might be useful to cap the stabilizer peptide to protect it from the enzymes that degrade it.

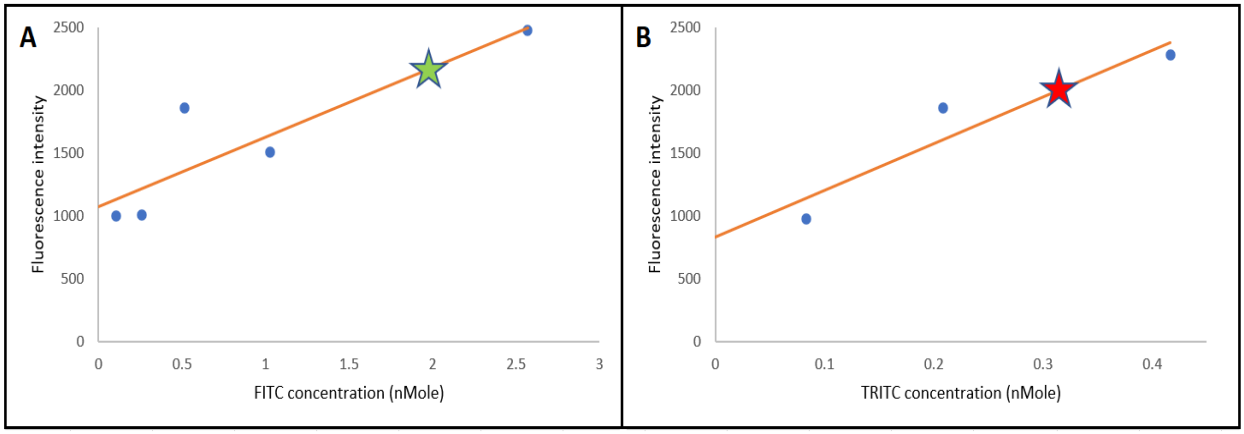

Figure 31: **The fluorescent intensity standard graphs of FITC/TRITC controls.**

A: Labeled destabilizer peptide average intensity from 50 slices of mouse heart (green star) corresponds to 2.05 nMole from the FITC standard graph. B: Labeled stabilizer peptide average intensity from 47 slices of mouse heart (red star) corresponds to 0.31 nMole from the TRITC standard graph.

5.3 Peptides Staining Pattern in the Cardiac Tissue

When the mice were injected with the peptides, the peptides traveled with the blood to reach the coronary arteries. From there, the peptides diffused through the capillaries into the

cardiac tissue. The cardiac arterioles were found stained with the labeled destabilizer peptide supporting the previous idea (Figure 32). The blue filter image shows the cardiac nuclei stained with DAPI (Figure 32A); however, the green filter image showed few arterioles bound to the labeled destabilizer (Figure 32B). Since the destabilizer peptide reached the heart in a higher concentration than the stabilizer peptide, the stained arterioles with the peptides were more evident with the destabilizer. In (Figure 33) an arteriole stained with the labeled stabilizer was imaged with the red filter.

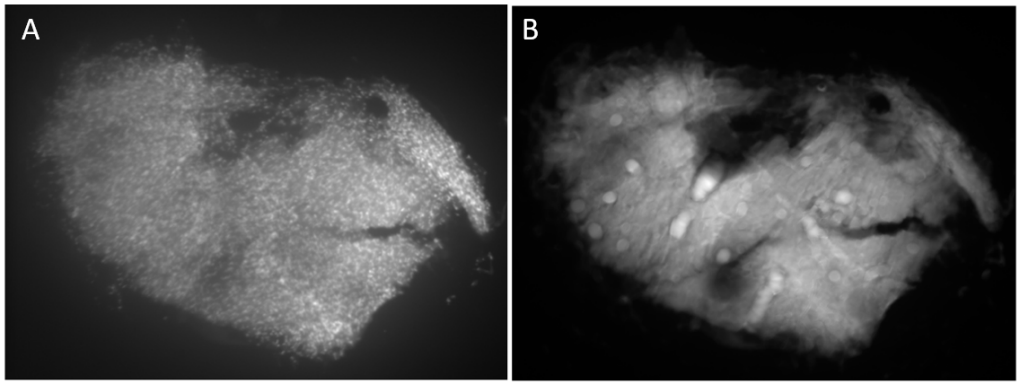

Figure 32: **Labeled destabilizer peptide-stained cardiac arterioles.**

A: Blue filter image showing cardiac nuclei stained with DAPI. B: Green filter image showing many arterioles bound to the FITC labeled destabilizer. Images dimensions are 0.8 x 0.7 mm.

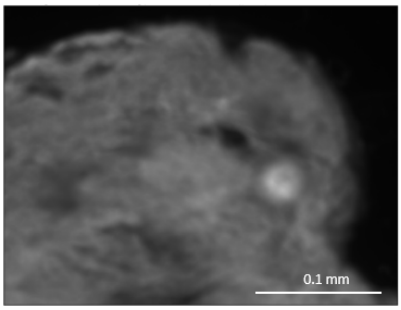

Figure 33: **Labeled stabilizer peptide bound to an arteriole in mouse cardiac tissue.**

The labeled peptide was bound to a blood vessel after 24 hours of peptide injection when imaged with the red filter. Image dimensions are 0.32 x 0.24 mm.

In addition to peptide binding to the blood vessels, the labeled destabilizer peptide was found bound to the T-tubules; it is possible that some of the peptide bound to the T-tubules before

it got into the cytoplasm of the cardiomyocyte (Figure 34). Further investigation will be undertaken to understand the nature of this binding, it might depend on the concentration of the peptide or the presence of an epitope on the T-tubules that the peptide recognized and bound to.

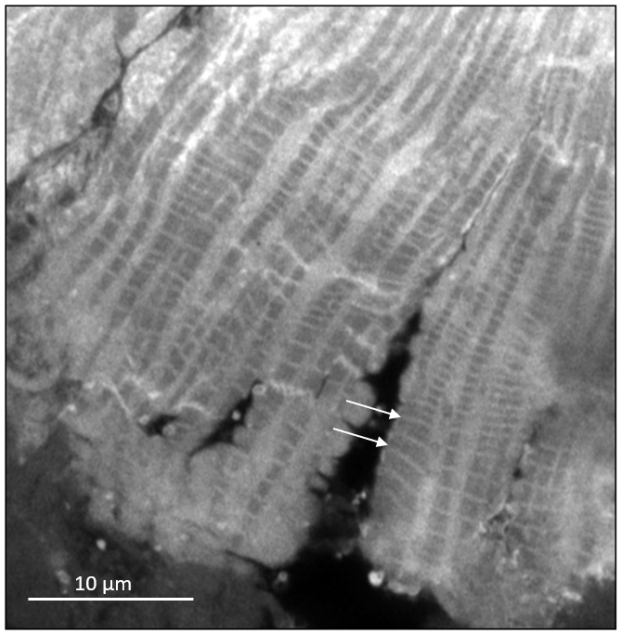

Figure 34: **Labeled destabilizer peptides bound to T-tubules in mouse cardiac tissue.**

T-tubules were stained with the destabilizer peptide from the apex of the heart, imaged with 63x oil, 1.4 NA planapochromat Airyscan confocal. White arrows point to 2 T-tubules. Image dimensions are 37 x 38 µm.

Moreover, both peptides reached into the cardiomyocytes and labeled some of the A-bands in the sarcomeres within the cardiac tissue (Figure 35). To confirm that the fluorescence in the tissues was related to the labeled peptides, the emission wavelengths were recorded for the fluorescent tissues. The destabilizer peptide emission graph coincides with the FITC emission graph from the literature (Figure 36A), and the stabilizer peptide emission graph coincides with the TRITC emission graph from the literature (Figure 36B). This result further supports that the mice cardiac tissues absorbed the labeled peptide that interfered with cardiac function, as it was found that the labeled destabilizer peptide caused a significant increase in cardiac output in 24 hours compared to the pre-injection levels (unpublished data). However, the labeled stabilizer did

not cause a significant change in the cardiac output, even though the unlabeled stabilizer peptide did.

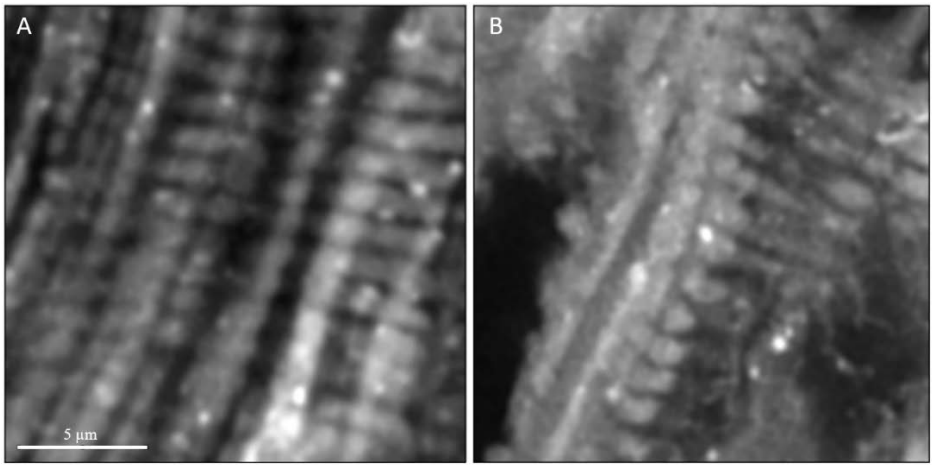

Figure 35: **Labeled peptides stained some sarcomeres in mice cardiac tissue.**

A: Labeled stabilizer peptide in the left atrium of the mouse heart is labeling the A-bands in sarcomeres. B: Labeled destabilizer peptide in the left ventricle is labeling the A-bands. Imaged with 63x oil, 1.4 NA planapochromat Airyscan confocal. Images dimensions are 18 x 18 µm.

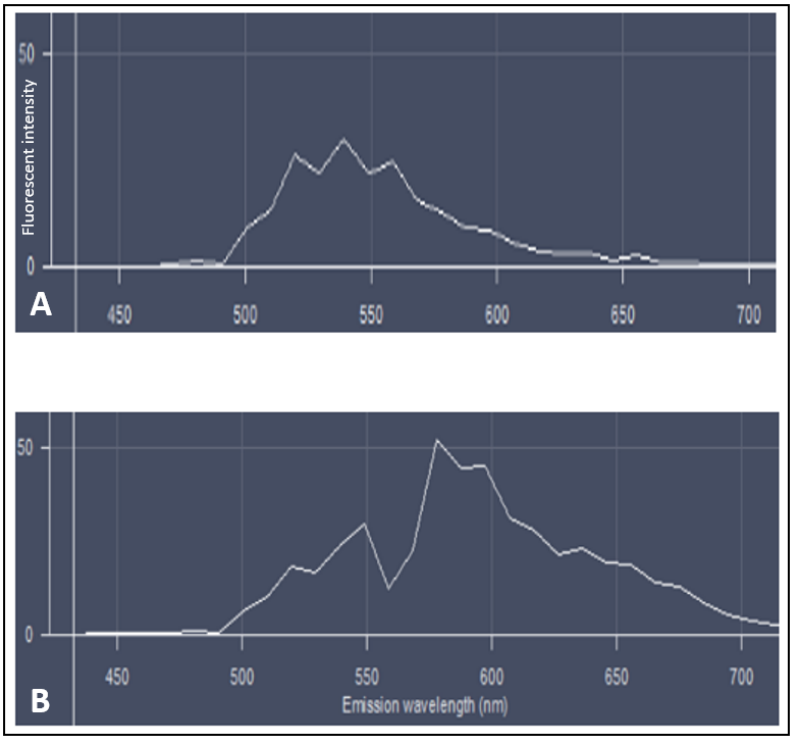

Figure 36: **Emission wavelength graphs of the labeled peptides.**

A: The emission graph of the destabilizer peptide coincides with FITC emission graph that has a peak close to 520 nm. B: The stabilizer peptide's emission graph coincides with the TRITC emission graph with a peak close to 570 nm.

5.4 Labeled Peptides Effect on Sarcomere Lengths

To detect if the labeled peptides altered cardiac muscle contraction, sarcomere lengths were measured from DIC images of cardiac tissue extracted after 24 hours of labeled peptides injection using the water immersion Apo-C 40X 1.6X NA. Shorter sarcomeres in comparison to the control indicate the possible effect of the peptide in increasing muscle contraction as it was hypothesized with the destabilizer peptide, however, if the sarcomere length is longer than the control, then the peptide relaxes the sarcomeres as expected with the stabilizer peptide in reducing muscle contraction.

The control sarcomere was measured from the cardiac tissue of one mouse injected with tannic acid; the average of 184 sarcomeres was 1.15 ± 0.108 microns. Meanwhile, the average of 160 sarcomeres from the cardiac tissue of one mouse injected with labeled destabilizer peptide-tannic acid was 1.11 ± 0.12 microns. However, the average of 160 sarcomeres from the cardiac tissue of one mouse injected with labeled stabilizer peptide-tannic acid was 1.48 ± 0.17 microns (Table 11). The stabilizer peptide had the longest sarcomeres as it possibly induced the cardiac muscle to relax. It had a wider I-band than the destabilizer peptide with a thicker A-band (Figure 37). The average sarcomere lengths that were measured significantly differed from the control (p-values calculated from Student's t-test were 4.4E-57 and 2.2E-4 in stabilizer and destabilizer peptides versus control, respectively).

Table 11: Sarcomere lengths in cardiac tissue with TA, destabilizer, and stabilizer peptides

Sample	Sarcomere length average (micron)	n
Control/TA	1.15 ± 0.108	184
Stabilizer peptide	1.48 ± 0.173	160
Destabilizer peptide	1.11 ± 0.120	160

n is the number of sarcomeres measured from one mouse each

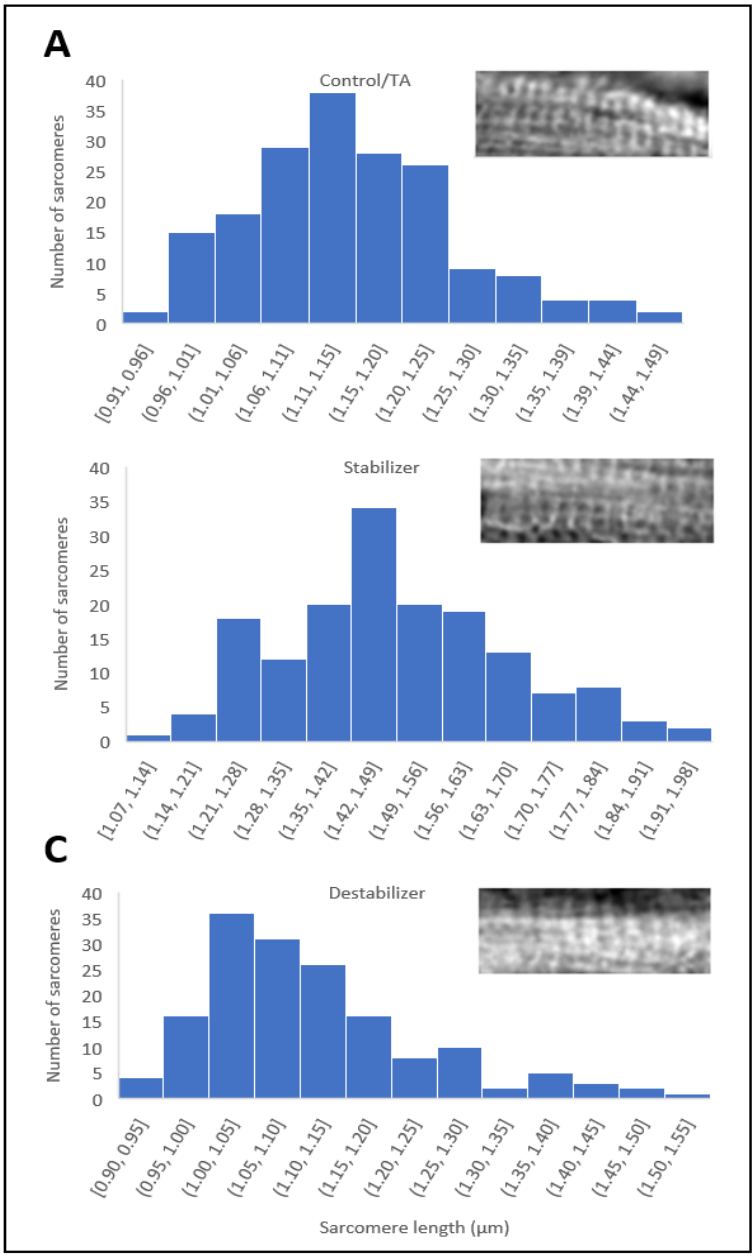

Figure 37: **Sarcomere lengths distribution among the measured sarcomeres from mice injected with tannic acid (control), labeled stabilizer, and labeled destabilizer peptides.**

A: The distribution of 184 sarcomeres from DIC images of cardiac tissue from mouse injected with tannic acid was measured with an average of 1.15 ± 0.108 micron (p-value =0.01 from chi- squared test). B: The distribution of 160 sarcomeres from DIC images of cardiac tissue from mouse injected with labeled stabilizer peptide were measured with an average of 1.48 ± 0.173 micron (p-value =0.09, from chi-squared test indicating normal distribution). The microscopic image on the right shows a wider I-band as the myofibril was extended. C: Distribution of 160 sarcomeres from DIC images of cardiac tissue from mouse injected with labeled destabilizer peptide were measured with an average of 1.11 ± 0.120 micron (p-value < 0.005 from chi- squared test). The microscopic image on the right shows a wider A-band as the myofibril was relatively contracted. Images dimensions are 19.5x7.8 microns.

The estimated sarcomere lengths indicated that peptides' effects on mice hearts are dose and time dependent. For example, if the hearts were extracted after 6 hours of the injection, they probably would indicate different sarcomere lengths. Injecting more mice with various concentrations of labeled and unlabeled peptides and extracting the hearts at different times will provide more accurate data about the effect of the peptides on cardiac tissue as will be performed very soon.

5.5 Conclusion

Tannic acid seems to aid anti-S2 peptides reaching the mice's hearts after intravenous injection. The injected 0.1 mM fluorescently labeled peptides were detected in the heart tissue using epifluorescence and confocal microscopes. The amount of destabilizer peptide that reached the heart was approximately 6X more than the stabilizer peptide. It is possible that some of the peptides were degraded by the proteases of the blood (112). This provokes the search to improve the stability of the administered peptides to reduce their potential for degradation.

Super-resolution microscopy images showed labeled peptides bound to the coronary arterioles before they entered the cardiac tissues, while some labeled destabilizer peptides bound to the T-tubules. Some A-bands within the cardiomyocyte sarcomeres were also detected and labeled with the conjugated peptides. The average sarcomere length calculated from cardiac tissue extracted after 24 hours from labeled stabilizer peptide injection indicated longer sarcomeres than control. However, with labeled destabilizer, the average sarcomere length was slightly shorter than the control.

The anti-S2 peptides demonstrated promising results, which may qualify them to be tested as therapeutic drugs in treating cardiomyopathies in the future. However, further trials are needed to optimize the dose, the frequency, and the administration method of the peptides into the body

to obtain the desired effect. The sequence of the amino acids of the peptides might be adjusted to have a more potent effect and/or to protect them from degradation.

CHAPTER 6

DISCUSSION AND CONCLUSION

Even though myosin thick filaments have identical sequence, yet each can be present in a different state (113). During muscle contraction, one of the myosin heads stays in the folded state, stabilizing the free head and alternating between the folded and free states (114). Myosin S2 has a significant role in stabilizing the folded head by interacting with it. Some mutations in the cardiac myosin S2 disrupt the stability of the folded head, leading to hypertrophic cardiomyopathies. This invoked the idea of designing synthetic peptides to reach the heart and modulate its contraction. The destabilizer peptide simulated the mutation's effect in destabilizing myosin heads to increase muscle contraction, and the stabilizer worked on reducing muscle contraction.

Anti-S2 peptides, the stabilizer and destabilizer, were appended to tannic acid to allow them to reach the heart and interfere with cardiac contractility. The 19 residues destabilizer peptide was designed to have a similar sequence to myosin S2 except in a few residues, which were replaced with other residues to allow the peptide to bind to the myosin S2 monomer stronger than the other monomer, thus disrupting the dimer formation. Therefore, when two destabilizer peptides bind to the myosin S2 dimer, the heads stay in the ON state endorsing muscle contraction. However, the stabilizer peptide is a 17 residues synthetic peptide composed mostly of positively charged amino acids that recognize the negative amino acids on myosin S2 and potentially wraps around it, thus stabilizing the OFF state.

Both the stabilizer and destabilizer peptides were tested using dynamic and mechanical computational simulation to detect the nature of binding with myosin S2 (102). The stabilizer was able to induce 9 times more stability on the E930del mutated myosin according to the mechanical

simulation data. While the destabilizer binding force to the myosin was 3 times stronger than the myosin dimerization force, inducing instability in the dimer.

Anti-S2 peptides were tested using different assays like gravitational force spectroscopy (GFS), fluorescence resonance energy transfer (FRET), fluorescence anisotropy, in vitro motility assay, and many other experiments. For example, the FERT assay proved that the stabilizer peptide had a lower lifetime and the destabilizer peptide had a higher lifetime in myosin S2 from striated muscle (115).

The amount of sarcomere shortening in myofibrils after the addition of ATP was assessed in the presence and absence of the anti-S2 peptides. The sarcomeres with the stabilizer peptide displayed longer sarcomeres compared to the control, meaning that it induced muscle relaxation. However, the sarcomeres treated with the destabilizer peptide had an increase in sarcomere shortening due to the increase in muscle contraction (116).

In this study, the anti-S2 peptides were further tested using spectroscopic and microscopic experiments. The MF20, MF30, and polyclonal antibodies that bind to LMM or myosin S2 were used to simulate myosin mutations, and they helped in understanding the binding of the synthetic peptides to myosin S2. MF20 was used as a control in some experiments, while it was also used to validate the expansion microscopy technique.

6.1 Anti-S2 Peptides/Antibodies Bind to Myosin S2 with High Affinity

The change in the anisotropy reading confirmed the binding of the stabilizer and destabilizer peptide to myosin S2. The myosin dimer is almost 100X heavier than the anti-S2 peptide, therefore, when it was added to the fluorescently labeled peptides, it reduced peptides rotation in the solution causing an increase in the anisotropy reading.

Fluorescence anisotropy and TIRFS showed that fluorescently labeled anti-S2 peptides and

antibodies have a high affinity to myosin. However, previous work in the lab estimated the peptides' affinity to myosin using cELISA to be higher when unlabeled, meaning that the fluorescent labeling of the peptides reduces their affinity to myosin (116).

The addition of anti-S2 peptides or antibodies to myosin stabilized the unfolded myosin upon binding, and they also shifted some of the unbound myosin from the folded into the unfolded state to maintain the equilibrium between the two states. This was extrapolated from the binding graphs that favored the sigmoidal fitting over the hyperbolic fitting. On the other hand, when myosin was added to the anti-S2 peptides or antibodies, the folded and unfolded states of myosin stayed in equilibrium, and no shifting was noticed in fluorescence anisotropy.

Based on the concerted and sequential equations, MF30 and destabilizer peptide bind cooperatively to myosin, which means binding the antibody or the peptide to myosin S2 breaks up the dimer, thus allowing more antibodies or peptides to bind. The stabilizer peptide displayed cooperative binding too, the way the peptide wraps around myosin S2 possibly affects stabilizing the OFF state, which probably causes disruption to the interacting heads motifs in the filament and makes other myosins S2 accessible for more peptides.

6.2 Anti-S2 Peptides Modulate Myosin S2 Helicity

As the stabilizer peptide wraps around the wild type myosin, it stabilizes and improves the helicity of the coiled-coil. It was found that only one stabilizer peptide binds to the wt myosin. However, two stabilizer peptides are needed in the mutated cardiac myosin with E930del to stabilize it and improve the helical content of the myosin dimer. Meanwhile, the destabilizer peptide unzipped the cardiac myosin S2 coiled-coil reducing the helical content of S2, and it was found that 2 destabilizer peptides were needed to disrupt the helicity, one peptide at each strand.

Destabilizer peptides binding to myosin are thought to stabilize the unfolded state despite reducing the helicity of that segment.

6.3 Expansion Microscopy Disclosed Anti-S2 Peptides and Antibodies Staining Patterns in Myofibril

Expansion microscopy images for sarcomeres stained with MF20 revealed a similar staining pattern as other super-resolution photolocalization and Airyscan microscopic images. Expanded images of MF20 and MF30 revealed strong labeling of the P-zones next to the M-line in the middle of the sarcomere, then gradually decreased fluorescent intensity toward the edges of the A-band at the D-zone. This pattern of staining is believed to be due to the rigor condition of the myofibrils, where myosin and actin overlap and extend through the D-, C-, and parts of P-zones in the A-band. Myosin S2 accessibility was reduced at the overlapped region due to myosin heads binding to actin filament, leading to reduced labeling in this area.

The reduction in the fluorescence intensity at the C-zone was more distinct with MF30 than MF20 due to the competition with MyBPC. MF30 and MF20 competed with MyBPC to bind at myosin S2 and at the N-terminus of LMM, respectively. This competition was more distinct in dual and triple-labeled myofibrils; the more antibodies used, the more decrease in the fluorescent intensity at the C-zone detected. This competition was further confirmed when ablated MyBPC cardiac tissue labeled with MF30 revealed labeling for the A-band without reduction at the C-zone. This supports the notion that MyBPC blocks the C-zone and competes with the antibody/peptide preventing them from binding.

The stabilizer and destabilizer peptides labeled the P-zone strongly with a gradual decrease in the fluorescent intensity toward the edges of the A-band. Peptides labeling were reduced at the C-zone due to S2 blockage by MyBPC. The stabilizer peptide has a slight increase in the fluorescent intensity at the edge of the D-zone. This increase can be explained by the effect of the

stabilizer peptide in relaxing sarcomeres, reduction in actin-myosin interdigitation leaves more myosin S2 available for the stabilizer peptide to bind.

6.4 Stabilizer Staining Pattern is Affected by Myofibril Dual Labeling

The staining pattern of the stabilizer peptide was altered when the myofibril was dual labeled with stabilizer and destabilizer or anti-titin. Even though the stabilizer has a higher affinity to myosin S2 than the destabilizer peptide, the destabilizer design complements the myosin S2 strand and binds more specifically to it. The destabilizer peptide competed with the stabilizer peptide that blocked some areas within the A-band resulting in a different staining pattern from the stabilizer alone. Titin also possibly has epitopes where the stabilizer peptide recognizes and binds. This conviction was observed from the reduction in the labeling of the stabilizer peptide when the myofibril was dual labeled with anti-titin. On the other hand, myofibril double labeled with MF20 did not affect the staining pattern of the stabilizer peptide since the antibody binds to the LMM, not on S2, where the stabilizer peptide binds.

The destabilizer peptide staining pattern was not affected when the myofibril was dual labeled with the stabilizer peptide or anti-titin, suggesting that the presence of the stabilizer peptide did not affect the destabilizer binding and that the destabilizer does not interact with titin in myofibrils.

6.5 Anti-Titin Labeling Band Increased by Increasing Sarcomere Length and Altered by the Addition of MF30 and Anti-S2 Peptides

When a muscle sarcomere relaxes, titin extends by “springs” uncoiling along the sarcomere. The anti-titin that was used in this experiment has epitopes against the titin that is closer to the M-line. It was extrapolated from expansion microscopy images that the anti-titin band

increased by increasing sarcomere length, which suggests that titin epitopes move apart as the sarcomere relaxes.

It was observed that the destabilizer peptide did not alter the anti-titin staining pattern or the length of the labeling band in the dual-labeled myofibril. On the other hand, dual-labeling with stabilizer peptide affected both, and dual labeling with MF30 affected the length of the labeling band, not the staining pattern of anti-titin.

6.6 Anti-S2 Peptides In vivo Trials Reached the Heart and Labeled Some Sarcomeres

Intravenous injection of fluorescently labeled or unlabeled anti-S2 peptides into mice circulation traveled with the blood to reach the coronary arteries and arterioles of the heart; then they diffused through the capillaries into the extracellular matrix of the cardiomyocytes.

The fluorescently labeled peptides from the heart slices were detected through epifluorescence and confocal microscopes. The autofluorescence was estimated from the control heart of a mouse injected with tannic acid. The estimated fluorescence in the cardiac tissues after labeled peptides injection was higher than that from the control, confirming the presence of the peptides in the heart tissues.

Almost a third of the injected labeled destabilizer peptide reached the heart of the mouse, which is 6 times more than the labeled stabilizer peptide. The labeled peptides were found bound to some cardiac blood vessels as they diffused through them into the extracellular matrix, then to the sarcomeres, where they labeled some of the A-bands in the cardiac muscle sarcomeres. In addition, the labeled destabilizer peptide labeled some T-tubules within the cardiac tissue. This finding suggests a possible path of the peptides within the T-tubules before reaching the sarcomeres. It is also possible that the T-tubules have an antigen that the peptides recognized and bound to.

Echocardiography results indicated that the fluorescently labeled destabilizer peptide caused a statistically significant increase in cardiac output after 24 hours from the injection compared to the pre-injection level. However, no significant increase was noticed with the unlabeled destabilizer peptide (unpublished data). It is possible that the fluorophore protected the peptide from degradation inside the body; therefore, modifying the destabilizer peptide by capping it might protect the peptide from degradation before reaching the heart. The unlabeled stabilizer peptide caused a significant decrease in the stroke volume in 24 hours that was compensated by an increase in the heart rate resulting in no significant change in the cardiac output.

6.7 Labeled Peptides Effect on Sarcomere Lengths in Live Mice Cardiac Tissue

The stabilizer peptide is believed to stabilize the OFF-state myosin heads, making them unavailable for actin filament. When myosin heads are blocked, muscle contraction is reduced, leading to an extended sarcomere. The sarcomere lengths were measured in cardiac tissue extracted after 24 hours from injecting labeled stabilizer peptide, and it was found that the average sarcomere length was longer than the average length of the sarcomere from the control heart tissue suggesting the possible effect of stabilizer in relaxing cardiomyocyte.

On the other hand, labeled destabilizer peptide caused a slight shortening in cardiac sarcomere after 24 hours from the injection compared to the control, but not in the longer term. It is possible that the half-life of the destabilizer peptide is not long enough to promote muscle contraction after 24 hours, or maybe the injected dose was insufficient to induce cardiac muscle contraction.

6.8 Conclusion

Anti-S2 peptides and antibodies (MF20 and MF30) were determined to bind cooperatively with high affinity to myosin based on their binding graphs from TIRFS. As the destabilizer peptide

was designed to disrupt myosin stability by breaking S2 coiled-coil, absorbance spectroscopy indicated that the destabilizer peptide reduced the helical content of the synthetic myosin S2 by 14%. However, when the stabilizer peptide wrapped around myosin S2, it improved the helical content of the coiled-coil by 24% in wt myosin.

Expansion microscopy determined the binding sites of the fluorescently labeled anti-S2 peptides and antibodies in skeletal and cardiac myofibrils with high resolution. MyBPC prevented anti-S2 peptides and antibodies from binding to myosin at the C-zone. The competition between anti-myosin and MyBPC was further confirmed using cardiac tissue lacking MyBPC. MF30-labeled KO cardiac myofibril revealed intense labeling for the A-band without reduction at the C-zone, this finding indicated that MyBPC presence blocks the anti-myosin peptide from the C-zone. Anti-S2 peptides interaction with titin was also studied using an anti-titin antibody; It was noticed that the stabilizer labeling pattern in skeletal myofibril was affected by the presence of anti-titin; meanwhile, the destabilizer labeling pattern was not affected by anti-titin. Therefore, the possible interaction between stabilizer peptide and titin is expected, which might interfere with muscle contraction.

Anti-S2 peptides coupled with tannic acid were able to reach the heart in live mice after IV injections. Even though not all of the injected peptides reached inside the cardiomyocytes, they were able to alter the physiological function of the hearts. The amount of the destabilizer peptide that reached the heart after 24 hours from the injection was 6X higher than the stabilizer peptides. It was noticed that the anti-S2 peptides labeled some cardiomyocyte sarcomeres, T-tubules, and cardiac arterioles, which brings up the speculation about their route before reaching into the cardiomyocytes. Sarcomere length measured after 24 hours of injecting labeled stabilizer peptide revealed a more extended sarcomere than the control, however, slightly contracted sarcomeres

after destabilizer peptide injection was observed. Optimizing the administration methods of the peptides, dosage, and frequency, in addition to peptides' protection from degradation before reaching the heart make the peptides a promising drug in treating cardiomyopathies' diseases and saving lives.

I hypothesize that both the anti-S2 peptides and antibodies bind to myosin S2 with high affinity, compete with MyBPC, and possibly interact with titin, in which case the anti-S2 peptides have further impact on myosin helicity and reach the heart with the aid of tannic acid to modulate cardiomyocytes' contraction in live mice

Anti-S2 peptide bind to myosin S2

Fluorescence anisotropy

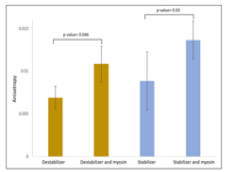

MF30 and polyclonal antibodies bind to the flexible S2, however MF20 binds to the LMM.
Anti-S2 peptides binding to myosin S2 extrapolated from the increase in anisotropy reading due to binding to the heavier myosin dimer slowing their rotation.

Anti-S2 peptides alter myosin dimer helicity

UV-absorbance spectroscopy

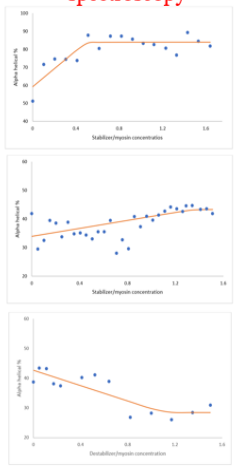

Stabilizer peptide increased myosin dimer helicity in wildtype and mutated synthetic myosin (1 peptide/dimer in wildtype and 2 peptides/dimer in mutated myosin).
Destabilizer peptide reduced myosin dimer helicity in synthetic cardiac myosin when 2 peptides bind to the dimer.

Anti-S2 peptides and antibodies have high affinity to myosin S2

Fluorescence spectroscopy

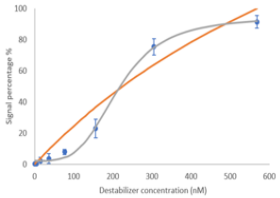

Fluorescently labeled anti-S2 peptides and antibodies bind to myosin with high affinity in the nanomolar range in a cooperative manner as indicated from the favorable sigmoidal fitting model and proved with the sequential and concerted equations.

Reagent (Sigmoidal fitting)	Kd (nM)
MF20	86.4 ±13
MF30	26.1 ±0.7
Stabilizer	55 ±3.3
Destabilizer	214 ±9.18

Anti-S2 peptides and antibodies compete with MyBPC and possibly interact with titin

Expansion microscopy

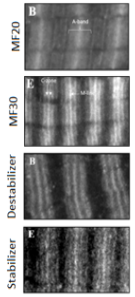

Fluorescently labeled anti-S2 peptides and antibodies labeled the P-zone strongly in skeletal myofibrils.
Decrease in the fluorescent intensities at the C-zone due to the competition with MyBPC.
Reduced labeling of the C- and D-zones are due to blocking myosin S2 during the rigor condition of the myofibrils.

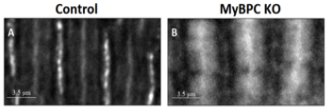

MyBPC ablation caused labeling for the whole A-band with no reduction at the C-zone compared to the control.

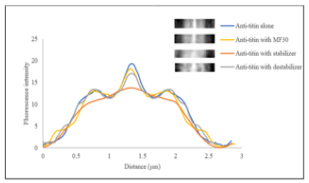

Anti-titin staining pattern was affected by the presence of stabilizer peptide. Possible binding of the stabilizer peptide to titin created this competition.
Anti-titin labeling band increased by increasing sarcomere length and affected by MF30 and stabilizer peptide presence.

Tannylated anti-S2 peptides reach the heart in live mice and modulate cardiomyocyte contraction

Fluorescence microscopy

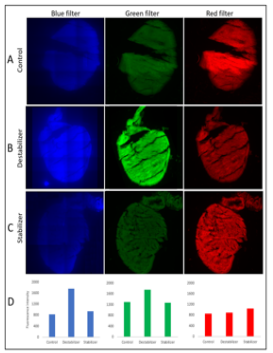

Fluorescently labeled anti-S2 peptides bound to tannic acid reached the mice hearts after IV injection. The peptides were detected with the epi-fluorescence and confocal microscopes after 24 hours of the injection.

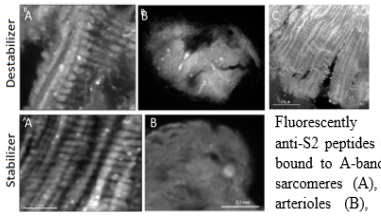

Fluorescently labeled anti-S2 peptides detected bound to A-band of the sarcomeres (A), cardiac arterioles (B), and T-tubules (C).

Sample	Sarcomere length average (micron)	n
Control/TA	1.15 ± 0.108	184
Stabilizer peptide	1.48 ± 0.173	160
Destabilizer peptide	1.11 ± 0.120	160

The average sarcomere length in cardiac tissue extracted after 24 hours from labeled stabilizer peptide injection indicated longer sarcomeres compared to the control. However, the average sarcomere length was slightly shorter with labeled destabilizer than the control.

REFERENCES

1. K. A. Clark, A. S. McElhinny, M. C. Beckerle, and C.C.G. 2002. Striated muscle cytoarchitecture: an intricate web of form and function. Annu. Rev. Cell Dev. Biol. 18:637–706.

2. Coffee Castro-Zena, P.G., and D.D. Root. 2013. Asymmetric myosin binding to the thin filament as revealed by a fluorescent nanocircuit. Arch. Biochem. Biophys. 535:14–21.

3. Linari, M., G. Piazzesi, I. Dobbie, N. Koubassova, M. Reconditi, T. Narayanan, O. Diat, M. Irving, and V. Lombardi. 2000. Interference fine structure and sarcomere length dependence of the axial x-ray pattern from active single muscle fibers. PNAS. 97:7226–7231.

4. Ojima, K., M. Oe, I. Nakajima, M. Shibata, S. Muroya, K. Chikuni, A. Hattori, and T. Nishimura. 2015. The importance of subfragment 2 and C-terminus of myosin heavy chain for thick filament assembly in skeletal muscle cells. Anim. Sci. J. 86:459–467.

5. Al-khayat, H.A. 2013. Three-dimensional structure of the human myosin thick filament : clinical implications. Glob. Cardiol. Sci. Pract. 36:283–302.

6. Herrel, A., J.J. Meyers, J. Timmermans, and K.C. Nishikawa. 2002. Review supercontracting muscle : producing tension over extreme muscle lengths. J. Exp. Biol. 205:2167–2173.

7. Jin, Y., L. Wei, W. Cai, Z. Lin, Z. Wu, Y. Peng, T. Kohmoto, R.L. Moss, Y. Ge, R. Biology, C. Pharmacology, T. Program, and P. Program. 2018. Complete characterization of cardiac myosin heavy chain (223 kDa) enabled by size-exclusion chromatography and middle- down mass spectrometry. Anal. Chem. 89:4922–4930.

8. Sugi, H., T. Kobayashi, T. Gross, K. Noguchi, T. Karr, and W.F. Harrington. 1992. Contraction characteristics and ATPase activity of skeletal muscle fibers in the presence of antibody to myosin subfragment 2. Proc. Natl. Acad. Sci. 89:6134–6137.

9. Esaki, S., Y. Ishii, M. Nishikawa, and T. Yanagida. 2007. Cooperative actions between myosin heads bring effective functions. BioSystems. 88:293–300.

10. Root, D.D., V.K. Yadavalli, J.G. Forbes, and K. Wang. 2006. Coiled-coil nanomechanics and uncoiling and unfolding of the superhelix and α-helices of myosin. Biophys. J. 90:2852–2866.

11. Alamo, L., J.S. Ware, A. Pinto, R.E. Gillilan, J.G. Seidman, C.E. Seidman, and R. Padrón. 2017. Effects of myosin variants on interacting-heads motif explain distinct hypertrophic and dilated cardiomyopathy phenotypes. Elife. 6:1–31.

12. Consuelas, V.A.; Minas, D.J. 2012. Actin: structure, functions and disease. .

13. Otterbein, L.R., P. Graceffa, and R. Dominguez. 2001. The crystal structure of uncomplexed actin in the ADP state. Science. 293:708–711.

14. Ricca, B.L., and R.S. Rock. 2010. The stepping pattern of myosin X is adapted for processive motility on bundled actin. Biophys. J. 99:1818–1826.

15. Rode, C., T. Siebert, A. Tomalka, R. Blickhan, and C. Rode. 2016. Myosin filament sliding through the Z-disc relates striated muscle fibre structure to function. R. Soc. 283:10–13.

16. Kremneva, E., M.H. Makkonen, A. Skwarek-maruszewska, G. Gateva, and A. Michelot. 2014. Cofilin-2 Controls Actin Filament Length in Muscle Sarcomeres. Dev. Cell. 31:215–226.

17. Tu, D., Y. Li, H.K. Song, A. V Toms, C.J. Gould, S.B. Ficarro, D. Tu, Y. Li, H.K. Song, A. V Toms, C.J. Gould, S.B. Ficarro, J.A. Marto, B.L. Goode, and M.J. Eck. 2011. Crystal structure of a coiled-coil domain from human ROCK I. Public Libr. Sci. 6.

18. Lehman, W., D.J. Manstein, P.A. Penczek, S. Raunser, and M. Mu. 2015. Structure of the F-actin– –tropomyosin complex ¨. Nature. 519:114–132.

19. Gunning, P.W., and E.C. Hardeman. 2017. Tropomyosins. Curr. Biol. 27:8–13.

20. Gomes, A. V, J.D. Potter, and D. Szczesna-cordary. 2002. The role of troponins in muscle contraction. IUBMB Life. 54:323–333.

21. Parvatiyar, M.S., J.R. Pinto, D. Dweck, and J.D. Potter. 2010. Cardiac Troponin Mutations and Restrictive Cardiomyopathy. J. Biomed. Biotechnol. 2010:1–9.

22. Sadayappan, S., and P.P. De Tombe. 2014. Cardiac myosin binding protein-C as a central target of cardiac sarcomere signaling: A special mini review series. Pflugers Arch. Eur. J. Physiol. 466:195–200.

23. Craig, R., K.H. Lee, Y. Ji, I. Torre, and P.K. Luther. 2014. Structure , sarcomeric organization , and thin filament binding of cardiac myosin-binding protein-C. Pflügers Arch. - Eur. J. Physiol. 466:425–431.

24. Kampourakis, T., Z. Yan, M. Gautel, Y.-B. Sun, and M. Irving. 2014. Myosin binding protein-C activates thin filaments and inhibits thick filaments in heart muscle cells. Proc. Natl. Acad. Sci. 111:18763–18768.

25. Colegrave, M., and M. Peckham. 2014. Structural implications of β-cardiac myosin heavy chain mutations in human disease. Anat. Rec. 297:1670–1680.

26. Li, A., S.R. Nelson, S. Rahmanseresht, F. Braet, A.S. Cornachione, S.B. Previs, T.S. O'Leary, J.W. McNamara, D.E. Rassier, S. Sadayappan, M.J. Previs, and D.M. Warshaw. 2019. Skeletal MyBP-C isoforms tune the molecular contractility of divergent skeletal muscle systems. Proc. Natl. Acad. Sci. U. S. A. 116:21882–21892.

27. Masum, M.M., M.A. Al Sayeef, R. Shahrear, D. Banik, G. Biswas, and Z.A. Yesmin. 2019. Hypertrophic cardiomyopathy: The molecular genetics. Faridpur Med. Coll. J. 14:44–49.

28. Mcnamara, J.W., A. Li, N.J. Smith, S. Lal, R.M. Graham, K. Bezold, S.J. Van Dijk, G. Cristobal, S.P. Harris, and R. Cooke. 2016. Ablation of cardiac myosin binding protein-C disrupts the super-relaxed state of myosin in murine cardiomyocytes. J. Mol. Cell. Cardiol. 94:65–71.

29. Tskhovrebova, L., and J. Trinick. 2003. Titin: Properties and family relationships. Nat. Rev. Mol. cell Biol. 4:679–689.

30. Herzog, W., M. Duvall, and T.R. Leonard. 2012. Molecular mechanisms of muscle force regulation : A role for titin ? Am. Coll. Sport. Med. 40:50–57.

31. Martin M. LeWinter, and H.G. 2010. Cardiac titin - A multifunctional giant. Circ. J. 121:2137–2145.

32. Opitz, C.A., M. Kulke, M.C. Leake, C. Neagoe, H. Hinssen, R.J. Hajjar, and W.A. Linke. 2003. Damped elastic recoil of the titin spring in myofibrils of human myocardium. PNAS. 100:12688–12693.

33. Fabiato, A. 1983. Calcium-induced release of calcium from the cardiac sarcoplasmic reticulum. Am. J. Physiol. 245:C1–C14.

34. Gomes, A. V, J.D. Potter, and D. Szczesna-cordary. 2002. The role of troponins in muscle contraction. IUBMB Life. 54:323–333.

35. Molloy, J.E. 2005. Muscle contraction: actin filaments enter the fray. Biophys. J. 89:1–2.

36. Huxley, A.F. 2000. Cross-bridge action : present views , prospects , and unknowns. J. Biomech. 33:1189–1195.

37. Warning, N., and C. Copyright. 1989. Complete amino-acid sequence of subfragment-2 in adult chicken skeletal muscle myosin. Biol Chem Hoppe Seyler. 370:1027–1034.

38. Kawana, M., S.S. Sarkar, S. Sutton, K.M. Ruppel, and J.A. Spudich. 2017. Biophysical properties of human b -cardiac myosin with converter mutations that cause hypertrophic cardiomyopathy. Sci. Adv. 3:1–11.

39. Lu, R.C., and A. Wong. 1985. The amino acid sequence and stability predictions of the hinge region in myosin subfragment 2. J. Biol. Chem. 260:3456–3461.

40. Gundapaneni, D., J. Xu, and D.D. Root. 2005. High flexibility of the actomyosin crossbridge resides in skeletal muscle myosin subfragment-2 as demonstrated by a new single molecule assay. J. Struct. Biol. 149:117–126.

41. McNamara, J.W., R.R. Singh, and S. Sadayappan. 2019. Cardiac myosin binding protein-C phosphorylation regulates the super-relaxed state of myosin. Proc. Natl. Acad. Sci. U. S. A. 116:11731–11736.

42. Irving, M. 2017. Regulation of contraction by the thick filaments in skeletal muscle. Biophys. J. 113:2579–2594.

43. Woodhead, J.L., F. Zhao, R. Craig, E.H. Egelman, and L. Alamo. 2005. Atomic model of a myosin filament in the relaxed state. Nature. 436:1195–1199.

44. Blankenfeldt, W., N.H. Thomä, J.S. Wray, M. Gautel, and I. Schlichting. 2006. Crystal structures of human cardiac β-myosin II S2-Δ provide insight into the functional role of the S2 subfragment. Proc. Natl. Acad. Sci. U. S. A. 103:17713–17717.

45. Gruen, M., and M. Gautel. 1999. Mutations in b -myosin S2 that cause familial hypertrophic cardiomyopathy (FHC) abolish the interaction with the regulatory domain of myosin-binding protein-C. J. Mol. Biol. 286:933–949.

46. Richard, P., P. Charron, L. Carrier, C. Ledeuil, T. Cheav, C. Pichereau, A. Benaiche, R. Isnard, O. Dubourg, M. Burban, J. Gueffet, A. Millaire, M. Desnos, K. Schwartz, B. Hainque, M. Komajda, E. Del, and E. Del. 2003. Hypertrophic cardiomyopathy: distribution of disease genes, spectrum of mutations, and implications for a molecular diagnosis strategy. Circulation. 107:2227–2232.

47. Spudich, J.A. 2015. The myosin mesa and a possible unifying hypothesis for the molecular basis of human hypertrophic cardiomyopathy. Biochem. Soc. Trans. 43:64–72.

48. Parvari, R., and A. Levitas. 2012. The mutations associated with dilated cardiomyopathy. Biochem. Res. Int. 2012.

49. Singh, R.R., J.W. McNamara, and S. Sadayappan. 2021. Mutations in myosin S2 alter cardiac myosin-binding protein-C interaction in hypertrophic cardiomyopathy in a phosphorylation-dependent manner. J. Biol. Chem. 297.

50. Harvey, P.A., and L.A. Leinwand. 2011. Cellular mechanisms of cardiomyopathy. J. Cell Biol. 194:355–365.

51. Maron, B.J., and M.S. Maron. 2013. Hypertrophic cardiomyopathy. Lancet. 381:242–255.

52. Towbin, J.A. 2010. Hypertrophic Cardiomyopathy. October. 32:23–32.

53. Perry Elliott, W.J.M., and Hypertrophic. 2010. Hypertrophic cardiomyopathy. Seminar. 363:1881–1892.

54. Tominaga, M., A. Matsumori, I. Okada, T. Yamada, and C. Kawai. 1991. β-blocker treatment of dilated cardiomyopathy: Beneficial effect of carteolol in mice. Circulation. 83:2021–2028.

55. Rosing, D.R., U. Idänpään-Heikkilä, B.J. Maron, R.O. Bonow, and S.E. Epstein. 1985. Use of calcium-channel blocking drugs in hypertrophic cardiomyopathy. Am. J. Cardiol. 55.

56. WEAVER, W.D., D. HILL, C. FAHRENBRUCH, M. COPASS, J. MARTIN, L. COBB, and A. HALLSTROM. 1988. Use of the automatic external defibrillator in the management of out-of-hospital cardiac arrest. N. Engl. J. Med. 319:184.

57. Chanpimol, S., B. Seamon, H. Hernandez, M. Harris-love, and M.R. Blackman. 2017. The myosin mesa and the basis of hypercontractility caused by hypertrophic cardiomyopathy mutations. Nat. Struct. Mol. Biol. 24:525–533.

58. Brown, J. H., Yang, Y., Reshetnikova, L., Gourinath, S., Süveges, D., Kardos, J., Hóbor, F., Reutzel, R., Nyitray, L., & Cohen, C. 2008. An unstable head-rod junction may promote folding into the compact off-state conformation of regulated myosins. J. Mol. Biol. 24:1434–1443.

59. Shin, M., H.A. Lee, M. Lee, Y. Shin, J.J. Song, S.W. Kang, D.H. Nam, E.J. Jeon, M. Cho, M. Do, S. Park, M.S. Lee, J.H. Jang, S.W. Cho, K.S. Kim, and H. Lee. 2018. Targeting protein and peptide therapeutics to the heart via tannic acid modification. Nat. Biomed. Eng. 2:304–317.

60. Hass, A.F.S. and G.M. 1949. A new method for isolation and purification of mammalian striated myofibrils. Science (80-.). 109:486–487.

61. Perry, S. V. 1951. The adenosinetriphosphatase activity of myofibrils isolated from skeletal muscle. Biochem. J. 48:257–65.

62. Harris, S.P., C.R. Bartley, T.A. Hacker, K.S. McDonald, P.S. Douglas, M.L. Greaser, P.A. Powers, and R.L. Moss. 2002. Hypertrophic cardiomyopathy in cardiac myosin binding protein-C knockout mice. Circ. Res. 90:594–601.

63. Godt, R.E., and B.D. Lindley. 1982. Influence of temperature upon contractile activation and isometric force production in mechanically skinned muscle fibers of the frog. J. Gen. Physiol. 80:279–297.

64. Godfrey, J.E., and W.F. Harrington. 1970. Self-association in the myosin system at high ionic strength. I. sensitivity of interaction to pH and ionic environment. Biochemistry. 9:894–908.

65. Smith, B.J. 1984. SDS Polyacrylamide gel electrophoresis of proteins. In: Proteins. Methods in molecular biology. . pp. 41–56.

66. Jeremy M. Berg, John L. Tymoczko, Gregory J. Gatto, L.S. 2015. Biochemistry. 8th ed. New York: .

67. Begum, H., P. Murugesan, and A.D. Tangutur. 2022. Western blotting: A powerful staple in scientific and biomedical research. Biotechniques. 73:59–69.

68. Mahmood, T., and P.C. Yang. 2012. Western blot: Technique, theory, and trouble shooting. N. Am. J. Med. Sci. 4:429–434.

69. Root, D.D., and E. Reisler. 1989. Copper iodide staining of protein blots on nitrocellulose membranes. Anal. Biochem. 181:250–253.

70. Groves, W.E., F.C. Davis, and B.H. Sells. 1968. Spectrophotometric determination of microgram quantities of protein without nucleic acid interference. Anal. Biochem. 22:195–210.

71. L.Lang. 1969. Absorbance spectra in the Ultraviolet and visible range. J. Mol. Struct. 4:335–340.

72. Faassen, S.M., and B. Hitzmann. 2015. Fluorescence spectroscopy and chemometric modeling for bioprocess monitoring. Sensors (Switzerland). 15:10271–10291.

73. Ashutosh Sharma, S.G.S. 1999. Introduction to fluorescence spectroscopy. New York: Wiley: .

74. Beaven, G.H., and E.R. Holiday. 1952. Ultraviolet absorption spectra of proteins and amino acids. Adv. Protein Chem. 7:319–386.

75. María Florencia Pignataro, M.G.H. 2020. Evaluation of peptide / protein self-assembly and aggregation by spectroscopic methods. Molecules. 25:121–140.

76. Clore, G. Marius; Gronenborn, A.M. 1989. Determination of three-dimensional structures of proteins and nucleic acids in solution by nuclear magnetic resonance spectroscopy. Crit. Rev. Biochem. Mol. Biol. 24:479–564.

77. Academy, N., N. Academy, and U. States. 1961. The far ultraviolet absorption spectra of polypeptide and protein solutions and their dependence on conformation. Proc. Natl. Acad. Sci. 47:1775–1785.

78. Steiner, R.F. 2002. Fluorescence anisotropy: Theory and applications. Boston, MA: .

79. Zhang, H., Q. Wu, and M.Y. Berezin. 2015. Fluorescence anisotropy (polarization): from drug screening to precision medicine. Expert Opin Drug Discov. 10:1145–1161.

80. Yikun Chen, Yongxin Gao, Yujun He, Gang Zhang, Hui Wen, Yuchen Wang, Qin-Pei Wu, and H.C. 2021. Determining essential requirements for fluorophore selection in various fluorescence applications taking advantage of diverse structure–fluorescence information of chromone derivatives. J. Med. Chem. 64:1001–1017.

81. Heyduk, T., Y. Ma, H. Tang, and R.H. Ebright. 1996. Fluorescence anisotrophy: Rapid, quantitative assay for protein-DNA and protein-protein interaction. Methods Enzymol. 274:492–503.

82. Burke, T.J.; Loniello, K.R.; Beebe, J.A.; Ervin, K.M. 2003. Development and application of fluorescence polarization assays in drug discovery. Comb. Chem. High Throughput Screen. 6:183–194.

83. Gradinaru, C.C., D.O. Marushchak, M. Samim, and U.J. Krull. 2010. Fluorescence anisotropy: From single molecules to live cells. Analyst. 135:452–459.

84. Gijsbers, A., T. Nishigaki, and N. Sánchez-puig. 2016. Fluorescence anisotropy as a tool to study protein-protein interactions. J. Vis. Exp. 116:1–9.

85. Jameson;, D.M.. J.A.R. 2010. Fluorescence polarization/anisotropy in diagnostics and imaging. Chem. Rev. 110:1–54.

86. Lakowicz, J.R. 2006. Principles of fluorescence spectroscopy. Boston, MA: .

87. Jameson, D.M., and W.H. Sawyer. 1995. Fluorescence anisotropy applied to biomolecular interactions. Methods Enzymol. 246:283–300.

88. Yguerabide, J., H.F. Epstein, and L. Stryer. 1970. Segmental flexibility in an antibody molecule. J. Mol. Biol. 51:573–590.

89. Valeur, B. 2001. Molecular fluorescence: Principles and applications. .

90. Gelen, F., M. Butz, E.J. Rees, M. Erdelyi, T. Moschetti, M. Hyvonen, J.B. Edel, C.F. Kaminski, and F. Hollfelder. 2017. Quantitative affinity determination by fluorescence anisotropy measurements of individual nanoliter droplets. Anal. Chem. 89:1092–1101.

91. Hoyt, L.F. 1934. New table of the refractive index of pure glycerol at 20° C. Ind. Eng. Chem. 26:329–332.

92. Zwettler, F.U., M. Spindler, R. Benavente, M. Sauer, S. Reinhard, T. Klein, and A. Kurz. 2020. Tracking down the molecular architecture of the synaptonemal complex by expansion microscopy. Nat. Commun. 11.

93. Chozinski, T.J., A.R. Halpern, H. Okawa, H.J. Kim, G.J. Tremel, R.O.L. Wong, and J.C. Vaughan. 2016. Expansion microscopy with conventional antibodies and fluorescent proteins. Nat. Methods. 13:485–488.

94. Chozinski, T.J., A.R. Halpern, H. Okawa, H.J. Kim, G.J. Tremel, R.O.L. Wong, and J.C. Vaughan. 2016. Expansion microscopy with conventional antibodies and fluorescent proteins. Nat. Methods. 13:485–488.

95. Oheim, M., A. Salomon, and M. Brunstein. 2020. Supercritical angle fluorescence microscopy and spectroscopy. Biophys. J. 118:2339–2348.

96. Mercer, J.M. 2017. Cooperativity. Ref. Modul. Life Sci. 1–6.

97. Goldbeter, A. 1976. Kinetic cooperativity in the concerted model for allosteric enzymes. Biophys. Chem. 4:159–169.

98. Hess, V.L., and A. Szabo. 1979. Ligand binding to macromolecules: Allosteric and sequential models of cooperativity. J. Chem. Educ. 56:289–293.

99. Koshland, D.E., G. Némethy, and D. Filmer. 1966. Comparison of experimental binding data and theoretical models in proteins containing subunits. Biochemistry. 5:365–385.

100. Kawski, A. 1993. Fluorescence anisotropy: Theory and applications of rotational depolarization. Crit. Rev. Anal. Chem. 23:459–529.

101. Janeway, C.J., P. Travers, and M. Walport. 2001. The structure of a typical antibody molecule. .

102. Qadan, M.M. 2021. The development of potential therapeutic anti-myosin S2 peptides that modulate contraction and append to the heart homing adduct tannic acid without noticeable effect on their functions. Doctoral dissertation. University of North Texas.

103. Chang, R. 2005. Physical Chemistry for the biosciences. University Science Books.

104. Horovitz, A., and T. Mondal. 2021. Discriminating between concerted and Sequential allosteric Mechanisms by comparing equilibrium and kinetic hill coefficients. J. Phys. Chem. B. 125:70–73.

105. Woodhead, J. L., ; Craig, R. 2020. The mesa trail and the interacting heads motif of myosin II. Arch. Biochem. Biophys. 176:139–148.

106. Smith, D.J. 2008. Ultimate resolution in the electron microscope? Mater. Today. 11:30–38.

107. Mühlfeld, C., B. Rothen-Rutishauser, D. Vanhecke, F. Blank, P. Gehr, and M. Ochs. 2007. Visualization and quantitative analysis of nanoparticles in the respiratory tract by transmission electron microscopy. Part. Fibre Toxicol. 4:1–17.

108. Akel, A. 2010. Photoactivable quantum dots in super-resolution microscopy of muscle. Master thesis. University of North Texas.

109. Flashman, E., H. Watkins, and C. Redwood. 2007. Localization of the binding site of the C-terminal domain of cardiac myosin-binding protein-C on the myosin rod. Biochem. J. 401:97–102.

110. Lu, S.H.A., K.Z. Lee, P.W.C. Hsu, L.Y. Su, Y.C. Yeh, C.Y. Pan, and S.Y. Tsai. 2022. Alternative splicing mediated by RNA-binding protein RBM24 facilitates cardiac myofibrillogenesis in a differentiation stage- specific manner. Circ. Res. 130:112–129.

111. Perlman, R.L. 2016. Mouse models of human disease: An evolutionary perspective. Evol. Med. Public Heal. 2016:170–176.

112. Boöttger, R., R. Hoffmann, and D. Knappe. 2017. Differential stability of therapeutic peptides with different proteolytic cleavage sites in blood, plasma and serum. PLoS One. 12:1–15.

113. Rahmani, H., W. Ma, Z. Hu, N. Daneshparvar, D.W. Taylor, J.A. McCammon, T.C. Irving, R.J. Edwards, and K.A. Taylor. 2021. The myosin II coiled-coil domain atomic structure in its native environment. Proc. Natl. Acad. Sci. U. S. A. 118.

114. Woodhead, J.L., and R. Craig. 2020. The mesa trail and the interacting heads motif of myosin II. Arch. Biochem. Biophys. 680:108228.

115. Aboonasrshiraz, N. 2020. Impact of anti-S2 peptides on a variety of muscle myosin S2 isoforms and hypertrophic cardiomyopathy mutants revealed by fluorescence resonance energy transfer and gravitational force spectroscopy. Doctoral dissertation. University of North Texas.

116. Singh, R. 2017. Stability of myosin subfragment-2 modulates the force produced by acto-myosin interaction of striated muscle. Doctoral dissertation. University of North Texas.